

INVESTIGATION OF PARTICLE BREAKAGE PARAMETERS IN LOCKED-CYCLE BALL  
MILLING

A THESIS SUBMITTED TO  
THE GRADUATE SCHOOL OF NATURAL AND APPLIED SCIENCES  
OF  
MIDDLE EAST TECHNICAL UNIVERSITY

BY

CEMİL ACAR

IN PARTIAL FULFILLMENT OF THE REQUIREMENTS  
FOR  
THE DEGREE OF DOCTOR OF PHILOSOPHY  
IN  
MINING ENGINEERING

JANUARY 2013



Approval of the thesis:

**INVESTIGATION OF PARTICLE BREAKAGE PARAMETERS IN LOCKED-CYCLE  
BALL MILLING**

Submitted by **CEMIL ACAR** in partial fulfillment of the requirements for the degree of **Doctor of Philosophy in Mining Engineering Department, middle East Technical University** by,

Prof. Dr. Canan Özgen  
Dean, Graduate School of **Natural and Applied Sciences**

\_\_\_\_\_

Prof. Dr. Ali İhsan Arol  
Head of Department, **Mining Engineering**

\_\_\_\_\_

Prof. Dr. Çetin Hoşten  
Supervisor, **Mining Engineering Dept., METU**

\_\_\_\_\_

**Examining Committee Members:**

Prof. Dr. Ali İhsan Arol  
Mining Engineering Dept., METU

\_\_\_\_\_

Prof. Dr. Çetin Hoşten  
Mining Engineering Dept., METU

\_\_\_\_\_

Prof. Dr. Yavuz Topkaya  
Metallurgical and Materials Engineering Dept., METU

\_\_\_\_\_

Prof. Dr. Ümit Atalay  
Mining Engineering Dept., METU

\_\_\_\_\_

Prof. Dr. Hakan Benzer  
Mining Engineering Dept., Hacettepe University

\_\_\_\_\_

**Date:**

31.01.2013

**I hereby declare that all information in this document has been obtained and presented in accordance with academic rules and ethical conduct. I also declare that, as required by these rules and conduct, I have fully cited and referenced all material and results that are not original to this work.**

Name, Lastname : **Cemil Acar**

Signature :

## ABSTRACT

### INVESTIGATION OF THE PARTICLE BREAKAGE PARAMETERS IN LOCKED-CYCLE BALL MILLING

Acar, Cemil  
Ph.D., Department of Mining Engineering  
Supervisor: Prof. Dr. Çetin Hoşten

January 2013, 116 pages

Size reduction processes, particularly fine grinding systems, in mineral processing and cement production plants constitute a great portion of energy consumption and operating costs. Therefore, the grinding systems should be designed properly and operated under optimum conditions to achieve productive and cost effective operations. The use of simulation based on kinetic mathematical models of grinding has proven useful in this respect. The kinetic models contain two essential parameters, namely, breakage rate and breakage distribution functions, that are to be determined experimentally, and preferably in laboratory, or by back-calculation from the mill product size distribution for a given feed size distribution.

Experimental determination of the breakage parameters has been mostly carried out in laboratory batch mills using one-size-fraction material. The breakage rate parameter is obtained from the disappearance rate of this one-size-fraction material, while the breakage distribution parameters are estimated from the short-time grinding of the same material. Such laboratory methods using one-size fraction material, however, are not truly representative of industrial continuous mill operations where the mill contents have a distribution of particle sizes. There is evidence in the literature that the size distribution of the mill contents affects the breakage parameters.

This thesis study was undertaken with the main purpose of investigating the effect of the size distribution of the mill hold-up on the breakage parameters of quartz and calcite minerals in locked-cycle dry grinding experiments. The locked-cycle and one-size-fraction experiments were performed in the Bond ball mill instrumented with a torque-measuring device. Different closing screen sizes were used in the locked-cycle work to produce different size distributions of the mill hold-up, and the operating conditions were changed in the one-size-fraction experiments to obtain different power draws. Particle breakage parameters were assessed for these changing conditions.

Prior to the experiments related to the main purpose of the study, preliminary experiments were conducted for two reasons: (i) to find the power draw of the Bond mill in relation to the operating conditions with the intention of eliminating the use of costly torque-measuring devices by others; and (ii) to find the most accurate estimation method of breakage distribution functions among the three existing methods, namely, the “zero-order production of fines” method, the BII method, and the G-H method. The G-H method was found to be more appropriate for the current study.

The locked-cycle grinding experiments revealed that the breakage rate function of coarse fractions increased with increasing proportion of fines in the mill hold-up. Breakage distribution functions were found to be environment-dependent and non-normalizable by size in one-size-fraction and locked cycle grinding experiments. It was concluded that the cumulative basis breakage rate function could sufficiently represent the breakage characteristics of the two studied materials in a wide range of operating conditions. Therefore, it would be more appropriate to evaluate the breakage characteristics of materials ground in ball mills by linearized form of the size-discretized batch grinding equation using single parameter instead of dealing with two parameters which may not be independent of each other.

Keywords: Bond ball mill, locked-cycle grinding, breakage parameters.

## ÖZ

### KAPALI DEVRE BİLYALI DEĞİRMENLERDE PARÇA KIRILMA PARAMETRELERİNİN ARAŞTIRILMASI

Acar, Cemil  
Doktora, Maden Mühendisliği Bölümü  
Tez Danışmanı: Prof. Dr. Çetin Hoşten

January 2013, 116 Sayfa

Cevher hazırlama ve çimento üretim tesislerindeki boyut küçültme işlemleri, özellikle de ince öğütme sistemleri enerji sarfiyatının ve işletme maliyetlerinin büyük bir bölümünü oluşturmaktadır. Dolayısıyla üretken ve yüksek verimli operasyonlar için öğütme sistemleri uygun bir şekilde dizayn edilmeli ve optimum koşullarda çalıştırılmalıdır. Bu açıdan matematiksel öğütme kinetik modelleri tabanlı simülasyonların kullanımının yararlı olduğu kanıtlanmıştır. Kinetik modeller kırılma hızı fonksiyonu ve kırılma dağılımı fonksiyonu adı verilen ve tercihen laboratuvar koşullarında deneysel olarak, veya belirli bir boyut dağılımı olan besleme malının öğütülmesinden elde edilen ürün boyut dağılımı kullanılarak geriye hesaplama yöntemiyle elde edilen iki etkin parametre içerir.

Kırılma parametreleri deneysel olarak genellikle kesintili çalışan laboratuvar değirmenlerinde dar tane sınıfındaki malzemeler kullanılarak gerçekleştirilir. Kırılma hızı parametresi bu dar tane sınıfındaki malzemenin kaybolma hızından elde edilirken kırılma dağılımı parametreleri aynı malzemenin kısa süreli öğütme testlerinden tahmin edilir. Ancak bu tür dar tane sınıfındaki malzemelerin kullanıldığı yöntemler tane boyut dağılımına sahip değirmen içeriğinin öğütüldüğü kesintisiz çalışan endüstriyel öğütme işlemlerini tam olarak temsil etmemektedir. Literatürde değirmen içeriğinin boyut dağılımının kırılma parametrelerini etkilediğine dair bulgular mevcuttur.

Bu tez çalışması, değirmen içeriğinin sahip olduğu tane boyut dağılımının kapalı devre kuru öğütme deneylerinde kuvars ve kalsit minerallerinin kırılma parametrelerine etkisinin araştırılması amacıyla yapılmıştır. Kapalı devre ve dar tane sınıflı malzemelerle yapılan deneyler tork ölçüm aletine sahip Bond bilyalı değirmeninde gerçekleştirilmiştir. Kapalı devre öğütme deneylerinde farklı tane boyut dağılımına sahip değirmen içeriği oluşturabilmek için farklı test elekleri kullanılmıştır. Dar tane sınıfındaki malzemelerle yapılan deneylerde çalışma koşulları farklı değirmen güçleri elde edebilmek amacıyla değiştirilmiştir. Bu değişen koşullarda tane kırılma parametreleri değerlendirilmiştir.

Çalışmanın temel amacına yönelik deneyler öncesinde iki nedenle hazırlık deneyleri gerçekleştirilmiştir: (i) diğer araştırmacıların maliyeti yüksek tork ölçüm cihazı kullanmadan, çalışma şartlarına bağlı olarak Bond değirmeninin çektiği gücü tespit edebilmesini sağlamak; ve (ii) mevcut olan üç kırılma dağılımı tahmin yöntemi olan “zero-order production of fines” yöntemi, BII ve G-H yöntemi arasından en uygun olanı tespit etmek. Bu çalışma için G-H yönteminin daha uygun olduğu tespit edilmiştir.

Kapalı devre öğütme deneyleri iri boyuttaki malzemelerin kırılma hızı fonksiyonunun değirmen içeriğindeki ince malzeme oranının artmasıyla yükseldiğini ortaya koymuştur. Kırılma dağılımı parametrelerinin öğütme ortamına bağlı olduğu ve boyuta göre normalize edilemediği dar tane sınıfındaki malzemelerle ve kapalı devre öğütme deneyleriyle tespit edilmiştir. Kümülatif bazlı kırılma hızı fonksiyonunun çalışılan malzemelerin kırılma davranışlarını geniş bir çalışma şartı aralığında yeterli olarak temsil edebildiği sonucuna ulaşılmıştır. Bu sebeple, bilyalı değirmenlerde öğütülen malzemelerin kırılma karakterlerinin, birbirinden bağımsız olup olmadığı kesin olmayan iki parametre ile değerlendirilmek yerine, tek parametre kullanan ayırık tane boyu esaslı kesintili öğütme modelinin doğrusal formu ile değerlendirilmesi daha uygun olmaktadır.

Anahtar kelimeler: Bond bilyalı değirmeni, kapalı devre öğütme, kırılma parametreleri.

**...to my lovely family**

## AKNOWLEDGEMENTS

I would like to express my sincere thanks and appreciation to my supervisor, Prof. Dr. Çetin Hoşten for his supervision, guidance, support and patience during my thesis study.

I would to express my appreciation to Prof. Dr. Ali İhsan Arol and Prof. Dr. Yavuz Topkaya for their help, suggestions and support. I am particularly indebted to my colleagues, İlker Acar, Cihan Doğruöz, Doğa Kaya, Suzan Tahir, Osman Sivrikaya, Savaş Özün, Gülşen Tozsin and Esin Pekpak for their valuable friendship. Tahsin Işıksal, İsmail Kaya, Aytekin Arslan, Hülya Sakınmaz and Hamide Kan are gratefully acknowledged. I would also like to send my special thanks to Dr. Tuğcan Tuzcu for his contribution and support.

I am also grateful to all my friends for their support, help and friendship during the most difficult period of my life.

Finally, I am deeply grateful to each and every member of my crowded and lovely family for their endless patience, understanding and unconditional support throughout my life.

## TABLE OF CONTENTS

ABSTRACT .....	v
ÖZ .....	vi
ACKNOWLEDGEMENTS .....	viii
TABLE OF CONTENTS .....	ix
LIST OF TABLES .....	xi
LIST OF FIGURES.....	xiii
CHAPTERS	
1. INTRODUCTION.....	1
1.1. General .....	1
1.2. The Objectives and the Scope of the Thesis .....	2
2. BACKGROUND.....	5
2.1. General .....	5
2.2. Comminution in Mineral Processing .....	5
2.3. Comminution Principles.....	6
2.4. Energy-Size Reduction Relationships .....	7
2.5 Mathematical Models of Comminution Processes .....	8
2.5.1. Matrix Model .....	9
2.5.2. Kinetic Model .....	10
2.5.3. Discrete Element Method (DEM).....	11
2.6. Determination of Breakage Parameters .....	12
2.6.1. The Breakage Rate (Selection) Function .....	12
2.6.2. The Breakage Distribution Function.....	12
2.7. Previous Studies About Parameter Estimation and Scaling Up.....	14
2.8. Operating Variables in Batch Ball Mills .....	16
2.8.1. Mill Speed.....	16
2.8.2. Closing Screen.....	16
2.8.3. Ball Diameter and Ball Size Distribution .....	17
2.8.4. Specific Gravity and Grindability of Material .....	17
2.8.5. Material Size and Size Distribution .....	18
2.8.6. Fractional Ball Loading .....	18
2.8.7. Fractional Material Filling .....	18
3. EXPERIMENTAL MATERIAL AND METHODS .....	21
3.1. Materials.....	21
3.2. Grinding Equipment .....	22
3.3. Methods.....	24
3.3.1. Bond Ball Mill Grindability Test.....	24
3.3.2. Short-time Grinding Tests .....	26
4. POWER MEASUREMENTS IN THE BOND BALL MILL .....	27
4.1. General .....	27
4.2. Effects of Operating Parameters on Power Draw of the Mill .....	29
4.3. Determination of Mill Constant.....	31
4.4. Energy Efficiency in the Bond Ball Mill .....	33
5. A COMPARISON OF THE EXPERIMENTAL METHODS OF DETERMINING THE BREAKAGE DISTRIBUTION FUNCTIONS.....	37

5.1. Experimental $B_{ij}$ Estimation Methods .....	37
5.2. Experimental Study .....	39
5.3. Concluding Remarks .....	43
6. PARTICLE BREAKAGE PARAMETERS IN LOCKED-CYCLE BALL MILLING .....	45
6.1. The Effect of Material Size Distribution on the Breakage Parameters of Coarse Particles.....	45
6.2.1. The effect of Fractional Ball Charges on the Particle Breakage Parameters .....	52
6.2.2. The effect of Ball Size on Particle Breakage Parameters .....	56
6.2.3. The effect of Percent Circulating Load on the Particle Breakage Parameters .....	59
6.2.4. The effect of Grinding Environment on the Breakage Distribution Function .....	60
6.2.5. The Evaluation of Grinding Kinetics with the Linear Form of Batch Grinding Equation.....	65
7. CONCLUSION .....	91
REFERENCES .....	93
APPENDICES	
APPENDIX A: TORQUE AND POWER MEASUREMENTS .....	97
APPENDIX B: PARTICLE SIZE DISTRIBUTIONS OF MINERALS AFTER SHORT-TIME ..	101
GRINDING TESTS .....	101
CURRICULUM VITAE .....	115

## LIST OF TABLES

### TABLES

<b>Table 2.1.</b> Mass balance for a size-reduction process.....	9
<b>Table 3.1.</b> The specifications for ball mill, media and material.....	23
<b>Table 3.2.</b> Bond ball charge with recommended ball size ranges (Mosher and Tague, 2001) .....	24
<b>Table 6.1.</b> The percent amount of 6x8 mesh material in different mill hold-ups, and -6 mesh feed. ..	60
<b>Table A.1.</b> Mill torque versus mill speed for different ball sizes ( $\Phi_B=0.22$ ) .....	97
<b>Table A.2.</b> % of Max. mill power versus ball charge for different ball sizes. ....	97
<b>Table A.3.</b> Torque measurements with aged and new balls (Ball size: 19.05 mm, $n_c=0.75$ ).....	97
<b>Table A.4.</b> Material filling versus torque for different ball charges (Bond ball charge, $n_c=0.75$ ). ....	98
<b>Table A.5.</b> Material filling versus fineness of ground ( $\Phi_B=0.25$ , $n_c=0.75$ ). ....	98
<b>Table A.6.</b> Energy Efficiency in the Bond Ball Mill .....	99
<b>Table A.7.</b> Variation of fineness of material ( $d_{50}$ ) with charge conditions at 5 ( $n_c=0.75$ ) .....	100
<b>Table A.8.</b> Bond Grindability indices ( $W_i$ ) for quartz and calcite for different closing screens.....	100
<b>Table B.1.</b> Short-time grinding tests for quartz steady-state mill feed generated by 75 $\mu\text{m}$ closing screen. ....	101
<b>Table B.2.</b> Short-time grinding tests for quartz steady-state mill feed generated by 106 $\mu\text{m}$ closing screen. ....	101
<b>Table B.3.</b> Short-time grinding tests for quartz steady-state mill feed generated by 150 $\mu\text{m}$ closing screen. ....	102
<b>Table B.4.</b> Short-time grinding tests for quartz steady-state mill feed generated by 212 $\mu\text{m}$ closing screen. ....	102
<b>Table B.5.</b> Short-time grinding tests for quartz steady-state mill feed generated by 300 $\mu\text{m}$ closing screen. ....	103
<b>Table B.6.</b> Short-time grinding tests for calcite steady-state mill feed generated by 75 $\mu\text{m}$ closing screen. ....	103
<b>Table B.7.</b> Short-time grinding tests for calcite steady-state mill feed generated by 150 $\mu\text{m}$ closing screen. ....	104
<b>Table B.8.</b> Short-time grinding tests for calcite steady-state mill feed generated by 300 $\mu\text{m}$ closing screen. ....	104
<b>Table B.9.</b> Short-time grinding tests for quartz steady-state mill feed generated by 150 $\mu\text{m}$ closing screen (100% CL.) .....	105
<b>Table B.10.</b> Short-time grinding tests for quartz steady-state mill feed generated by 150 $\mu\text{m}$ closing screen (350% CL.) .....	105
<b>Table B.11.</b> Short-time grinding tests for calcite steady-state mill feed generated by 150 $\mu\text{m}$ closing screen (100% CL.) .....	106
<b>Table B.12.</b> Short-time grinding tests for -6 mesh quartz (Bond charge. $\Phi_B=0.22$ ) .....	106
<b>Table B.13.</b> Short-time grinding tests for -6 mesh calcite (Bond charge. $\Phi_B=0.22$ ).....	107
<b>Table B.14.</b> Short-time grinding tests for 6x8 mesh quartz (Bond charge. $\Phi_B=0.22$ ) .....	107
<b>Table B.15.</b> Short-time grinding tests for 6x8 mesh quartz (1 inch charge. $\Phi_B=0.22$ ) .....	108
<b>Table B.16.</b> Short-time grinding tests for 14x20 mesh quartz (Bond charge. $\Phi_B=0.22$ ) .....	108
<b>Table B.17.</b> Short-time grinding tests for 14x20 mesh quartz (1 inch charge. $\Phi_B=0.22$ ) .....	109
<b>Table B.18.</b> Short-time grinding tests for 48x65 mesh quartz (Bond charge. $\Phi_B=0.22$ ) .....	109
<b>Table B.19.</b> Short-time grinding tests for 48x65 mesh quartz (1 inch charge. $\Phi_B=0.22$ ) .....	109
<b>Table B.20.</b> Short-time grinding tests for 6x8 mesh quartz (Bond charge. $\Phi_B=0.28$ ) .....	110
<b>Table B.21.</b> Short-time grinding tests for 14x20 mesh quartz (Bond charge. $\Phi_B=0.28$ ) .....	110
<b>Table B.22.</b> Short-time grinding tests for 48x65 mesh quartz (Bond charge. $\Phi_B=0.28$ ) .....	110
<b>Table B.23.</b> Short-time grinding tests for 6x8 mesh quartz (Bond charge. $\Phi_B=0.35$ ) .....	111
<b>Table B.24.</b> Short-time grinding tests for 14x20 mesh quartz (Bond charge. $\Phi_B=0.35$ ) .....	111
<b>Table B.25.</b> Short-time grinding tests for 48x65 mesh quartz (Bondcharge. $\Phi_B=0.35$ ) .....	111

<b>Table B.26.</b> Short-time grinding tests for 6x8 mesh calcite (Bond charge. $\Phi_B=0.22$ ).....	112
<b>Table B.27.</b> Short-time grinding tests for 14x20 mesh calcite (Bond charge. $\Phi_B=0.22$ ).....	112
<b>Table B.28.</b> Short-time grinding tests for 48x65 mesh calcite (Bond charge. $\Phi_B=0.22$ ).....	112
<b>Table B.29.</b> Short-time grinding tests for 6x8 mesh calcite (Bond charge. $\Phi_B=0.28$ ).....	113
<b>Table B.30.</b> Short-time grinding tests for 14x20 mesh calcite (Bond charge. $\Phi_B=0.28$ ).....	113
<b>Table B.31.</b> Short-time grinding tests for 48x65 mesh calcite (Bond charge. $\Phi_B=0.28$ ).....	113
<b>Table B.32.</b> Short-time grinding tests for 6x8 mesh calcite (Bond charge. $\Phi_B=0.35$ ).....	114
<b>Table B.33.</b> Short-time grinding tests for 14x20 mesh calcite (Bond charge. $\Phi_B=0.35$ ).....	114
<b>Table B.34.</b> Short-time grinding tests for 48x65 mesh calcite (Bond charge. $\Phi_B=0.35$ ).....	114

## LIST OF FIGURES

### FIGURES

<b>Figure 3.1.</b> The Bond Work Indices of quartz and calcite samples determined for different closing screens using the standard Bond test procedure .....	21
<b>Figure 3.2.</b> The picture of Bond Mill set-up.....	22
<b>Figure 3.3.</b> The schematic representation of instrumented Bond ball mill.....	23
<b>Figure 4.1.</b> The schematic representation of tumbling mill including charge .....	28
<b>Figure 4.2.</b> Mill torque versus mill speed for different ball sizes ( $\Phi_B=0.22$ ) .....	29
<b>Figure 4.3.</b> Comparison of theoretical and experimental variation of power draw with ball loading .	30
<b>Figure 4.4.</b> Torque measurements in the Bond mill with aged and new balls (19 mm balls, 75% critical speed) .....	30
<b>Figure 4.5.</b> Typical variation of the mill torque with grinding time ( $n_c=0.75$ ).....	31
<b>Figure 4.6.</b> Determination of the constant K for the Bond ball mill ( $\Phi_M=0$ ).....	32
<b>Figure 4.7.</b> Comparison of experimental and calculated power draw of Bond mill including material and ball charges.....	32
<b>Figure 4.8.</b> Effect of material filling ( $\Phi_M$ ) on the torque draw of Bond ball mill for different $\Phi_B$ ( $n_c=0.75$ ) .....	33
<b>Figure 4.9.</b> a) Effect of $\Phi_M$ on the fineness of ground ( $n_c=0.75$ , $\Phi_B=0.25$ ).....	33
b) Fineness of ground as a function of $\Phi_M$ at different $\Phi_B$ ( $n_c=0.75$ ) .....	33
<b>Figure 4.10.</b> Specific grinding energy of material as a function of $\Phi_M$ at different $\Phi_B$ .....	34
<b>Figure 4.11.</b> Specific grinding energy of material as a function of $d_{50}$ at different $\Phi_B$ .....	34
<b>Figure 4.12.</b> Variation of fineness (efficiency of grinding) of material with charge dynamics ( $n_c=0.75$ ) .....	35
<b>Figure 5.1.</b> The disappearance of one-size-fraction quartz feeds ground with 1 inch and Bond ball charges .....	40
<b>Figure 5.2.</b> Cumulative breakage distribution functions of one-size-fraction quartz feeds plotted by (a) Zero-order, (b) BII and (c) G-H methods.....	41
<b>Figure 5.3.</b> Comparison of $B_{ij}$ values plotted by three different estimation methods on different size of feeds (a) -3.35+2.36 mm, (b) -1.18+0.85 mm, (c) -0.300+0.212 mm, ground with Bond ball charge.....	42
<b>Figure 6.1.</b> Cumulative size distribution of steady state mill hold-up of quartz (a) and calcite (b) before screening with different closing screens .....	46
<b>Figure 6.2.</b> Cumulative size distribution of steady state mill hold-up of quartz (a) and calcite (b) after screening with different closing screens .....	47
<b>Figure 6.3.</b> Cumulative size distributions of combined feeds quartz (a) and calcite (b) after screening of mill contents and addition of fresh feeds .....	47
<b>Figure 6.4.</b> The change in size distribution of steady state mill feeds quartz (left) and calcite (right) during short-time grinding tests .....	48
<b>Figure 6.5.</b> The disappearance of coarsest fraction (6x8 mesh) of quartz feed at steady state generated by different closing screens.....	49
<b>Figure 6.6.</b> The disappearance of coarsest fraction (6x8 mesh) of calcite feed at steady state generated by different closing screens.....	50
<b>Figure 6.7.</b> The change of the breakage rate of coarsest fraction (6x8 mesh) of quartz and calcite feeds at steady state generated by different closing screens .....	51
<b>Figure 6.8.</b> The disappearance of 6x8 mesh quartz as one-size-fraction feed and steady state mill content generated by 75 $\mu$ m test sieve .....	52
<b>Figure 6.9.</b> The disappearance of one-size-fraction quartz feeds at different ball charges ( $\Phi_B$ ), ( $\Phi_M=0.35$ ) .....	53
<b>Figure 6.10.</b> The disappearance of one-size-fraction calcite feeds at different ball charges ( $\Phi_B$ ), ( $\Phi_M=0.35$ ) .....	54

<b>Figure 6.11.</b> The change of the breakage rate of 6x8, 14x20, 48x65 mesh quartz and calcite feeds at different ball charges ( $\Phi_B$ ), ( $\Phi_M=0.35$ ) .....	54
<b>Figure 6.12.</b> The cumulative breakage distribution function ( $B_{ij}$ ) of 3 different one-size-fraction quartz feeds with specific energy values at different ball charges ( $\Phi_B$ ), ( $\Phi_M=0.35$ ) .....	55
<b>Figure 6.13.</b> The cumulative breakage distribution function ( $B_{ij}$ ) of 3 different one-size-fraction calcite feeds with specific energy values at different ball charges ( $\Phi_B$ ), ( $\Phi_M=0.35$ ) .....	56
<b>Figure 6.14.</b> The disappearance of 6x8 mesh quartz using Bond ball charge and 1 inch ball charge ..	57
<b>Figure 6.15.</b> The disappearance of 14x20 mesh quartz using Bond ball charge and 1 inch ball charge .....	57
<b>Figure 6.16.</b> The disappearance of 48x65 mesh quartz using Bond ball charge and 1 inch ball charge .....	58
<b>Figure 6.17.</b> The particle size distribution of 6x8 mesh, 14x20 mesh and 48x65 mesh quartz feeds after being ground with Bond Ball Charge and 1 inch ball charge .....	58
<b>Figure 6.18.</b> Size distributions of quartz (a) and calcite (b) feeds at different percent of circulating loads generated by 150 $\mu\text{m}$ closing screen.....	59
<b>Figure 6.19.</b> The disappearance of 6x8 mesh size fractions of quartz (a) and calcite (b) in -6 mesh feed and steady state mill feeds generated by 150 $\mu\text{m}$ closing screen at 100% and 250% circulating loads .....	60
<b>Figure 6.20.</b> The experimental and predicted (PBM) size distributions for 6x8 mesh quartz and calcite products for 90 seconds grinding time at 0.22 $\Phi_B$ .....	61
<b>Figure 6.21.</b> The experimental and predicted (PBM) size distributions for quartz products (75 $\mu\text{m}$ test sieve) for 90 and 120 seconds grinding time at 0.22 $\Phi_B$ .....	62
<b>Figure 6.22.</b> The experimental and predicted (PBM) size distributions for 14x20 mesh quartz and calcite products for 90 seconds grinding time at 0.22 $\Phi_B$ using $B_{ij}$ of 6x8 mesh and 14x20 mesh feeds.....	63
<b>Figure 6.23.</b> The experimental and predicted (PBM) size distributions for 48x65 mesh quartz and calcite products for 90 seconds grinding time at 0.22 $\Phi_B$ using $B_{ij}$ of 6x8 mesh and 48x65 mesh feeds.....	64
<b>Figure 6.24.</b> The variation of breakage rate functions by size for 6x8 mesh quartz and calcite minerals in narrow size 90 seconds of grinding.....	64
<b>Figure 6.25.</b> The variation of breakage rate functions by size for 14x20 mesh quartz and calcite minerals in narrow size 90 seconds of grinding.....	65
<b>Figure 6.26.</b> The variation of breakage rate functions by size for 48x65 mesh quartz and calcite minerals in narrow size 90 seconds of grinding.....	65
<b>Figure 6.27.</b> The linear batch grinding plots for quartz feeds at steady state generated by different closing screens .....	66
<b>Figure 6.28.</b> The linear batch grinding plots for calcite feeds at steady state generated by different closing screens .....	67
<b>Figure 6.29.</b> The linear batch grinding plots for quartz and calcite feeds at steady state generated 150 $\mu\text{m}$ closing screens at 100% Circulating Load.....	67
<b>Figure 6.30.</b> The linear batch grinding plots for -3.35 mm quartz and calcite feeds .....	67
<b>Figure 6.31.</b> The linear batch grinding plots for -3.35+2.36 mm (6x8 mesh) quartz feed ground by Bond ball size distribution and 1 inch balls ( $\Phi_B$ 0.22, $\Phi_M$ 0.35) .....	68
<b>Figure 6.32.</b> The linear batch grinding plots for -3.35+2.36 mm (6x8 mesh) quartz feed ground by Bond ball size distribution at $\Phi_B$ 0.28 and 0.35 .....	68
<b>Figure 6.33.</b> The linear batch grinding plots for -1.18+0.85 mm (14x20 mesh) quartz feed ground by Bond ball size distribution at $\Phi_B$ 0.22, 0.28 and 0.35 .....	68
<b>Figure 6.34.</b> The linear batch grinding plots for -0.300+0.212 mm (48x65 mesh) quartz feed ground by Bond ball size distribution at $\Phi_B$ 0.22, 0.28 and 0.35 .....	69
<b>Figure 6.35.</b> The linear batch grinding plots for -3.35+2.36 mm (6x8 mesh) calcite feed ground by Bond ball size distribution at $\Phi_B$ 0.22, 0.28 and 0.35 .....	69
<b>Figure 6.36.</b> The linear batch grinding plots for -1.18+0.85 mm (14x20 mesh) calcite feed ground by Bond ball size distribution at $\Phi_B$ 0.22, 0.28 and 0.35 .....	69
<b>Figure 6.37.</b> The linear batch grinding plots for -0.300+0.212 mm (48x65 mesh) calcite feed ground by Bond ball size distribution at $\Phi_B$ 0.22, 0.28 and 0.35 .....	70
<b>Figure 6.38.</b> Cumulative breakage rate function for quartz feed at steady state generated by different closing screens .....	70

<b>Figure 6.39.</b> Cumulative breakage rate function for calcite feed at steady state generated by different closing screens .....	71
<b>Figure 6.40.</b> Cumulative breakage rate function for one-size-fraction 6x8, 14x20 and 48x65 mesh quartz feeds at different ball charges, plotted by normalized size ( $\Phi_M=0.35$ ).....	71
<b>Figure 6.41.</b> Cumulative breakage rate function for one-size-fraction 6x8, 14x20 and 48x65 mesh calcite feeds at different ball charges, plotted by normalized size ( $\Phi_M=0.35$ ). .....	72
<b>Figure 6.42.</b> The experimental and predicted size distributions for quartz feed generated by 75 $\mu\text{m}$ closing screen, and its products for short grinding times .....	73
<b>Figure 6.43.</b> The experimental and predicted size distributions for quartz feed generated by 106 $\mu\text{m}$ closing screen, and its products for short grinding times .....	73
<b>Figure 6.44.</b> The experimental and predicted size distributions for quartz feed generated by 150 $\mu\text{m}$ closing screen, and its products for short grinding times .....	74
<b>Figure 6.45.</b> The experimental and predicted size distributions for quartz feed generated by 212 $\mu\text{m}$ closing screen, and its products for short grinding times .....	74
<b>Figure 6.46.</b> The experimental and predicted size distributions for quartz feed generated by 300 $\mu\text{m}$ closing screen, and its products for short grinding times .....	75
<b>Figure 6.47.</b> The experimental and predicted size distributions for calcite feed generated by 75 $\mu\text{m}$ closing screen, and its products for short grinding times .....	75
<b>Figure 6.48.</b> The experimental and predicted size distributions for calcite feed generated by 150 $\mu\text{m}$ closing screen, and its products for short grinding times .....	76
<b>Figure 6.49.</b> The experimental and predicted size distributions for calcite feed generated by 300 $\mu\text{m}$ closing screen, and its products for short grinding times .....	76
<b>Figure 6.50.</b> The experimental and predicted size distributions for quartz feed generated by 150 $\mu\text{m}$ closing screen at 100% circulating load, and its products for short grinding times .....	77
<b>Figure 6.51.</b> The experimental and predicted size distributions for calcite feed generated by 150 $\mu\text{m}$ closing screen at 100% circulating load, and its products for short grinding times .....	77
<b>Figure 6.52.</b> The experimental and predicted size distributions for -6 mesh quartz feed, and its products for short grinding times .....	78
<b>Figure 6.53.</b> The experimental and predicted size distributions for -6 mesh calcite feed, and its products for short grinding times .....	78
<b>Figure 6.54.</b> The experimental and predicted size distributions for 6x8 mesh quartz products for short grinding times at 0.22 $\Phi_B$ .....	79
<b>Figure 6.55.</b> The experimental and predicted size distributions for 6x8 mesh quartz products for short grinding times at 0.22 $\Phi_B$ , 1 inch balls.....	79
<b>Figure 6.56.</b> The experimental and predicted size distributions for 14x20 mesh quartz products for short grinding times at 0.22 $\Phi_B$ .....	80
<b>Figure 6.57.</b> The experimental and predicted size distributions for 48x65 mesh quartz products for short grinding times at 0.22 $\Phi_B$ .....	80
<b>Figure 6.58.</b> The experimental and predicted size distributions for 6x8 mesh quartz products for short grinding times at 0.28 $\Phi_B$ .....	81
<b>Figure 6.59.</b> The experimental and predicted size distributions for 14x20 mesh quartz products for short grinding times at 0.28 $\Phi_B$ .....	81
<b>Figure 6.60.</b> The experimental and predicted size distributions for 48x65 mesh quartz products for short grinding times at 0.28 $\Phi_B$ .....	82
<b>Figure 6.61.</b> The experimental and predicted size distributions for 6x8 mesh quartz products for short grinding times at 0.35 $\Phi_B$ .....	82
<b>Figure 6.62.</b> The experimental and predicted size distributions for 14x20 mesh quartz products for short grinding times at 0.35 $\Phi_B$ .....	83
<b>Figure 6.63.</b> The experimental and predicted size distributions for 48x65 mesh quartz products for short grinding times at 0.35 $\Phi_B$ .....	83
<b>Figure 6.64.</b> The experimental and predicted size distributions for 6x8 mesh calcite products for short grinding times at 0.22 $\Phi_B$ .....	84
<b>Figure 6.65.</b> The experimental and predicted size distributions for 14x20 mesh calcite products for short grinding times at 0.22 $\Phi_B$ .....	84
<b>Figure 6.66.</b> The experimental and predicted size distributions for 48x65 mesh calcite products for short grinding times at 0.22 $\Phi_B$ .....	85
<b>Figure 6.67.</b> The experimental and predicted size distributions for 6x8 mesh calcite products for short grinding times at 0.28 $\Phi_B$ .....	85

<b>Figure 6.68.</b> The experimental and predicted size distributions for 14x20 mesh calcite products for short grinding times at 0.28 $\Phi_B$ .....	86
<b>Figure 6.69.</b> The experimental and predicted size distributions for 48x65 mesh calcite products for short grinding times at 0.28 $\Phi_B$ .....	86
<b>Figure 6.70.</b> The experimental and predicted size distributions for 6x8 mesh calcite products for short grinding times at 0.35 $\Phi_B$ .....	87
<b>Figure 6.71.</b> The experimental and predicted size distributions for 14x20 mesh calcite products for short grinding times at 0.35 $\Phi_B$ .....	87
<b>Figure 6.72.</b> The experimental and predicted size distributions for 48x65 mesh calcite products for short grinding times at 0.35 $\Phi_B$ .....	88
<b>Figure 6.73.</b> The experimental and predicted (PBM and Linear form) size distributions for 6x8 mesh quartz and calcite products for 90 seconds grinding time at 0.22 $\Phi_B$ .....	88
<b>Figure 6.74.</b> The repeatability of 6x8 mesh quartz short-time grinding test .....	89

## CHAPTER 1

### INTRODUCTION

#### 1.1. General

The development in technology necessitates the use of high quality raw material for the industries to manufacture advanced products. The mineral industry, being the raw material supplier for a variety of industries, has to renew itself continually to meet specific requirements. For the mineral beneficiation, achievement of the desired degree of liberation of mineral species at a particle size as coarse as possible, and then, separation of the liberated minerals with a high efficiency is the main issue. In addition, comminution stage – combination of crushing and grinding operations - should be designed and operated properly as size and size distribution of particles play an important role during the concentration processes in terms of both technical and economical considerations. Besides, in some cases, size and size distribution may be the desired specification for industries such as cement, paint, glass etc. Hence, comminution has a major effect on the economic viability of mineral processing plants.

It is a well known fact that size reduction of particles is an energy-intensive process (Narayanan, 1987; Narayanan and Whiten, 1988; Kawatra, 1992; Ramasamy et al., 2005). Mineral processing plants consider energy consumption in the size-reduction operations as an important variable in determining the economic viability of the process (Verma and Rajamani, 1992). Comminution can account for more than 50% of the total power consumption in a typical mineral processing plant (Narayanan, 1987; Narayanan and Whiten, 1988), a tremendous portion of which is due to size reduction of very fine sizes, that is, grinding. Investigations revealed that less than 1% of applied energy is utilized for grinding (Fuerstenau and Abouzeid, 2002) while the rest is lost in movement of machinery, generating noise and heat (Rowland, 1998). Another statistics indicate that comminution is responsible for approximately 3% of consumption of electricity generated in the industrialized countries of the world (Narayanan, 1987). According to the U.S. Energy Information Administration's recent statistics, comminution comprised 1.14% of the energy used by the industrial sector and 0.39% of the overall national energy consumption (Tromans, 2008). These and many other statistics reveal the importance of size reduction processes and the reason for the extensive amount of effort made on this subject over the last half an age.

Due to the nature of comminution, energy required for breakage of unit mass of particles in terms of creating new surface area is inversely proportional with particle size. Hence, most of the studies carried out on this subject have focused on grinding operations but hardly any fundamental changes in grinding systems have been achieved so far. Instead, generally the investigators have been interested in improving the performance of conventional applications.

Among many grinding systems available today, such as rod mill, hammer mill, disk mills, high pressure grinding rolls etc., ball mills have been the most popular grinding equipments since their first implementation in the mineral processing industry. As the breakage in ball mills is a stochastic process, whether the ball-particle interactions in the mill will result with a breakage is a matter of probability. Theoretical and experimental methods developed in order to estimate the system output have been successful to a certain extent. The first generation mathematical model used in the description of size reduction processes is Bond's grinding equation (Bond, 1961).

Until 1970's the energy-size reduction relationship was the main form of mathematical model used in the description of size reduction processes. In these models, some measure of product fineness (80% passing size, specific surface area, size modulus) is selected as the dependent variable and the energy input per unit mass of material being ground acts as the independent variable. In some cases these models have been useful for the correlation of experimental data, but, usually, they have been found to be inadequate for meaningful process simulation (Herbst and Fuerstenau, 1973).

Recently, considerable improvements have been made in the development of phenomenological grinding models derived from population balance considerations. In these models a set of dependent variables is employed, corresponding to the set of mass fractions which constitute the product size distribution, and energy input is abandoned in favor of residence time as the dependent variable. The phenomenological models have been shown to provide accurate simulations of entire size distribution of ground products in grinding mills (Herbst and Fuerstenau, 1973).

Population balance models for batch grinding operations utilize two parameters; breakage rate function (or selection function)  $K_i$ , and the breakage distribution function ( $B_{ij}$ ). These parameters are very important for predicting the evolution of the entire particle size distribution in grinding systems. Good approximation of these functions helps better simulation, scale-up and optimization of grinding processes (Hoşten and Avşar, 2004).

Although the breakage rate function ( $K_i$ ) is widely accepted by the researchers to be dependent on the milling environment (size distribution of the feed, grinding media specifications, fractional media and material charges, mill speed) (Herbst and Fuerstenau, 1973; Austin et al., 1982; Fuerstenau and Abouzeid, 1991; Verma and Rajamani, 1992;), there are some contradictions on the relationship between milling environment and the breakage distribution function ( $B_{ij}$ ). Many researchers with the help of experimental results and empirical formulae, stated that  $B_{ij}$  is independent of milling conditions (Shoji et al., 1982; Fuerstenau and Abouzeid, 1990; Fuerstenau et al., 2004) while there are some others disagree with this statement (Meloy and Williams, 1992; Zhang and Kavetsky, 1993).

In general, population balance models consider  $B_{ij}$  to be normalizable with respect to size and independent of grinding environment. Therefore, it attributes all the variations on particle size distribution to the breakage rate function. This is questionable as these two parameters may not be independent so the both of the parameters may not be realistic although the model gives a reasonable estimation. Breakage parameters that population balance models contain are energy-dependent. They need to be determined experimentally in the laboratory and scaled up accordingly on the basis of the specific energy (energy per unit mass of product) consumed (Herbst and Fuerstenau, 1980) or the net power drawn (Morrell and Man, 1997). As the Bond (1961) approach remains to be a standard, the Bond mill is the most appropriate laboratory equipment for determining the energy-dependent breakage parameters of the population balance models. This approach may have the advantage of combining the traditional Bond method with the simulation approach using population balance models. The dependence of scaling up on mill power necessitates the accurate determination of the net grinding power draw in the Bond mill.

An alternative method for the evaluation of breakage kinetics is linearized form of the batch grinding equation. This method utilizes cumulative size basis rate of breakage assuming distribution of particles to be independent of size (compensation condition (Austin et al., 1984)). The advantage of this scheme is that the reasonable approximations can be achieved by utilizing a single cumulative breakage rate function.

## **1.2. The Objectives and the Scope of the Thesis**

The purpose of this study is to determine the particle breakage parameters and evaluate their behavior in different milling conditions in locked-cycle ball mill simulating the industrial scale continuous grinding circuits so as to provide a better basis for the design and operation of industrial mills. Power draw of the mill has been measured under different operating conditions in order to determine the

effects of operating variables and evaluate the efficiency of grinding. It is also intended to combine Bond approach and Population Balance Model to establish a meaningful approach representing the grinding operations in tumbling mills by observing the energy dependency of breakage parameters.

Calcite and quartz samples have been used as feed materials. The kinetic tests were performed with narrowly sized (one-size-fraction) materials and the steady state mill hold-up materials having different size distributions were generated by Bond Grindability Tests using different closing screens. The parameters were tested at different feed size, size distribution, grinding media, fractional media filling and percent circulating load variables. Experiments have been carried out in a standard Bond ball mill with a torque transducer.

The effects of grinding media and material charge conditions on torque and power draw of the laboratory scale Bond ball mill were investigated under dry grinding conditions. The mill constant  $K$  of Morrell's empirical power equation was determined. The optimum operating conditions for the Bond ball mill were determined.

Three methods for the estimation of breakage distribution functions, namely, zero-order production of fines, BII and G-H, were compared with the intention that the dissimilarities in these methods may be one of the reasons for the disagreements in the literature on the environment dependency of breakage parameters.

The breakage parameters were observed in one-size-fraction material and in closed-cycle milling conditions. The effect of grinding environment on the breakage parameters were pointed out. The reliability of linear form of batch grinding equation was evaluated in prediction of product size distributions.



## CHAPTER 2

### BACKGROUND

#### 2.1. General

Most of the valuable minerals are found as finely disseminated and firmly associated with the gangue in the nature so it is not practical to utilize them without processing. First, they must be unlocked or liberated to a sufficient degree by means of size reduction equipment. Then, the unlocked particles are subjected to an appropriate separation process. Achieving the desired degree of liberation at a particle size as coarse as possible is the crucial point for the economic viability of the process in terms of both the energy expenditure of the size reduction stage and the applicability of appropriate separation techniques. Therefore, the ore preparation plants should be well designed and operated properly.

#### 2.2. Comminution in Mineral Processing

Size reduction operations from crushing at coarse sizes to grinding to ultrafine sizes are generally defined by a combined name that is comminution. The aim of comminution is:

- to ease handling and transportation,
- liberation of valuable minerals from the gangue,
- to increase the specific surface area to ease chemical reactions,
- to prepare appropriate material for subsequent processes,
- to meet market demand concerning particle size and shape specifications.

Blasting and excavating the fresh material in quarries for the ease of handling and transportation can be considered to be the first stage in comminution. In mineral processing plants, particle size of excavated material is further reduced by subsequent crushing and grinding equipment each of which has certain range of operating size and reduction ratio since size reduction over many orders of magnitude cannot be efficiently carried out in a single machine. It may take a few or several stages to achieve the desired product size depending on the material characteristics. In general, crushing is a dry process and particles are broken by compression in between two rigid surfaces or by impact against a rigid surface with a high velocity. Gyratory and jaw crushers are widely used in the plants for the primary crushing issue. Their products are further crushed to a few millimeters by different type of roll and cone crushers. Then, in grinding stage, particle size of crushed material is further reduced to desired size by abrasion or impact, or combined effect of these two with certain proportion. It can be performed either wet or dry but the former one is preferred unless there is any technical constraint as it is more effective than the latter one. The conventional grinding mills using rods and balls, autogenous (AG) and semi-autogenous (SAG) mills are commonly used for this stage.

Recently, a relatively new comminution device, the high pressure grinding rolls (HPGR) has become popular as it is proved to be 20- 50% more efficient than conventional systems. In HPGR, a bed of particles is fed to the two counter-rotating rolls one of which is rigidly mounted and the other is pushed by a hydraulic force. Under very high pressure, an energy efficient inter-particle breakage occurs within the particle bed. This reduces mechanical wear and provides great reduction ratio so it may take the secondary and tertiary crushers and even grinding systems place when it is operated as closed circuit.

The minerals have unique crystal lattices comprised of atoms and different type of physical and chemical bonds. The crystal lattice of the mineral and the size and amount of the discontinuities in the material structure are the main properties which determine the breakage characteristics. The type of forces acting on the particles, the surrounding environment and the energy of impact are the other effective parameters. These all make breakage in a comminution device rather a complex process. Being influenced by these parameters, particles are broken into finer products with different size and shapes or may remain unbroken. The estimation of product size distribution by utilizing the aforementioned parameters has been attracting researchers' attention for decades as it is very important for producing high quality materials. Although each comminution device has unique breakage mechanism, the particle breakage occurs in basic comminution principles which were given in detail in the next part.

### 2.3. Comminution Principles

Particle fracture simply depends on the nature of the particle (brittle or ductile) and the type of force applied. Most of the minerals are brittle at coarse sizes so the strain (change in dimensions of a solid,  $\epsilon$ ) is proportional to the applied stress (force per unit area,  $\sigma$ ) until the point of fracture, as defined by Hooke's law (Encyc. Britannica, 2012):

$$\sigma = \frac{F}{A} = Y\epsilon \quad (2.1)$$

where Y is the proportionality constant denoted as Young's modulus.

Griffith stated that the low fracture strength observed in his experiments, as well as the size-dependence of strength, was due to the presence of microscopic flaws in the material (Griffith, 1921). This means that a fracture originates from pre-existing cracks and, with applied energy, can be propagated into larger cracks leading particle breakage.

$$\sigma_c \cong \sqrt{\frac{2\gamma Y}{L}} \quad (2.2)$$

where  $\sigma_c$  is the critical applied (tensile) stress normal to the crack axis,  $\gamma$  is the energy required to create unit area of new surface, and L is the crack length. According to Griffith's theory, smaller particles are stronger as they have fewer cracks. Moreover, materials may behave more ductile as the particle size decreases so higher energy is required to overcome plastic deformation. This means that greater energy density, hence greater applied stress, is necessary to create continuous cracks in smaller particles.

The breakage of particles occurs in different shapes and distributions according to the type of applied forces such as compression, impact and abrasion. The crushers which compressive force dominates between two rigid surfaces, such as jaw, gyratory and cone crushers, produce large number of small fragments with small number of large fragments. Impact of a rigid surface to a particle at very high velocity transfers considerable amount of energy to the particle causing it to break to large number of middle-size and very small fragments. Rubbing of two particles each other or a particle with a hard surface causes tearing out of fines from the original coarse particles. This type of force generates large amount of fines with worn or smoothed coarse particles as it is the case in ball mills operated in slow rate at which cascading action dominates.

## 2.4. Energy-Size Reduction Relationships

Comminution theories concern with the energy input-particle size relationship from a given feed size (Wills and Atkinson, 1993). The existing theories proposed to describe this relationship stem from a common empirical equation proposed by Walker et al. (1937):

$$dE = -\frac{C}{x^n} dx \quad (2.3)$$

where,

dE : infinitesimal change in specific energy

dx : infinitesimal size change

x : initial particle size

C : constant

n : constant (related to the material and the manner in which it is broken)

According to this proposition, change in particle size is proportional to the energy expended per unit weight of material, and energy required to make a small change in size of an object is proportional to the size change and inversely proportional to the object size to some power n (Charles, 1957). Various theories have been proposed based on this mathematical expression, none of which is entirely satisfactory (Wills and Atkinson, 1993), but they are considered to be valid for certain size ranges.

Rittinger's postulate, proposed in 1857, states that energy required for size reduction of a unit amount of solid is proportional to the fresh surface area created (Austin and Klimpel, 1964; Austin et al. 1984; Wills and Napier-Munn, 2006). The proposed theory can be formulated by integrating Walker's general equation and assigning a value of 2 to the exponent n.

$$\int_0^{E_R} dE = \int_{x_1}^{x_2} -C_R \frac{dx}{x^2} \Rightarrow E_R = C_R \left( \frac{1}{x_2} - \frac{1}{x_1} \right) \quad (2.4)$$

where, the  $x_1$  and  $x_2$  are the feed and product size, respectively.

Kick (1883) proposed an alternative theory that, for geometrically equivalent size reduction, the energy per unit volume is constant (Austin and Klimpel, 1964; Austin et al. 1984; Wills and Napier-Munn, 2006), which means that energy consumed is proportional to the size reduction ratio irrespective of the starting size. This seems to be a reasonable hypothesis from similarity considerations although it does not agree with Rittinger's postulate. Similarly, Kick's theory can be formulated by integrating eq. 2.1 and assigning a value of 1 to the exponent n.

$$\int_0^{E_K} dE = \int_{x_1}^{x_2} -C_K \frac{dx}{x} \Rightarrow E_K = -C_K \ln\left(\frac{x_1}{x_2}\right) \quad (2.5)$$

The investigations on these theories resulted in that Kick's theory is valid for coarse sizes while Rittinger's one is valid for very fine particles even below a few microns. A typical comminution plant in industry handles wide range of particle size from coarse lumps to a few microns so neither of the aforementioned theories is considered to be fully applicable in crushing and grinding operations.

In the light of the Rittinger's and Kick's comminution theories, Bond proposed 'The third theory of comminution' in 1952. Basically, he stated that the energy required in comminution is proportional to the new crack length created. When a particle of diameter  $x$  is broken, the average strain energy per unit volume is proportional to the particle volume  $x^3$  while the cracks form on a surface area which is proportional to  $x^2$ . The number of particles of similar shape in a unit volume varies as  $1/x^3$ . Therefore, the energy input should be proportional to;

$$\frac{\sqrt{x^3 \cdot x^2}}{x^3} = \frac{1}{\sqrt{x}} \quad (2.6)$$

This is the basis of the third theory of comminution (Bond, 1952). As the aforementioned methods are not satisfactory for comminution systems, an equation between two would be more applicable (Austin and Klimpel, 1964; Austin et al. 1984). Bond's law can be stated mathematically by integrating the general energy-size reduction equation and assigning a value of 1.5 to the exponent n.

$$E_B = C_B \left( \frac{1}{\sqrt{x_2}} - \frac{1}{\sqrt{x_1}} \right) \quad (2.7)$$

Bond (1952) defined a work index ( $W_i$ ) representing the energy (kWh/ton) required to reduce the size of a material from infinite size to 80% passing 100  $\mu\text{m}$ . It is basically a measure of the grindability (hardness) of material but it also includes the mechanical efficiency of the machine.

$$W_i = C_B \left( \frac{1}{\sqrt{100}} - \frac{1}{\sqrt{\infty}} \right) = \frac{C_B}{10} \quad (2.8)$$

According to the descriptions above, the energy input (kWh/t) to the machine for reducing the certain size of feed to a definite product size is,

$$W(kWh/t) = 10W_i \left( \frac{1}{\sqrt{P_{80}}} - \frac{1}{\sqrt{F_{80}}} \right) \quad (2.9)$$

where,  $F_{80}$  and  $P_{80}$  are the 80% passing size of feed and product, respectively. The output holds for certain material and mill specifications but it can be calibrated for different conditions by applying some efficiency factors. He also developed standard laboratory tests for the determination of crushability and grindability indices in 1952 and modified them in 1961 (Bond, 1961; Jankovic et. al, 2010). The crushability index is determined by the impact crushing tests of rock specimens. Grindability indices for rod mills and ball mills are determined by separate laboratory procedures for relatively fine minerals. The explanation of Bond Grindability Test for ball mills and the calculation of  $W_i$  were given in detail in the next chapter as they were utilized in this study.

The industrialization and technological developments have brought along the requirement for production of high quality raw materials with certain desired specifications, such as shape, size, and size distribution. For the grinding issues, achievement of this is only possible by controlling the system with a mathematical model describing the grinding kinetics of the material to be ground. Although Bond is an indispensable approach for the determination of energy-size reduction relationship and still widely utilized in design and scale-up issues in size reduction applications, it is inadequate for simulating grinding systems thoroughly. This enhanced the investigations on establishing new mathematical models which describe grinding kinetics of material and provide precise data for simulation.

## 2.5 Mathematical Models of Comminution Processes

The aforementioned empirical energy-size reduction relationships give highly oversimplified descriptions of the fracture process so they are not capable of yielding sufficient information for process simulation. Unlikely, mechanistic approach which is based on recognition of physical events that occur during comminution has been found to provide reasonable data which are sufficient for simulation (Lynch, 1977). The basic idea underlying mechanistic approach is that the distribution function after 'n' steps in a repetitive breakage process which can be described by a probability function and a distribution function is asymptotically log-normal, and this conforms to characteristic

size distributions of comminuted products. This concept has been used as the matrix and kinetic models (Epstein, 1948). Both models are based on three basic concepts;

- probability of breakage (selection or a breakage-rate function)
- characteristic size distribution after breakage (distribution or appearance function)
- differential movement of particles through or out of a continuous mill (discharge-rate or classification function).

### 2.5.1. Matrix Model

The matrix model considers comminution as a succession of breakage events. The product of each event is considered to be the feed of following event. The probability of breakage of each size range and the size distribution of each broken product is arranged in a matrix model. In this model, the feed and the product from a size-reduction process may be expressed as sizing distributions in terms of  $n$  size ranges (Lynch, 1977).

**Table 2.1.** Mass balance for a size-reduction process

Size Fraction	Feed	Product						
1	$f_1$	$p_{1,1}$	0	0	.	.	0	0
2	$f_2$	$p_{2,1}$	$p_{2,2}$	0	.	.	0	0
3	$f_3$	$p_{3,1}$	$p_{3,2}$	$p_{3,3}$	.	.	0	0
.	.	.	.	.	.	.	.	.
.	.	.	.	.	.	.	.	.
$n$	$f_n$	$p_{n,1}$	$p_{n,2}$	$p_{n,3}$	.	.	$p_{n,n}$	0
$n+1$	$f_{n+1}$	$p_{n+1,1}$	$p_{n+1,2}$	$p_{n+1,3}$	.	.	$p_{n+1,n}$	$p_{n+1,n+1}$

The 3<sup>rd</sup> column in the table refers to the products of breakage of the top size range in the feed, 4<sup>th</sup> column to the second size range and so on. The elements in the product have been written in the form  $p_{i,j}$  where 'i' refers to the size range in which the element occurs and 'j' refers to the size of the feed particle from which it came. Then,

$$p_{i,j} = X_{i,j} f_j \quad (2.10)$$

where,  $X_{i,j}$  is the mass fraction of the particles in the  $i^{\text{th}}$  fraction broken from  $j^{\text{th}}$  size. The detailed information on matrix model was given by Lynch (1977).

#### 2.5.1.1. The Perfect Mixing and Multi-Segment Ball Mill Models

The perfect mixing ball mill model is the simplest case of multi-segment models which contain only one segment. When expressed in matrix form, this model could be considered to be a matrix model that combines some better aspects (Lynch, 1977).

$$f_i - \left(\frac{k_i}{d_i}\right)p_i + \sum_{j=1}^i b_{i,j} \left(\frac{k_j}{d_j}\right)p_j - p_i = 0 \quad (2.11)$$

where,  $f_i$  and  $p_i$  are the feed and product vectors, respectively.  $d_i$  is discharge rate,  $k_i$  is diagonal rate matrix, and  $b_{i,j}$  is the triangular distribution function matrix.

In the multi-segment ball mill model, the effects of breakage rate, differential transport of the material and the variation of contents along the mill are described by dividing the mill into a number of perfectly mixed segments. The  $k_i$  is assumed to be the same for all segments while discharge rate factor  $d_i$  varies for each segment depending on the amount of coarse material present. The perfect

mixing and multi-segment ball mill models are the special case of population balance model so they are not going to be detailed here. The detailed information and the derivation of the equations of these models can be found in Whiten and Roberts (1974), Kavetsky and Whiten (1982), Lynch (1977), and Avşar (2003).

## 2.5.2. Kinetic Model

The kinetic model considers comminution as a continuous process and the longer the period of grinding, the greater the size reduction attained. It can be expressed both in terms of continuous functions and as discretized distributions. In discretized form, it shows close resemblance to matrix models (Lynch, 1977).

### 2.5.2.1. Population Balance Model

The population balance models (PBM) have been used in many branches of modern science dealing with particulate materials. As the particle moves through a processing environment, its external (physical coordinates) and internal (size, shape, chemical composition, surface specific energy, mineralogical composition etc.) properties change. The basic principle of PBM is to track the instantaneous characteristics and movement of particles. The derivation of batch population balance equation was cited in Tuzcu (2010).

The exact conservation law, which is that a mass entering to a system must either accumulate within the system or leave it, is used in the analysis of particle size distribution (Tuzcu, 2010).

$$Accumulation = Input - Output + Net Generation \quad (2.12)$$

As this phenomenon happen due to breakage of a particle in a collision event, the number of particles will change suddenly leaving a fraction and appearing in lower fractions, which are called birth and death events. If this phenomenon is applied to the particles having set of properties,  $Z^{(1)}, Z^{(2)}, \dots, Z^{(n)}$ :

$$Accumulation = \frac{\partial(V\bar{\psi})}{\partial t} \quad (2.13)$$

$$Input - Output = (Q_{in}\psi_{in} - Q_{out}\psi_{out}) \quad (2.14)$$

where,  $V$  is the tank volume,  $\bar{\psi}$  is the average number fraction of particles per unit volume.  $Q_{in}$  and  $Q_{out}$  are the volume flow rate of material fed and leave from the system.

$$Net Generation = V \left[ (\bar{B} - \bar{D}) - \sum_{j=1}^j \frac{\partial}{\partial Z^{(j)}} (v^{(j)}\psi) \right] \quad (2.15)$$

where,  $\bar{B}$  and  $\bar{D}$  are the rate of birth and death per unit volume, respectively.  $v^{(j)}$  is the rate of change of the  $j^{th}$  property. Then;

$$\frac{\partial(V\bar{\psi})}{\partial t} = (Q_{in}\psi_{in} - Q_{out}\psi_{out}) + V \left[ (\bar{B} - \bar{D}) - \sum_{j=1}^j \frac{\partial}{\partial Z^{(j)}} (v^{(j)}\psi) \right] \quad (2.16)$$

This general form is called macroscopic population balance equation and can be used to describe changing property of any particulate system after making necessary modifications. For a batch grinding system, one can not mention about input, output and continuous rate of change of any property. Then, the accumulation can be defined as the summation of birth and death events. If  $x$  refers to the particle size;

$$\frac{\partial}{\partial t} [V\bar{\psi}(x,t)] = V[\bar{B}(x) - \bar{D}(x)] \quad (2.17)$$

The particle born in the fraction of  $x$  is generated by the breakage of coarser fraction,  $y$ . The progeny particles of  $y$  are distributed into the smaller size fractions with a function which is called breakage distribution function,  $b(x,y)$ . The fractional breakage rates of the particles are  $K(x)$ ,  $K(y)$ . Then the birth and death terms can be described as;

$$V\bar{B}(x) = \int_x^{x_{\max}} b(x,y)K(y)V\bar{\psi}(y,t)dy \quad (2.18)$$

$$V\bar{D}(x) = K(x)V\bar{\psi}(x,t) \quad (2.19)$$

If these terms are substituted in the previous equation;

$$\frac{\partial}{\partial t} [V\bar{\psi}(x,t)] = -K(x)V\bar{\psi}(x,t) + \int_x^{x_{\max}} b(x,y)K(y)V\bar{\psi}(y,t)dy \quad (2.20)$$

The equation can be discretized by the size intervals for more convenient use. The parent size fraction is denoted by  $j$  and the daughter size fraction is denoted by  $i$ . Then, if the terms  $V\bar{\psi}(x,t)$  and  $V\bar{\psi}(y,t)$  are replaced by time dependent mass fractions  $m_i$  and  $m_j$ , the size-discretized/time-continuous batch population balance model is obtained.

$$\frac{dm_i(t)}{dt} = -K_i(t)m_i(t) + \sum_{j=1}^{i-1} K_j(t) b_{ij}m_j(t) \quad (2.21)$$

where  $K_i(t)$  is the breakage rate function for material in the  $i$ th size class at time  $t$ , and  $b_{ij}$  is the breakage distribution function which gives the fraction of material reporting to size class  $i$  when material in the  $j$ th size class is comminuted. For last a few decades, PBM has been used successfully by many researchers in order to carry out mathematical analysis of the grinding kinetics of materials to be ground. This study is also based on the investigation of particle breakage parameters of PBM in closed-cycle ball milling in order to provide more representative data for design and operation of industrial ball mills.

### 2.5.3. Discrete Element Method (DEM)

This method deals with each element and the interaction between the elements within the process. In general, it estimates the product size distribution considering the collision energy spectra and the breakage parameters.

Discrete element method (DEM) is a numerical method for computing the motion and interactions of a particulate system composed of large number of small particles. With the developments in computing power and numerical algorithms, it has become possible to numerically simulate the motion of millions of particles on a single processor. Today DEM is becoming widely accepted as an effective method of solving engineering problems in granular and discontinuous materials, especially in granular flows, powder mechanics, and rock mechanics (Munjiza, 2004). Mishra and Rajamani (1992) and Rajamani et al. (1993) utilized collision energy spectra in ball mills which was computed by DEM based simulation of the experimental mill. Recently, the micro-scale ball mill modelling has become more popular after the combination of collision spectra and particle breakage studies (Tuzcu and Rajamani, 2011).

## 2.6. Determination of Breakage Parameters

Batch grinding operations have been modeled as a first-order kinetic process for decades by employing two parameters; breakage rate parameters (or selection functions)  $K_i$ , and the breakage distribution function ( $B_{ij}$ ) (Fuerstenau et al., 2004). The breakage rate functions describe the probability of breakage of particles of different sizes and have units of 1/time. The dimensionless breakage distribution parameters (or functions) quantify the mass fraction of the breakage product of a given particle size reporting into finer sizes. These parameters play a vital role in predicting the evolution of the entire particle size distribution in a grinding environment, and a knowledge of their true values is essential for simulation, scale-up, control and optimization of grinding processes (Hoşten and Avşar, 2004). They are determined from the size distributions obtained by short-time grinding tests which are generally applied to one-size-fraction feeds.

### 2.6.1. The Breakage Rate (Selection) Function

Assuming first order kinetics, the breakage rate is obtained by evaluating the slope of semi-log plots of the fraction retained versus time which generally shows straight line (Sand, 2004).

$$\ln(R_i(t)) = -K_i t \quad (2.22)$$

where  $R_i$  is the cumulative fraction retained on the lower screen of the size interval  $i$ . Provided that the breakage parameters for the coarsest fraction ( $B_{i1}$ ,  $K_i$ ) in the mill feed have been determined, and assuming  $B_{ij}$  to be normalizable, the  $K_2$ ,  $K_3$ , ...,  $K_{n-1}$  can be calculated by the use of rearranged form of G-H solution given by Purker et al. (1986).

$$K_i = \frac{-G_i - H_i t - K_{i-1} B_{i,i-1} \frac{R_{i-1}(t)}{R_i(t)} + \sum_{j=1}^{i-2} (K_{j+1} B_{i,j+1} - K_j B_{i,j}) \frac{R_j(t)}{R_i(t)}}{1 - \frac{R_{i-1}(t)}{R_i(t)}} \quad (2.23)$$

where

$$G_i = -K_i + \sum_{j=1}^{i-1} \frac{R_j(0)}{R_i(0)} (K_{j+1} B_{i,j+1} - K_j B_{i,j}) \quad (2.23a)$$

and

$$H_i = \sum_{j=1}^{i-1} \frac{R_j(0)}{R_i(0)} (K_{j+1} B_{i,j+1} - K_j B_{i,j}) (G_j - G_i) \quad (2.23b)$$

### 2.6.2. The Breakage Distribution Function

There are many methods of estimating the breakage distribution function described in the literature which are based on non-linear optimization techniques and direct experimental schemes for measuring the feed size distribution parameters from short-time grinding of one-size-fraction feed (Kapur, 1982). According to Subasinghe (2004) they are based on the nature of the terms in the right hand-side of the Kapur's size-discretized batch grinding equation (2.24) for a given ore and type of mill being used. The  $B_{ij}$  estimation methods mentioned below were cited in Sand and Subasinghe (2004);

$$\frac{dR_i(t)}{dt} = -K_i R_i(t) + \sum_{j=1}^{i-1} [K_{j+1} B_{i,j+1} - K_j B_{ij}] R_j(t) \quad \text{for } i = 1, 2, 3, \dots, n \quad (2.24)$$

When the right hand side of eq. 2.24 is small it leads to a first order relationship known as linearized form of the batch grinding equation (eq. 2.25). This form of the batch grinding equation utilizes cumulative size basis rate of breakage without using breakage distribution function assuming

compensation condition is valid. The advantage of this scheme is that the reasonable approximations can be achieved by utilizing a single parameter which implicitly represents the change in breakage rate and distribution functions.

$$R(x_i, t) = R(x_i, 0) \exp(-z_i t^{p_i}) \quad (2.25)$$

where,  $R(x_i, t)$  and  $R(x_i, 0)$  are the mass retained of mineral  $m$  coarser than size  $i$  at time  $t$  and 0, respectively.  $z_i$  is the rate of breakage of mineral coarser than size  $i$ .  $p_i$  is a function which corrects the equation for non-first order kinetics.

Herbst and Fuerstenau (1968) assumed the right hand-side of the eq. 2.24 to be constant for smaller sizes in the initial stages of grinding a coarse ore. This is called zero order production of fines and used to estimate grinding characteristics such as breakage rate and distribution functions.

$$\frac{dY_i(t)}{dt} = F_i \quad (2.26)$$

where  $Y_i(t) = 1 - R_i(t)$  and  $F_i$  is the production rate of fines. A sufficient condition for this phenomenon to occur is  $B_{ij}K_j = F_i$  for  $j=1, \dots, i-1$ .

Austin and Luckie (1972) proposed three methods of estimating  $B_{ij}$ . BII is the one based on the solution of batch grinding equation given by the compensation condition and is claimed to correct for the secondary breakage.

$$B_{i,1} \cong \frac{\log[(1 - P_i(0))/(1 - P_i(t))]}{\log[(1 - P_2(0))/(1 - P_2(t))]}, \quad i > 1 \quad (2.27)$$

where  $P_i$  is the mass fraction of material in a certain size.

Kapur (1982) developed a method (G-H) for estimating breakage distribution functions;

$$\ln \frac{R_i(t)}{R_i(0)} = G_i t + \frac{H_i}{2!} t^2 + \frac{I_i t^3}{3!} + \dots \quad (2.28)$$

where  $G_i, H_i, I_i, \dots$  are coefficients of the series expansion which were defined in eq. 2.23. When a single sized feed is used then for all size fractions  $R_i(0) = 1.0$ . In addition, if short grind times are used then the higher order terms of eq. 2.28 may be neglected. He also showed that the coefficients are related to the breakage rate of the top size and the cumulative breakage distribution function, i.e. for  $i = 2, 3, 4, \dots$

Klimpel and Austin (1984) suggested a mathematical expression for obtaining  $B_{ij}$  which describes it as a sum of two components arising from impact and shatter breakage, respectively.

$$B_{ij} = \phi \left( \frac{x_i}{x_j} \right)^\gamma + (1 - \phi) \left( \frac{x_i}{x_j} \right)^\beta \quad (2.29)$$

Assuming  $B_{ij}$  to be normalizable and independent of grinding environment, the model parameters  $\phi, \gamma, \beta$  can be directly determined via single particle breakage tests such as drop weight and slow compression. However, this method cannot simulate the complex grinding environment within a tumbling mill. As the case study aims to examine the reliability of this assumption, this method was not utilized in this study. Instead, aforementioned methods, Zero Order Production of Fines (Herbst and Fuerstenau, 1968), BII (Austin and Luckie, 1972) and G-H (Kapur, 1982), were compared and the most reliable one for the entire range of operating conditions was preferred for determination of  $B_{ij}$ .

These kinds of methods lump together the entire spectrum of stress application events which prevail in a system under certain operating conditions. The appropriately defined average of these individual events is then considered to characterize the over-all breakage properties (Herbst and Fuerstenau, 1968) so as to allow one to analyze the environmental effect on breakage parameters.

In general,  $B_{ij}$  is considered to be normalizable with respect to size and independent of grinding environment in population balance models. Therefore, all the variations on particle size distribution are attributed to the breakage rate function. However, this is questionable as these two parameters may not be independent and distribution function may be environment dependent, too. As the breakage rate functions for the lower size fractions are calculated considering the  $B_{ij}$  fixed in eq. 2.23, both of the obtained parameters may not be realistic although the model provides a reasonable estimation.

## 2.7. Previous Studies About Parameter Estimation and Scaling Up

For decades, numerous studies have been carried out by many researchers in order to determine the particle breakage behavior and effects of parameters in a ball mill using concepts of breakage rate function and breakage distribution function. Most of the recent studies have been carried out in the light of these investigations. It is not practical to mention all of these investigations here. Some of these important studies were summarized below.

Yang et. al. (1967) investigated the relationship between the torque and operating parameters in a 254x292 mm laboratory batch ball mill. They concluded that the fractional ball loading  $\Phi_B$  is proportional to the net torque up to 0.5, then torque decreases with increasing  $\Phi_B$ . They also found that fractional material filling  $\Phi_M$  has a negligible effect on torque values. Size and size distribution of feed is not effective after the first 20 revolutions of the mill. Torque increases with increasing mill speed up to critical speed,  $n_c$ . Then, sharp decrease was observed. In wet grinding experiments, formation and breaking up of a cake of the grinding material resulted in unstable torque-readings. Decreasing the slurry density solved this problem. They also studied the effects of ball size for different milling conditions and found that it has different effects for dry and wet grinding.

Gumtz and Fuerstenau (1970) simulated the locked-cycle grinding process by using the dolomite batch grinding data and discretized batch-grinding model. They concluded that product material in closed-circuit grinding has the form of the natural feed material and depends much more on the mechanics of the comminution process than on the nature of the mill feed. This simulation also confirmed the linear relationship between the logarithm of the product rate and the logarithm of the product size in locked-cycle grinding. A reason as to why this relationship has the same slope as the log-log size distribution for the natural feed material was also presented in their study. An example of modeling for an unusual (bimodal, deficient in fines) feed-size distribution was discussed; this simulation also served as an example of the overriding importance of the mechanics of the comminution process. The reason for the lack of a proportional relation between batch and locked-cycle grindabilities was investigated. It was shown that this relationship was to be expected and that the discretized batch-grinding model provides a path by which tedious locked cycle testing may be eliminated in the light of appropriately interpreted batch data. The relationship between production rate and percent circulating load was reconstructed using batch data and the simulation procedure.

Herbst and Fuerstenau (1973) analyzed the kinetics of dolomite grinding in a dry batch ball mill. They concluded that the breakage rate is proportional to the specific power input to the mill, and the breakage distribution function is independent of time and milling environment. These approximations made it easy to generate the batch grinding model in which the kinetics of breakage for different mill operating conditions are normalized with respect to the specific energy input to the mill. They showed that normalized model provides relatively accurate predictions of batch grinding behavior over a wide range of ball loads, material fillings and mill speeds.

Magdalinovic (1988) studied the calculation of energy required for grinding in a ball mill. The Bond work index  $W_i$  is not a material constant but it changes with change of size of the ground product.

Therefore, there are some difficulties and errors when the energy consumption is determined according to this formula without having a  $W_i$  determined experimentally. Magdalinovic considered this problem in his study and found that the change of the mass passing a test screen  $G$  could be related to the aperture size  $P_k$  of the screen by the formula:  $G = K_1 \sqrt{P_k}$ . The grinding-product size,  $P$ , in a Bond ball mill, which is given by the aperture size which passes 80% of the grinding product as a function of the aperture size of the test screen  $P_k$  can be expressed by the formula  $P = P_k / K_2$ . He stated that these functions for  $G$  and  $P$  enable  $W_i$  to be calculated for any other size of grinding product if  $W_i$  and  $P_k$  is known.

Fuerstenau and Abouzeid (1991) investigated the effect of fine particles on the kinetics and energetics of grinding coarse particles by the use of PBM. To determine the effect of material environment on grinding parameters and specific energy distribution, mixtures of coarse (10x14 mesh) and fine (minus 100 mesh) material at different mass ratios were comminuted in a dry-batch ball mill. They concluded that the breakage distribution function is environment independent, whereas the breakage rate function of the coarse particles increases with increasing fine ratio in the feed. Furthermore, the energy split factors indicate that the specific energy consumed by coarse material increases as the ratio of coarse to fine material in the mill feed decreases. If the grinding of coarse-fine particle mixtures is carried out wet, the breakage rate of the coarse particles is markedly enhanced over all feed compositions, probably because the fines are suspended in the liquid and thereby effectively removed from the grinding zone.

Rajamani and Guo (1992) studied the acceleration and deceleration of breakage rates of all individual size classes in wet ball mills when the grinding environment is varied. He used natural spline techniques combined with the  $G-H$  scheme. Examination of wet grinding data showed acceleration of breakage rates in coarser sizes and deceleration in finer sizes. Whenever there is an increase of breakage rates with the production of finer particles the following mechanism may hold: the finer particles increase the contact points for transmission of the applied force to coarser particles which results in faster breakage. In industrial practice, it is generally believed that by increasing the hydrocyclone efficiency, the fines recycled to the mill can be decreased and corresponding quantity of fresh feed can be added to increase circuit capacity. This study showed that removing the fines might decrease breakage rates and so the recycle mass rate can increase; as a result, the circuit capacity may not increase at all.

Effect of milling environment on the breakage rates in dry and wet grinding is investigated by Verma and Rajamani (1992). They determined the time dependence of breakage rates by  $G-H$  plot using limestone and copper. They concluded that each fraction has different breakage rate and there are some variations on breakage rates with time which do not follow a general trend. They also studied the effect of grinding additives on breakage rates.

Zhang and Kavetsky (1993) investigated the particle breakage mechanisms in a batch ball mill using back-calculation. They estimated the breakage rate and distribution function parameters for two industrial ore samples and three types of cement clinker using dry batch ball mill data. Unique parameter estimates were obtained through a back-calculation approach using non-linear least squares fitting. Investigation showed that breakage distribution and rate parameters did not conform to the commonly used functional forms. They also concluded that the breakage rate function correlates to material property and particle size, and the breakage rate function also changes with material type and mill content size distribution.

Hoşten and Avşar (2004) studied the variation of back calculated breakage rate parameters in Bond mill grinding. They carried out kinetic experiments with one-size-fraction feeds and standard locked-cycle Bond grindability tests with natural size cement and trass samples. Size discretized population balance model of batch grinding and invariant breakage distribution parameters from short-time grinding experiments were used in order to back-calculate the breakage rate parameters. The results were found to be varying depending on either grinding time or the feed size distribution. They could not find a single set of parameters representing whole grinding path in the Bond grindability test, and therefore the simulation of Bond test with one set of parameters failed.

## 2.8. Operating Variables in Batch Ball Mills

There are some variables affecting the breakage kinetics and energetics of a mineral in batch ball mill. Effects of these parameters can be evaluated by changing one parameter in each experiment. In a laboratory scale Bond Ball Mill, the parameters which can be evaluated are;

- mill speed
- closing screen
- ball diameter and ball size distribution
- specific gravity and grindability of material
- material size distribution
- fractional ball loading
- fractional material filling
- volumetric solid fraction in the slurry (in wet grinding)

Since the experiments in this study were carried out in a standard Bond Ball Mill, mill diameter, length and lifters are not considered as variables. As the experiments were performed in dry conditions, volumetric solid fraction of the slurry was not tested as a variable.

### 2.8.1. Mill Speed

Generally the rotational speed is reported as a percentage of the critical speed ( $n_c$ ), which grinding medium and material stick to the inner surface of the mill and move together;

$$n_c = \frac{42.3}{\sqrt{(D-d)}} \text{ rev/min} \quad (2.30)$$

where  $D$  and  $d$  are the inside diameter of the mill and the diameter of the largest ball (or rod) in meter, respectively.

Mills are run at a speed of 50-90% of critical speed which is chosen according to the economic considerations. The higher the speed, the more is the capacity, but there is not that much increase in efficiency (i.e. kWh/t) above 40-50% of critical speed (Wills, 1985). Lower speeds are used for abrasive grinding and higher speeds are used for high capacity coarse grinding with the help of impact motion. Laboratory scale Bond Ball Mill is driven at a speed of 70 rpm, which corresponds to the 85% of the critical speed.

The net power required to turn a mill increases as a function of rotational speed. Similarly, the specific rates of breakage vary with the rotational speed. Austin et al, (1984) stated that the maximum power occurs at different fractions of critical speed for different mills depending on their specifications. The maximum power is usually in the range of 70-85% of  $n_c$ . Within the range of speed near the maximum power draw, there are relatively small changes in the specific breakage rates with rotational speed. Austin provided an equation for the variation of breakage rates with fractional critical mill speeds ( $\phi_c$ );

$$K_i \propto (\phi_c - 0.1) \left( \frac{1}{1 + \exp[15.7(\phi_c - 0.94)]} \right), \quad 0.4 < \phi_c < 0.9 \quad (2.31)$$

### 2.8.2. Closing Screen

Bond work index ( $W_i$ ) is generally calculated by the use of -3,35 mm (6 mesh) material, but the aperture of closing screen can be adjusted according to the product that is obtained in industry since

the result can be changed with different closing screens depending on the breakage characteristics of minerals.

On the other hand, changing the closing screen will change the gram of required size of product per revolution, and at steady state, the size distribution of material in mill so the proportion of fine and coarse material will change. At steady state, the greatest proportion in the mill hold-up is composed of the particles just above the closing screen, which can be investigated as the effect of coarse to fine ratio in ball mills.

### 2.8.3. Ball Diameter and Ball Size Distribution

In conventional ball mills, large balls are known to be responsible for the breakage of coarse particles and small balls are supposed to grind the fine ones. Although the Bond ball mill has a special ball size distribution, different size distributions and different one-size-fraction ball loads can be used in order to find the effects of ball diameter and ball size distribution. Austin et al. (1984) showed that, for the same material, the breakage rate function varies with ball diameter ( $d$ ):

$$a = \frac{\bar{a}}{d^{\xi}} \quad (2.32)$$

$$\mu = \bar{\mu} \cdot d^{\eta} \quad (2.33)$$

where  $\bar{a}$  and  $\bar{\mu}$  are the proportionality constants,  $\xi$  and  $\eta$  are constant exponent factors. He stated that the greater impact force of a collision involving a larger ball gives higher proportion of fines. On the other hand, the rates of breakage of smaller sizes are higher for smaller ball diameters. Thus, these two results partially compensate each other. Katubilwa and Moys (2009) and Katubilwa et al. (2011) investigated the effect of ball size and ball size distribution on the breakage rates of materials. They provided an optimum ball size distribution for coal grinding. They concluded that the effect of ball size is limited for large diameters. Furthermore, small diameter balls are more effective in producing fines. This was already shown by Austin et al. (1984) that as ball size decreases, total number of balls increase for the equal weight of charge so the number of impact increases. Katubilwa et al. (2011) also stated that the effect of ball size could vary for different operating conditions. Erdem and Ergün (2009) investigated the variation of breakage rates with ball diameter in industrial mills and concluded that the breakage rate was strongly related to the maximum ball diameter in the ball charge.

For a given ball diameter, the particle size at which the breakage rate function is maximum can be determined by (Austin et al., 1984):

$$x_m = \mu \cdot \left( \frac{\alpha}{\Lambda - \alpha} \right)^{1/\Lambda}, \quad \text{for } \Lambda > \alpha \quad (2.34)$$

### 2.8.4. Specific Gravity and Grindability of Material

Use of different type of materials with different grindability indices (hard, medium and soft) will help finding the effect of grindability of material to the breakage characteristics. However, in order to keep the total volume and weight of the mill hold-up equal, the materials should have same specific gravity (e.g. quartz and calcite).

### 2.8.5. Material Size and Size Distribution

Although Bond Ball Mill uses -3.35 mm material as feed, effect of material size distribution can be evaluated by using different size distributions such as one-size-fraction, larger or finer top size, or different proportion of one-size-fraction material in feed in order to determine the effect of one size in breakage kinetics as it is done by Fuerstenau and Abouzeid (1991) for determination of the effect of fine particles on the kinetics and energetics of grinding coarse particles. However, as the feeds were generated artificially, the representativeness of the results for the industrial operations was questionable. The following empirical equation is used for the definition of variation of breakage rate function with particle size (Austin et al., 1984):

$$K_i = a_i x_i^\alpha \frac{1}{1 + \left(\frac{x_i}{\mu}\right)^\Lambda} \quad (2.35)$$

where  $x_i$  is the upper size of the interval.  $a_i$  and  $\mu$  are the parameters which are the function of the mill conditions.  $\alpha$  and  $\Lambda$  and  $K$  are the parameters which are the function of the material.

In this study, material size distributions were changed by applying a standard Bond Grindability Test to the feeds with different closing screens. These naturally generated steady-state mill hold-up materials had different size distributions even though they were not as distinct as artificial feeds. Therefore, it is expected that the results should be more representative of the industrial operations.

### 2.8.6. Fractional Ball Loading

Fractional ball loading ( $\Phi_B$ ) is defined as the proportion of ball bulk volume, which includes the voids between the balls, to the mill inside volume:

$$\Phi_B = \frac{M_B}{(1 - \varepsilon_B)\rho_B V} \quad (2.36)$$

where  $M_B$ ,  $\varepsilon_B$ ,  $\rho_B$ , and  $V$  are ball mass, porosity in ball charge, ball density, and mill volume, respectively. For Bond Ball Mill,  $\Phi_B$  is 0.22 although it is generally in the range of 0.35-0.45 for industrial scale ball mills.

Since it is the major part of the total weight in the mill, fractional ball loading is directly proportional to the required motor power. Therefore, the relationship between fractional ball loading, breakage functions, and power parameters were investigated at different ball/mill volume ratios.

### 2.8.7. Fractional Material Filling

Fractional material filling ( $\Phi_M$ ) is defined as the proportion of material bulk volume, which includes the voids between the particles, to the void volume between the ball charge:

$$\Phi_M = (M_M / M_B)(\rho_B / \rho_M) \left\{ \frac{(1 - \varepsilon_B)}{(1 - \varepsilon_M)\varepsilon_B} \right\} \quad (2.37)$$

where  $M_M$ ,  $\rho_M$  and  $\varepsilon_M$  are material mass, density and porosity, respectively. For standard ball charge in the Bond mill, proportion of the void space between the balls to the ball loading was 40.6%, which was measured by replacement of water. 35% of this void space (equal to 700 ml) was filled with material for Bond work index tests although 100% material filling is preferred in industrial scale grinding.

Fractional material filling affects the total weight in the mill and the mill torque to a little extent. However, there is another effect of material filling, that is, particulate material filling restrains the regular movement of balls in mill, which results in increase in net torque. Different fractional material filling ratios and replacement of material with equal weight of ball charge can be tested in order to investigate the effects of this parameter. This variable was tested in mill power measurements. In parameter estimation tests, it was kept constant at 0.35.



## CHAPTER 3

### EXPERIMENTAL MATERIAL AND METHODS

#### 3.1. Materials

Grinding experiments were conducted with quartz and calcite. The quartz sample was supplied by Kaltun Mininc Co. from from Muğla-Yatağan district, and calcite sample was supplied by Omya Mining Co. from Muğla-Yatağan district. These two homogenous samples have very close densities (quartz:  $2.68 \text{ g/cm}^3$ , calcite:  $2.70 \text{ g/cm}^3$ ) but different degrees of hardness on the Mohs scale (quartz:7, calcite:3). The Bond Work Indices of these two samples determined for different closing screens using the standard Bond test procedure (Bond, 1961; Austin et al., 1984) are shown in Figure 3.1.

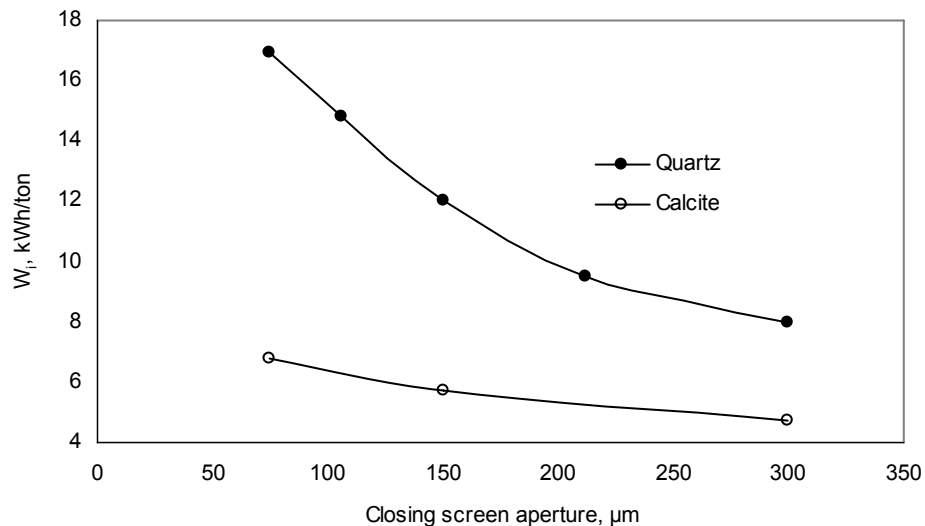


**Figure 3.1.** The Bond Work Indices of quartz and calcite samples determined for different closing screens using the standard Bond test procedure

For the experimental study, three one-size-fraction samples of  $-3.35+2.36 \text{ mm}$  (6x8 mesh),  $-1.18+0.850 \text{ mm}$  (14x20 mesh), and  $-0.300+0.212 \text{ mm}$  (48x65 mesh) quartz and calcite feeds with certain weights that corresponds to the 700 ml or  $0.35 \Phi_M$  (proportion of material bulk volume, which includes the voids between the particles, to the void volume between the ball charge) were prepared by dry laboratory screening. Also, steady state mill hold up materials were prepared by standard Bond Grindability Test procedure using 75, 106, 150, 212, 300  $\mu\text{m}$  closing screens.

Two types of ball charges were used in short-time grinding experiments one of which was composed of 1 inch steel balls and the other was standard Bond ball charge. The  $\Phi_B$  (proportion of ball bulk volume, which includes the voids between the balls, to the mill inside volume) was selected as 0.22 (approximately 22,650 g as it is the standard for Bond Grindability Test). The higher  $\Phi_B$  conditions (0.28, 0.35) were also tested.

Experiments were carried out under dry grinding conditions in a standard Bond ball mill (305x305 mm) with smooth inside surface at 70 rpm (nearly 85% of critical speed). After short-time (15, 30, 45, 60, 90, 120, 150 sec) grinding experiments, ground material were analyzed by wet and dry screening procedure. For power measurements, different mill speeds were also tested.

### 3.2. Grinding Equipment

The determination of breakage parameters under conditions smartly simulating the closed-cycle continuous ball mills in industrial operations is fundamental part of experimental setup. The experimental unit, shown in Figure 3.2, is an instrumented Bond ball mill (305 mm x 305 mm) having smooth inner surface. A torque transducer (Magtrol, TMB 308/411) is implemented between the motor and mill drum by using flexible couplings (Rexnord, BSD-966-62-000 CBC Single) in order to measure the torque drawn by the mill to avoid efficiency losses caused by the electrical motor (Asynchronous AC-0.37 kW). Mill speed can be adjusted between 20-82 rpm by an inverter.



Figure 3.2. The picture of Bond Mill set-up

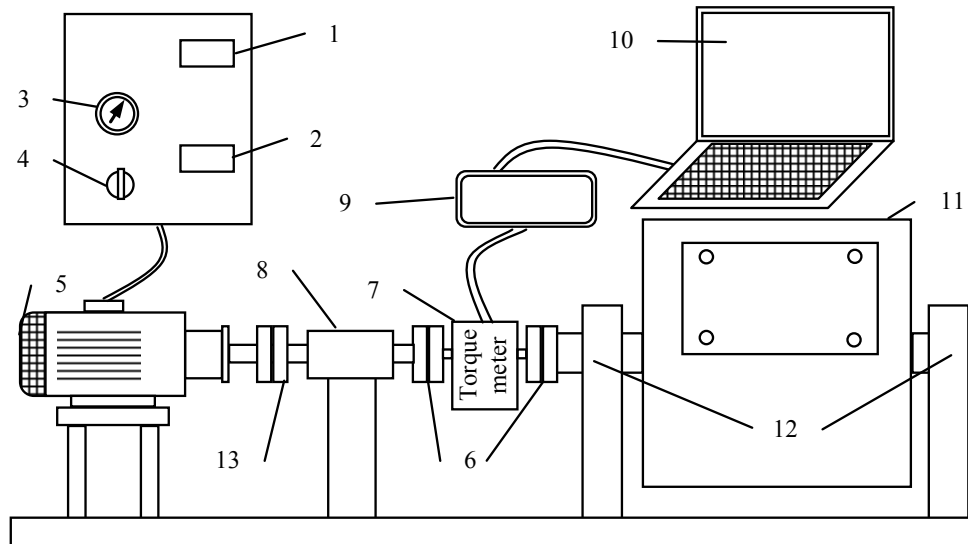


**Figure 3.3.** The schematic representation of instrumented Bond ball mill

- |                                    |                            |
|------------------------------------|----------------------------|
| 1. Digital tachometer              | 7. Torque transducer       |
| 2. Digital counter                 | 8. Centering bearing       |
| 3. Inverter rpm switch             | 9. Monitor                 |
| 4. Main switch                     | 10. PC                     |
| 5. Asynchronous AC motor (0.37 kW) | 11. Mill drum (305x305 mm) |
| 6. Flexible couplings              | 12. Bearings               |
|                                    | 13. Miniature coupling     |

**Table 3.1.** The specifications for ball mill, media and material

Mill	Inside diameter, D (mm)		305					
	Length, L (mm)		305					
	Volume, V (cm <sup>3</sup> )		22272.5					
	Rotational speed, rpm		70					
	Critical speed, n <sub>c</sub> , rpm		82					
	Motor power, kW		0.37					
Grinding media (balls)	Standard charge (0.22 Φ <sub>B</sub> )	Diameter, d(mm)	15.87	19.05	25.4	31.75	38.1	Total
		Number	94	71	10	67	43	285
	Density, g/cm <sup>3</sup>		7.78					
	Total weight, gr (std. charge)		22,650					
	Fractional ball loading, Φ <sub>B</sub>		0.22, 0.28, 0.35					
	Porosity in ball charge, ε <sub>B</sub> (%)		40.6					
Material			Quartz			Calcite		
	Density, gr/cm <sup>3</sup>		2.68			2.70		
	Mohs hardness		7			3		
	Size, mm		-3.35			-3.35		

### 3.3. Methods

The experiments were carried out by one-size-fraction feeds with different size fractions and feeds with natural size distributions. Furthermore, in order to simulate industrial continuous milling environment, steady state mill hold-up materials were prepared by Bond Grindability Test Procedure. Then, new fresh feeds were added to the prepared steady state material and short-time grinding tests were performed. The detailed information of applied test procedures is given below.

#### 3.3.1. Bond Ball Mill Grindability Test

Bond (1961) developed standard laboratory tests for the determination of crushability and grindability indices in 1952 and modified them in 1961. These indices are the measure of material's resistivity to breakage and are utilized in his empirical energy-size-reduction relationship equation in order to estimate the energy requirement of comminution processes. The basic principle for the grindability tests is achieving the steady state milling conditions simulating the industrial closed-cycle grinding applications with a certain (250% for ball milling) circulating load by using test sieve (closing screen) with an appropriate aperture size ( $P_1$ ). At steady state, the amount of fresh feed added and the product removed from the mill should be equal in weight for a certain grinding time. The procedure and the conditions for Bond Ball Mill Grindability Test utilized in this study were explained below.

The Physical Bond Ball Mill Parameters were given in Table 3.1. The inner surface of the 305x305 mm mill should be smooth with rounded edges. The rotational speed of the mill is 70 rpm. Perfectly round steel balls with different nominal diameters and different sizes were used as grinding media. The density of steel balls is 7.78 g/cm<sup>3</sup>. However, instead of nominal diameters, average ball size range was recommended as grinding media thinking that steel balls can be worn during grinding and it may be difficult to find exact size of balls. This flexibility caused an inconsistency in researches so different ball size distributions can be encountered in the literature (Mosher and Tague, 2001).

**Table 3.2.** Bond ball charge with recommended ball size ranges (Mosher and Tague, 2001)

<b>Bond Original</b>		<b>Recommended Range</b>		<b>Average</b>	<b>Total</b>
<b>Size</b>	<b>Number</b>	<b>Top</b>	<b>Bottom</b>	<b>Mass/Ball</b>	<b>Mass</b>
<b>Inches</b>		<b>Inches</b>	<b>Inches</b>	<b>g</b>	<b>g</b>
1.45	43	1.50	1.25	205	8806
1.17	67	1.25	1.12	108	7209
1	10	1.12	0.88	67.2	672
0.75	71	0.88	0.63	28.3	2009
0.61	94	0.63	0.50	15.2	1429
<b>Total</b>	<b>285</b>				<b>20125</b>

If the balls are new and glossy, they may slip rather than rolling in the mill because of low friction so it is better to roll them with abrasive material like quartz for a few hours before starting the experiment.

Test material should be -6 mesh (-3.35 mm), which has a natural size distribution. The recommended amount of material is around 10 kg. It can be achieved by controlled crushing of coarse material in order to prevent over-crushing. During preparation, it should be noted that every single particle was broken at least ones. All of the feed should be passed from 6 mesh sieve, completely. In some cases, a little amount of flakey particles may remain unbroken no matter how narrow the crusher gap is. Then,

they can be removed if the amount is negligible. Appropriate amount of (250-400 g) representative sample obtained by systematic sampling techniques is screened from a sieve series starting from 2360 mm and progressing according to  $\sqrt{2}$  rule. The 80% passing size ( $P_{80}$ ), and the percent of test sieve undersize values are noted. Test sieve size should be selected according to the industrial application. It is generally between 75-300  $\mu\text{m}$ .

700 ml of representative material is prepared via 1 liter volume of graduate cylinder. The material must be compacted in the graduate cylinder. The compaction can be achieved by a vibrating table or tapping it manually by hand for 30 seconds. The prepared material is weighed in order to keep it constant for the next cycles. It is then fed to the mill filled with grinding media.

For the first cycle, the mill is set to a random number of revolutions with the speed of 70 rpm. This number can be determined by experience considering the material hardness and test sieve size. For example, 100 revolutions are appropriate for the first cycle if quartz feed is tested with 106  $\mu\text{m}$  sieve. For 75  $\mu\text{m}$  test sieve, this number can be increased to 200 revolutions. If the material type is unknown, it is better starting with around 50 revolutions. Once the mill stops, the material is removed, and the balls and the inside of the mill are cleaned via a brush. The ground material is dry screened from the test sieve for certain time. The undersize is weighed and removed. The equal amount of fresh feed is added to the mill hold-up. Then, the amount of undersize produced per revolution for the first cycle ( $Gpr_1$ ) is calculated as follows;

$$Gpr_1 = \frac{W_{P1} - (W_{F1}xU)}{R_1} \quad (3.1)$$

where

$W_{P1}$  = Weight of undersize material for the  $i^{\text{th}}$  cycle, g

$W_{F1}$  = Weight of fresh feed for the  $i^{\text{th}}$  cycle, g

$U$  = Percent of undersize material in the fresh feed, g

$R_1$  = Number of revolution for the  $i^{\text{th}}$  cycle

For the second cycle, the aim is to simulate 250% circulating load (mill hold-up). For this purpose, the required number of mill revolution can be calculated as;

$$R_2 = \frac{\left(\frac{W_{F1}}{3.5}\right) - (W_{P1}xU)}{Gpr_1} \quad (3.2)$$

Then, the procedure is repeated until the number of revolution ( $R_i$ ) is the same or very close for last 3 cycles. Then the eq. 3.1 and eq. 3.2 can be generalized as;

$$Gpr_i = \frac{W_{Pi} - (W_{Fi}xU)}{R_i} \quad (3.3)$$

$$R_i = \frac{\left(\frac{W_{F1}}{3.5}\right) - (W_{Pi-1}xU)}{Gpr_{i-1}} \quad (3.4)$$

It should be noted that  $W_{Pi-1} = W_{Fi}$ , and, at steady state,

$$W_{Pn} = W_{Fi} = W_{Pn-1} \quad (3.5)$$

For Bond testing, suggested deviation from the highest and lowest Gpr value is 3% for the test closure. Inconsistent values indicate instability. The suggested minimum number of cycles is seven, no matter how fast the steady state conditions are achieved (Mosher and Tague, 2001).

For the first cycle, the percent of test sieve undersize in the feed should be less than 10% for the reliability of results. Otherwise, before starting the experiment, the first 700 ml feed should be screened from test sieve and equal amount of fresh feed should be added.

When the steady state conditions achieved, the products of last 3 cycles are mixed and appropriate amount of sample is taken for the sieve analysis in order to determine 80% passing size of product ( $P_{80}$ ). Then the Bond Ball Mill Work Index ( $W_i$ ) is calculated as;

$$W_i(kWh/t) = \frac{49.1}{P_1^{0.23} \times Gpr^{0.82} \times \left( \frac{10}{\sqrt{P_{80}}} - \frac{10}{\sqrt{F_{80}}} \right)} \quad (3.6)$$

The experimentally determined  $W_i$  is used in the eq. 2.9 to calculate the energy input (kWh/t) to the mill for reducing the feed to a definite size of product defined by 80% passing size.

The Bond Ball Mill Tests in this study were performed by the use of different test sieves (75, 106, 150, 212 and 300  $\mu\text{m}$ ). Therefore, mill contents with different size distributions, which are assumed to represent the industrial mill contents, were achieved. They were used in short-time grinding tests in order to evaluate the effect of milling environment on the breakage parameters of the population balance model.

### 3.3.2. Short-time Grinding Tests

Short-time grinding tests were performed for the evaluation of grinding kinetics of quartz and calcite feeds. For steady state mill contents, test conditions were similar to the Bond Test. For one-size-fraction feeds, two different ball charges, standard Bond ball charge, and 1-inch ball charge were used as grinding media. The fractional material filling  $\Phi_M$  kept constant at 0.35 while fractional ball charge  $\Phi_B$  was changed as 0.22, 0.28 and 0.35.

The ball charge and the feed were put into the mill layer by layer. The grinding times were set as 15, 30, 45, 60, 90, 120, 150 seconds, cumulatively. After each cycle, wet and dry sieve analyses were performed with representative samples. Then, the samples were added to the ground mill content. The whole ground mill content were again put into the mill layer by layer for further short-time grinding. The procedure was repeated until 150 seconds of grinding achieved. The obtained size distribution data were evaluated for the determination of breakage parameters using Kapur's G-H method described in detail in Chapter 5.

## CHAPTER 4

### POWER MEASUREMENTS IN THE BOND BALL MILL

#### 4.1. General

Despite its shortcomings, the traditional Bond approach has been the most common scale-up procedure for full-scale continuous grinding mill design (Herbst and Fuerstenau, 1980; Austin et al., 1984). An alternative design approach is using population balance models of grinding mills as a basis for scale-up from laboratory batch grinding tests. Such population balance models contain energy-dependent breakage parameters that are to be experimentally determined in the laboratory and scaled up accordingly on the basis of the specific energy (energy per unit mass of product) consumed (Herbst and Fuerstenau, 1980) or the net power drawn (Morrell and Man, 1997). As the Bond approach remains to be a standard, the Bond mill is the most appropriate laboratory equipment for determining the energy-dependent breakage parameters of the population balance models. This approach may have the advantage of combining the traditional Bond method with the simulation approach using population balance models. The dependence of scaling up on mill power necessitates the accurate determination of the net grinding power draw in the Bond mill.

Bond approach is very useful tool for the estimation of specific grinding energy (kWh/t) and the power draw of tumbling mills. It utilizes a few data such as grindability index,  $W_i$ , of ore and 80% passing size of feed ( $F_{80}$ ), and product ( $P_{80}$ ) in microns.

$$W(\text{kWh/t}) = 10W_i \left( \frac{1}{\sqrt{P_{80}}} - \frac{1}{\sqrt{F_{80}}} \right) \quad (4.1)$$

then, the power is the product of specific energy and output rate,  $Q$  (t/h).

$$P(\text{kW}) = W \times Q \quad (4.2)$$

In tumbling mills, power is consumed by the rotation of mills which have certain amount of grinding media and material to be ground filling the voids in the media charge. Fractional material filling ( $\Phi_M$ ) is defined as the proportion of material bulk volume (including the voids between particles) to the void volume in the ball charge. Fractional ball loading ( $\Phi_B$ ) is defined as the proportion of ball bulk volume (including voids between the balls) to the mill inside volume. The values of  $\Phi_M$  and  $\Phi_B$  vary to a certain extent depending on the operation; the preferred values are  $\Phi_M = 1.0$  and  $\Phi_B = 0.35-0.50$ . Although the power consumption ( $P$ ) of a tumbling mill can be closely predicted by the use of empirical equations, it is directly related to the torque ( $\tau$ ) required to rotate the mill and to the speed ( $N$ ) of the mill. From basic principles, the mill power in kilowatts is then given by the following expression:

$$kW = \frac{2\pi N \tau}{60,000} \quad (4.3)$$

where  $N$  is mill speed (rpm),  $\tau$  is the torque (N.m) generated by the mill charge. Referring to Figure 4.1, the torque developed by the mill charge is approximated by the product of the charge weight,  $W$  (in newtons), and the torque arm,  $r_c \sin \theta$  (in meters):

$$\tau \approx W r_c \sin \theta \quad (4.4)$$

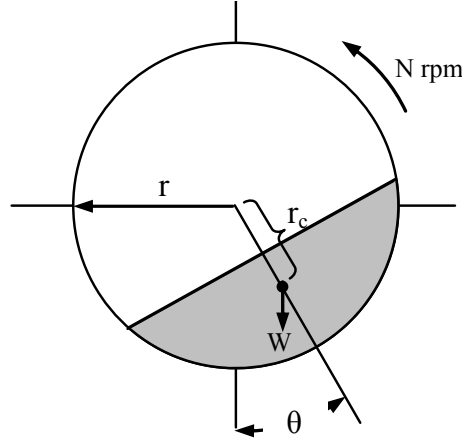


**Figure 4.1.** The schematic representation of tumbling mill including charge

Equation 4.4 is only an approximation and it does not take into account the contributions to power draw made by many other factors (Morrell, 1996). Among these factors are the mill contents size distribution and the interactions between the balls, material and mill shell. These interactions affect the net power draw depending on the operating conditions such as fractional material filling ( $\Phi_M$ ) and ball loading ( $\Phi_B$ ).

Loveday (1978) calculated the net power draw of the ball mills by the use of mill diameter  $D$  and length  $L$ , total charge density  $\rho_c$ , and a constant called power number  $P_N$ , which considers all the charge motions in the mill such as mill speed, attrition, abrasion, friction, etc...

$$kW_{(net)} = P_N \rho_c D^{2.5} L \quad (4.5)$$

Turner (1982) used the same formula with some changes to calculate the net power draw for dry grinding mills. He separated the effect of mill speed from  $P_N$ , and defined a constant for the rest of the charge motions. In his formula, mill speed is directly proportional to the net power draw in the form of fractional critical speed  $n_c$ .

$$kW_{(net)} = 2.208 \rho_c D^{2.5} L N_c \quad (4.6)$$

Morrell (1996) developed an empirical model that separately considers the effect of mill diameter ( $D$ ), length ( $L$ ), total charge density ( $\rho_c$ ), material filling and mill speed on the net power draw of industrial tumbling mills:

$$kW_{(net)} = K D^{2.5} L_e \rho_c \alpha \delta \quad (4.7)$$

$$\alpha = \phi_T (\omega - \phi_T) / \omega^2 \quad (4.8)$$

where  $L_e$  is effective mill length,  $\alpha$  and  $\delta$  are the non-linear functions of total mill filling ( $\Phi_T$ ) and mill speed, respectively.  $\omega$  is an empirical parameter being a function of the critical speed.  $K$  is a

calibration constant which is unique for each mill and reflect the losses due to attrition, abrasion and friction, which are related with the motion of the mill charge.

The purpose of this part of the study is to investigate variations in the net power drawn by the Bond ball mill under different operating conditions of dry grinding so that more accurate estimations of the specific energy of comminution can be made for scale-up purposes. The operating parameters of the test work were mill speed, ball loading, ball size, material filling and mill contents size distribution. Calibration of Morrell's empirical power equation (eq. 4.7) for the Bond mill was attempted with the intention of predicting the specific grinding energy consumption in laboratory tests conducted in the Bond mill that was not equipped with the costly torque or power measuring devices.

#### 4.2. Effects of Operating Parameters on Power Draw of the Mill

Calcite, stage-crushed to -3.35 mm (6 mesh), was used as feed material. The effect of ball size at different mill speeds was first investigated with 3 ball sizes (Figure 4.2) without any feed material charge. Austin et al. (1984) carried out similar investigation with two different ball sizes and concluded that the effect of ball size on power draw of the mills was negligible. Therefore, for normal ranges of ball sizes, any mixture of ball charges were to draw the same power independent of ball sizes. However, Figure 4.2 indicates that there is an increase in torque with decreasing ball size, confirming the findings of Yang et al. (1967). The 3% error bars on the 1 inch curve indicate more than 7% increase in torque as the ball size is reduced from 31.75 mm to 19.05 mm. The smaller the ball size the higher is the total surface area where friction takes place. It can be concluded that higher friction causes difficulty in tumbling of balls so the angle of repose increases. For a given ball size the mill speed has no appreciable effect on the torque for mill speeds below the corresponding critical speeds for the studied ball sizes (79-81 rpm). However, the power drawn by the mill increases with increasing mill speed up to the critical speed in accordance with the power draw formula (eq. 4.3).

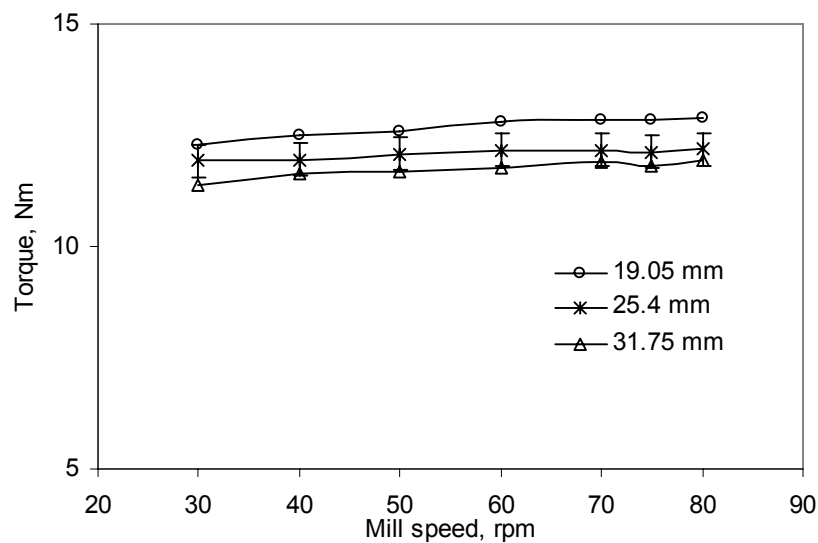
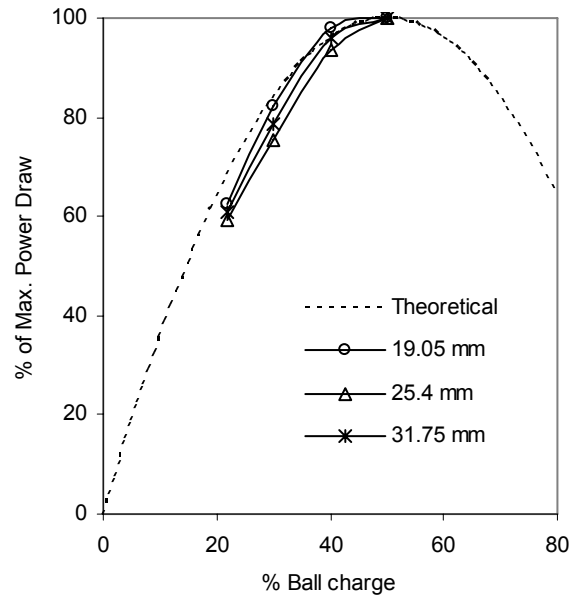


Figure 4.2. Mill torque versus mill speed for different ball sizes ( $\Phi_B=0.22$ )

The experimental variation of power draw with ball loading complies with the theoretical curves generated by the Bond equation (Austin et al., 1984) between 0.2-0.5  $\Phi_B$  with small deviations for all ball sizes (Figure 4.3). These deviations may be due to the slippage of balls and uncertain gravity center of charge during tumbling.



**Figure 4.3.** Comparison of theoretical and experimental variation of power draw with ball loading

As ball-to-ball and ball-to-wall frictions are important in torque measurements, surface roughness of the balls is to affect the torque to a certain extent. To see this effect, mill torque measurements were separately conducted with the new balls and aged balls at different ball charges of three different ball sizes, without any feed material. Only one set of results is shown in Figure 4.4 for 19-mm balls, which indicates that there is, in fact, a considerable increase in the measured torque in the case of aged balls having rougher surfaces. The similar trend was observed with the other two ball sizes (25.4 mm and 31.8 mm).

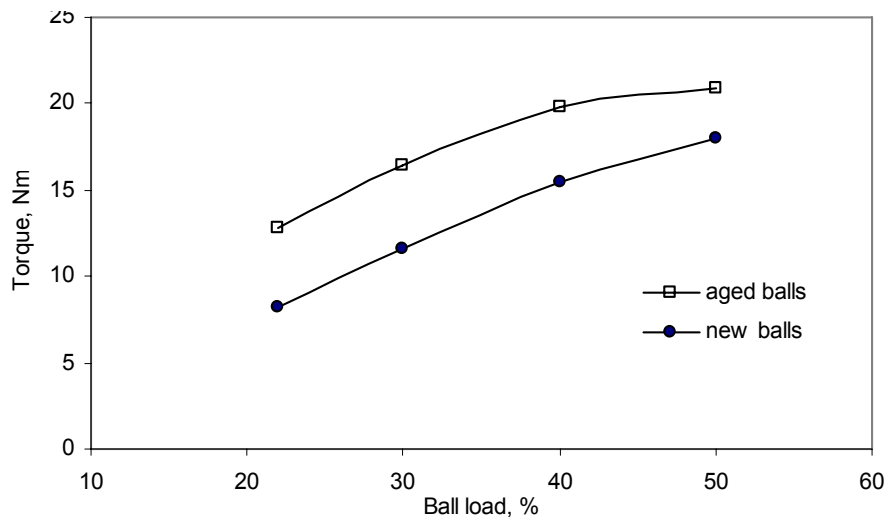


**Figure 4.4.** Torque measurements in the Bond mill with aged and new balls (19 mm balls, 75% critical speed)

Effect of fineness of the material being ground on the mill torque and power draw was also investigated in this study. Austin et al. (1984) stated that grinding of coarse feed draws significantly higher power than finer one. Some of our experiments carried out with calcite as feed material

confirm their results for certain conditions. However, especially when  $\Phi_M$  is above 0.4, torque values follow three different path during 15-20 minutes of grinding. Initially, it gradually decreases and then shows an increase up to a certain point. Then, it is almost fixed at this value. Figure 4.5 shows the change in the mill torque with time for  $\Phi_M$  lower and greater than 0.4. Although the time for critical points changes, the general shape of the curves are the same for all fractional ball loadings. Austin et al. (1984) considered this to be a problem in laboratory scale measurements and claimed that it was not seen in industrial operations. The reason for the increase in torque draw was first thought to be the coating of newly generated fines on the balls. However, experiments carried out with quartz in this study disproved this inference as the grinding of the quartz followed a similar trend, while it did not cause ball coating. Therefore, the reason for the increase in the torque after a certain time must be the change in the charge dynamics due to changing fineness of the material being ground.

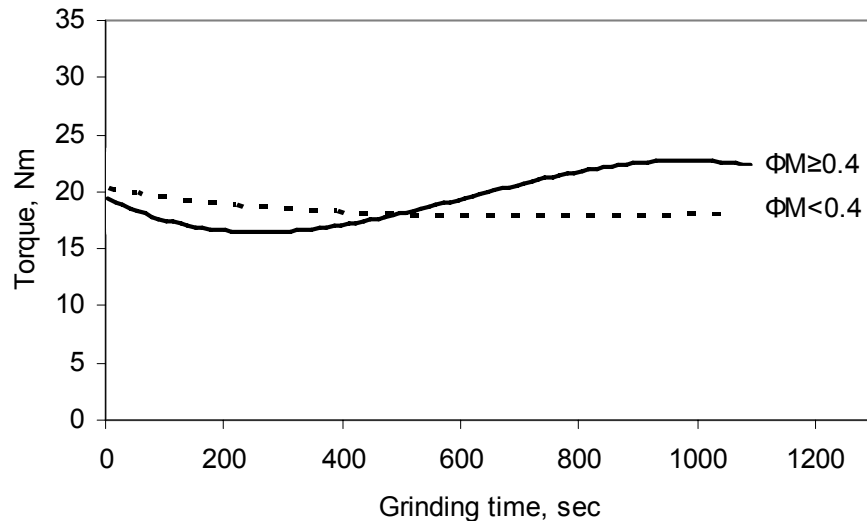


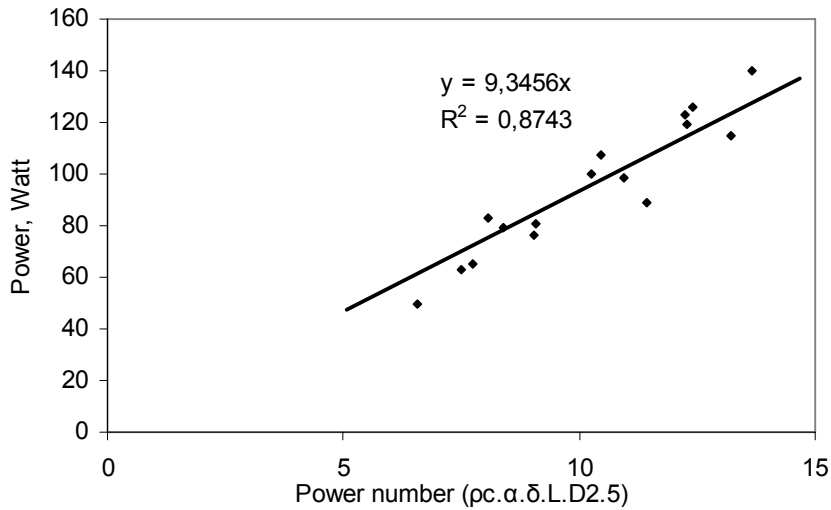
**Figure 4.5.** Typical variation of the mill torque with grinding time ( $n_c=0.75$ )

### 4.3. Determination of Mill Constant

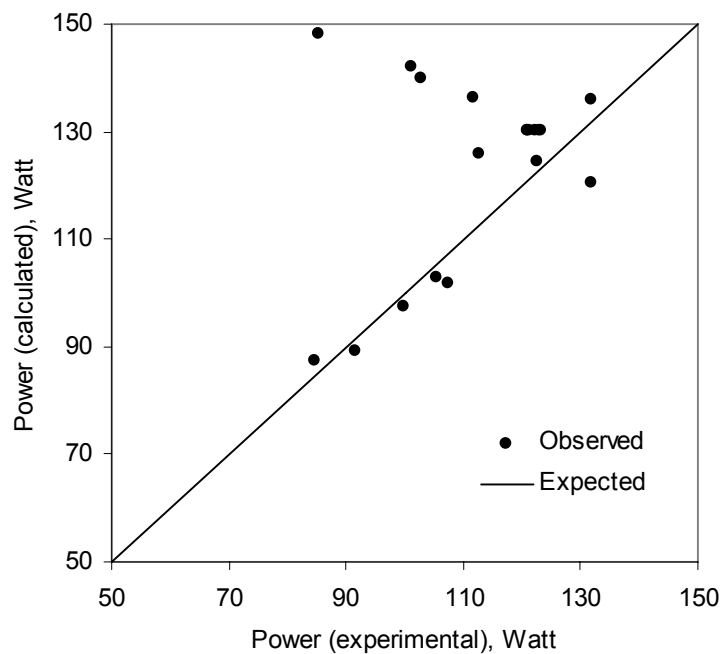
Scaling up breakage rate parameters of the population balance models from laboratory grinding tests requires the measurement of the power draw of the laboratory mills. An accurate prediction of this power draw by a power equation similar to Morrell's equation (eq. 4.7) would eliminate the use of costly torque measuring devices or digital energy meters. For this purpose, calibration of Morrell's equation was attempted for the Bond mill by determining the K value from a set of power values obtained by the operation of the Bond ball mill under different mill speeds and ball charges, but first without material filling, then with material filling.

The power data were plotted against a group of variables, referred to as the power number, so that the slope of this plot yields the value of the empirical constant K (Figure 4.6). This plot indicates a good correlation, yielding a value of 9.35 for the constant K. Morrell (1996) reported the values of 7.98 and 9.10 for overflow mills and grate mills, respectively.

The experiments carried out with material filling, however, indicate a deviation from the linear correlation between the power draw and the power number (Figure 4.7), especially at high levels of material filling,  $\Phi_M$ , and ball loading,  $\Phi_B$ , where the Morrell equation loses its validity for the Bond mill.

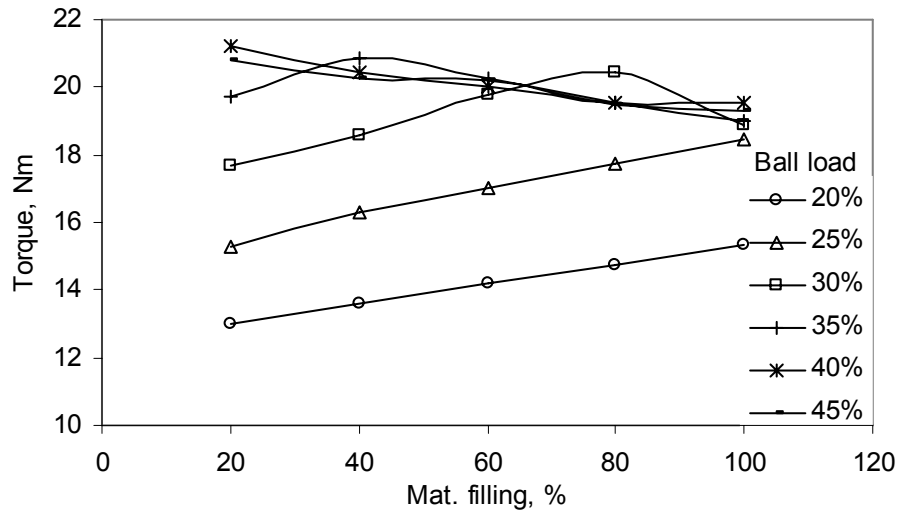


**Figure 4.6.** Determination of the constant K for the Bond ball mill ( $\Phi_M=0$ )



**Figure 4.7.** Comparison of experimental and calculated power draw of Bond mill including material and ball charges

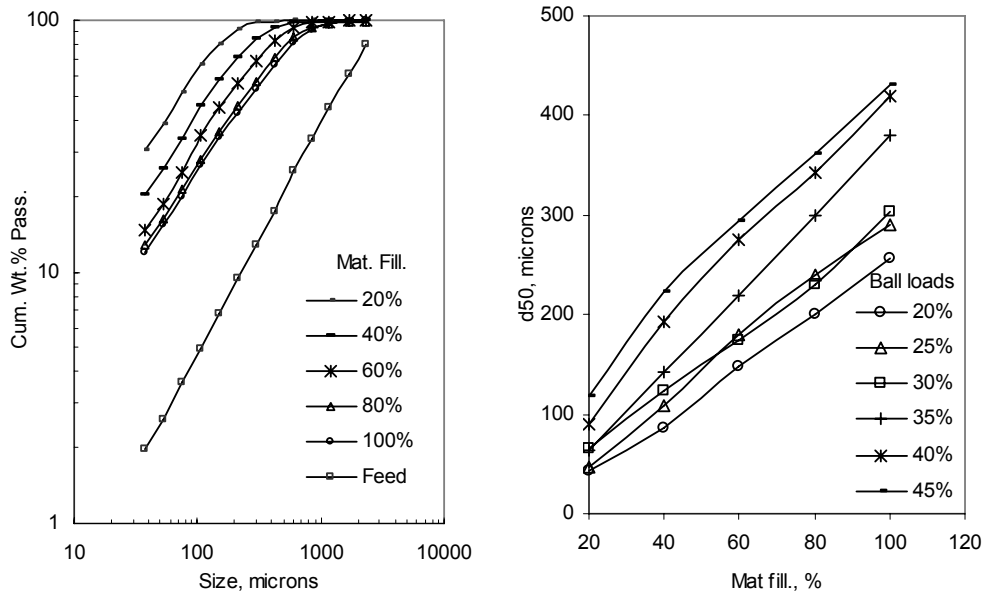
To further delineate the effects of material filling and ball loading, experiments were performed at various values of these two variables, and the results are shown in Figure 4.8. At low ball loadings (20% and 25%), the torque increases with increasing material filling. At 30% ball loading, the torque decreases after 80% material filling. At higher ball loadings, the torque decreases with increasing material filling, leading to unmatching results with the Morrell equation. The maximum torque and power draw is expected at  $0.5 \Phi_B$  but, at relatively higher  $\Phi_B$  values, the presence of feed manipulates ideal conditions causing the length of torque arm to decrease which results in lower torque values. The change in torque values is due to the change of mill charge and the change in the length of torque arm because of frictions between balls, mill shell and material so it is not related to the efficiency of grinding and fineness of material.



**Figure 4.8.** Effect of material filling ( $\Phi_M$ ) on the torque draw of Bond ball mill for different  $\Phi_B$  ( $n_c=0.75$ )

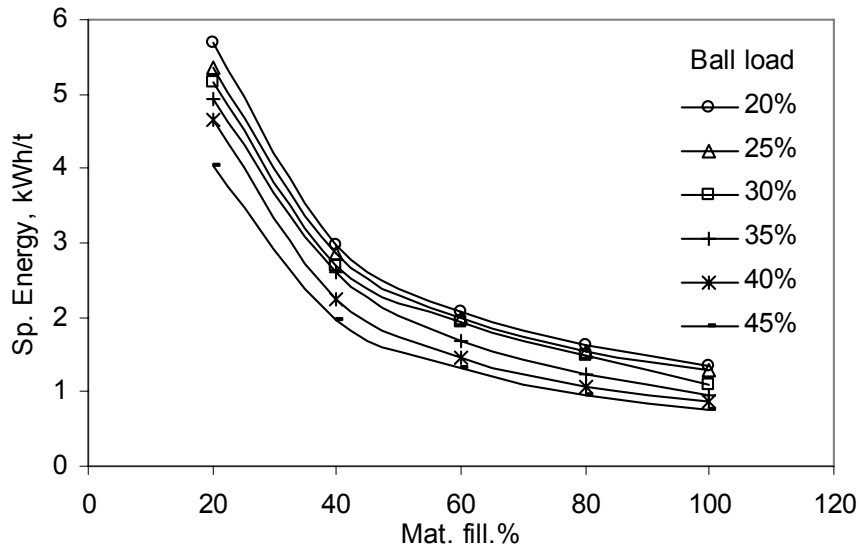
#### 4.4. Energy Efficiency in the Bond Ball Mill

Effect of material filling ( $\Phi_M$ ) on the grindability of material was investigated for different fractional ball loadings ( $\Phi_B$ ). Calcite was ground for 3 minutes under different operating conditions and a certain fractional critical speed ( $n_c$ ). For all  $\Phi_B$ , it is straightforward that increasing the material filling negatively affects the fineness of ground. One of the experimental results is shown in Figure 4.9-a. 50% passing size of the products ( $d_{50}$ ) was considered to be representative for the fineness of materials, and  $d_{50}$  vs.  $\Phi_M$  was plotted for different  $\Phi_B$  values (Figure 4.9-b). It is seen that the products become finer at low  $\Phi_M$  and  $\Phi_B$  values. It is a well known fact that the increase in fineness of material is due to the increase in number of impact per unit mass of material. The most energy efficient grinding conditions can be analyzed with the data of specific power consumption and fineness of material, which will be mentioned about hereafter.



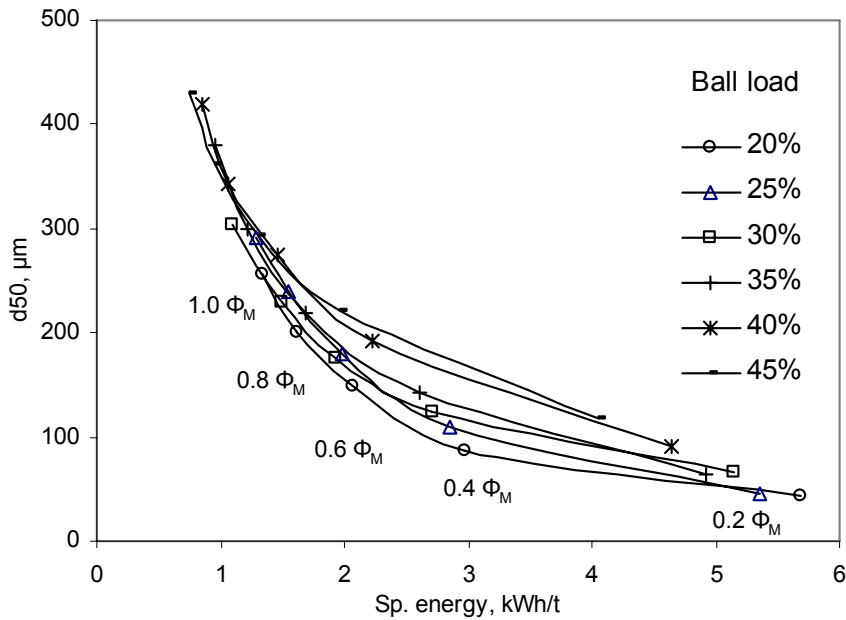
**Figure 4.9.** a) Effect of  $\Phi_M$  on the fineness of ground ( $n_c=0.75$ ,  $\Phi_B=0.25$ )  
 b) Fineness of ground as a function of  $\Phi_M$  at different  $\Phi_B$  ( $n_c=0.75$ )

Figure 4.10 shows the decrease in specific energy consumption with increasing  $\Phi_B$  and  $\Phi_M$ . This figure implies that the loss of energy is higher for low fractional charges. Moreover, 45-50% material filling is very crucial point for all fractional ball charges as the specific energy consumptions increase dramatically below that point.



**Figure 4.10.** Specific grinding energy of material as a function of  $\Phi_M$  at different  $\Phi_B$

Another graph obtained from the same experimental data is the expected result of increasing specific energy consumption with decreasing product size for all ball loading conditions (Figure 4.11). The  $d_{50}$  values decreases with increasing specific energy and  $\Phi_M$ . This graph also shows that below a certain  $d_{50}$  size, in this graph it is about 150  $\mu\text{m}$ , the specific energy consumption increases dramatically.



**Figure 4.11.** Specific grinding energy of material as a function of  $d_{50}$  at different  $\Phi_B$

Grinding operations can be considered effective if and only if the specific energy consumption is quite low, capacity is high and wear is reasonable (Austin et al., 1984). In this study, most energy efficient operating conditions were determined for the Bond ball mill without considering the wear and capacity. The power draws for all tested conditions were determined. Then, the specific energy consumptions were equalized at 5 kWh/t by adjusting the grinding time, and the finenesses ( $d_{50}$ ) of the products were evaluated as the representative values for the efficiency of grinding. Results are shown in Figure 4.12.

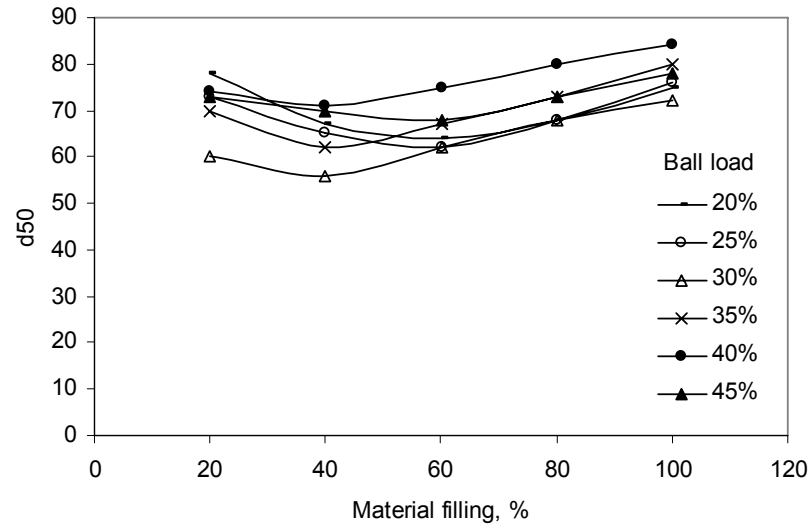


**Figure 4.12.** Variation of fineness (efficiency of grinding) of material with charge dynamics ( $n_c=0.75$ )

In industrial operations, it is common practice to operate the ball mills with 0.3-0.4  $\Phi_B$  and with a  $\Phi_M$  close to 1.0. Austin et al. (1981) concluded by the help of an empirical formula that the specific grinding energy is lowest at  $\Phi_M = 0.83$  and  $\Phi_B = 0.15$  for laboratory scale grinding mills. However, according to the experimental results shown in Figure 4.12,  $\Phi_M = 0.40$  and  $\Phi_B = 0.30$  are the optimum operating conditions for the Bond ball mill since finest  $d_{50}$  value was achieved for the same specific grinding energy at that conditions. It can be also stated that the efficiency of grinding is highest at  $\Phi_M = 0.4-0.6$  for all ball loading conditions. Moreover, the highest mill capacities were achieved at these conditions considering the grinding times and weight of material ground in the mill corresponding the 5 kWh/t specific energy consumption.

The effects of grinding media and material charge dynamics on torque and power draw of the Bond ball mill were investigated under dry grinding conditions. Results showed that grinding media consisting of smaller balls draw more power because of higher friction. Similarly, aged balls draw more power than new ones because of the same reason. Mill speed does not affect the torque up to the critical speed, while it directly affects the power draw. At material fillings above 0.4, the mill torque decreases with increasing material filling for the ball loads of 30% and higher (up to 45%). The mill constant K of Morrell's empirical power equation is 9.35 when no material is charged. However, the power equation is not valid for high material and ball charges. Fineness of the material affects the mill torque. At material fillings less than 0.4, the torque decreases with increasing grinding time (increasing fineness); but at higher material fillings, the torque decreases first and then increases again towards its steady value.



## CHAPTER 5

### A COMPARISON OF THE EXPERIMENTAL METHODS OF DETERMINING THE BREAKAGE DISTRIBUTION FUNCTIONS

Determination of the breakage rate function for the coarsest size fraction in the feed is quite straightforward while, except for back-calculation, mainly three different breakage distribution functions ( $B_{ij}$ ) estimation methods, namely, zero-order production of fines (Herbst and Fuerstenau, 1968), BII (Austin and Luckie, 1972), and G-H (Kapur, 1981), are available which are based on experimental studies for measuring the feed size distribution parameters from short-time grinding of one-size-fraction feeds (Sand and Subasinghe, 2004).

Formerly, many investigators stated that the breakage rate parameter of feed particles in a dry-batch mill remains unchanged over relatively long grinding times provided that the operating conditions are kept constant (Fuerstenau and Abouzeid, 1991). It means that breakage rate parameter is independent of both time and size consist of the material charge inside the mill. Recent studies indicated that the breakage rate parameters are considered size consist-dependent in that the values of breakage rate parameters depend upon the amount of fines produced in the mill and also upon the properties of the constituent minerals in mixture grinding (Venkataraman and Fuerstenau, 1984; Hoşten and Avşar, 2004). This is verified by Fuerstenau and Abouzeid (1991) with the investigation of effect of different amount of -100 mesh quartz and dolomite on the breakage rate of 10x14 mesh feeds. Rajamani and Guo's study (1992) also indicated the change in breakage rates in wet ball mills as the grinding environment is varied.

On the other hand, several investigators (Fuerstenau and Kapur, 2004; Shoji et al., 1982; Venkataraman and Fuerstenau, 1984; Fuerstenau and Abouzeid, 1991; Rajamani and Guo, 1992) stated that breakage distribution parameters of a mineral are independent of both time and milling environment. However, some scientists argue with this opinion by claiming that the breakage distribution functions of materials are related to particle size and material properties (Zhang and Kavetsky, 1993). It is intended that the use of different  $B_{ij}$  estimation methods maybe one of the reason for the debates on its relationship with size consist and milling environment.

The purpose of this study is to compare and evaluate these three methods with the help of an experimental study using quartz, and determining the most appropriate method that will be utilized for the study in Chapter 6. Short-time grinding experiments were carried out in a standard Bond ball mill with three narrowly sized (one-size-fraction) quartz samples and two different ball charges. The experimental data was then used for the determination of  $B_{ij}$  values to find out if aforementioned methods yield any significant differences. Also, by evaluating these methods, it was intended to clarify whether the breakage distribution function depends on the milling environment and particle size by using three different one-size-fraction quartz feeds and two different types of ball charges. The breakage rate parameters for the tested materials were also evaluated.

#### 5.1. Experimental $B_{ij}$ Estimation Methods

In the literature, there are many experimental  $B_{ij}$  estimation methods which are based on size-discretized batch grinding equation (Sand and Subasinghe, 2004) as mentioned before. In this study,

three main ones, namely, Zero-order production of fines (Herbst and Fuerstenau, 1968), BII (Austin and Luckie, 1972), and G-H (Kapur, 1981) were evaluated.

Herbst and Fuerstenau (1968) showed that, for a size which is small compared to feed size, the production rate of less-than-size material is approximately constant for a protracted grinding time. They described it as the zero-order production of fines and utilized this condition to determine the breakage parameters.

$$\frac{dM_i(t)}{dt} = F_i(\text{constant}) = \sum_{j=1}^n \frac{dm_j(t)}{dt} \quad (5.1)$$

where  $M_i$  is the cumulative fraction of undersize.

$$F_i = \sum_{r=1}^n \sum_{j=1}^{i-1} b_{rj} K_j m_j(t) = \sum_{j=1}^{i-1} B_{ij} K_j m_j(t) \quad (5.2)$$

$$\text{since } B_{ij} = \sum_{r=1}^n b_{rj}$$

$$B_{ij} K_j \cong F_i \text{ (compensation condition)} \quad (5.3)$$

for fine sizes and short grinding times,

$$\sum_{j=1}^{i-1} m_j(t) \cong 1 \quad (5.4)$$

If the feed is one-size-fraction,  $j=1$

$$B_{i1} = \frac{F_i}{K_1} \quad 1 < i \leq n \quad (5.5)$$

Austin and Luckie (1972) described three  $B_{ij}$  estimation methods with varying degrees of accuracy. BII is the one based on the solution of batch grinding equation given by the compensation condition and is claimed to be correct for the secondary breakage. For the top size, at approximate compensation conditions,

$$1 - P_i(t) \cong [1 - P_i(0)] \exp(-B_{i,1} K_1 t) \quad i > 1 \quad (5.6)$$

where  $P_i$  is the mass fraction of material in a certain size. For the top size interval, first-order breakage gives

$$1 - P_2(t) = [1 - P_2(0)] \exp(-K_1 t) \quad (5.7)$$

since  $B_{21} = 1$ , then,

$$-K_1 t = \ln[(1 - P_2(t))/(1 - P_2(0))] \quad (5.8)$$

$$-B_{i,1} K_1 t \approx \ln[(1 - P_i(t))/(1 - P_i(0))] \quad (5.9)$$

and

$$B_{i,1} \cong \frac{\log[(1 - P_i(0))/(1 - P_i(t))]}{\log[(1 - P_2(0))/(1 - P_2(t))]}, \quad i > 1 \quad (5.10)$$

Kapur (1982) developed an alternative procedure which is based on an expanded version of the first order relationship. This method is an improvement of zero order production of fines and the BII method.

$$\ln \frac{R_i(t)}{R_i(0)} = G_i t + \frac{H_i t^2}{2!} + \frac{I_i t^3}{3!} + \dots \quad (5.11)$$

where  $R_i$  is the cumulative fraction retained on the lower screen of the  $i$ th size-interval and  $G, H, I, \dots$  are coefficients of the expanding series. For short grinding times, higher order terms of eq. 5.11 can be neglected:

$$\ln \frac{R_i(t)}{R_i(0)} = G_i t + \frac{H_i t^2}{2!}, \quad i = 1, 2, 3, \dots \quad (5.12)$$

Kapur showed that the coefficients are related to the  $K_1$  and  $B_{i,1}$ ,

$$G_i = -K_1 B_{i,1} \quad (5.13)$$

if we combine the eq. 2.22 and eq. 5.13, for the top size fraction,

$$\frac{\ln R_i(t)}{\ln R_i(0)} = B_{i,1} - \frac{H_i}{2K_1} t \quad (5.14)$$

Breakage distribution function can be estimated as the intercepts of a straight line relationship between the left-hand sides of eq. 5.14 vs. time.

## 5.2. Experimental Study

The quartz sample supplied from Aydın-Çine district in Turkey was used as feed material. Three one-size-fraction samples (-3.35+2.36 mm, -1.18+0.850 mm, -0.300+0.212 mm) with nearly 1050 g weight that corresponds to the 700 ml or 0.35  $\Phi_M$  (proportion of material bulk volume, which includes the voids between the particles, to the void volume between the ball charge) were prepared by dry laboratory screening.

Two types of ball charges were used in short grinding experiments one of which is composed of 1 inch one-size-fraction steel balls and the other is standard Bond ball charge which both corresponds to nearly 22,650 g or 0.22-0.23  $\Phi_B$  (proportion of ball bulk volume, which includes the voids between the balls, to the mill inside volume).

Experiments were carried out under dry grinding conditions in standard Bond ball mill (305x305 mm) with smooth inside surface at 70 rpm (nearly 85% of critical speed). After short-time (15, 30, 45, 60, 90, 120, 150 sec) grinding experiments, ground material were analyzed by wet and dry screening procedure.

Figure 5.1 shows the dependence of breakage rate parameters on particle size as it had already been stated in several investigations (Austin et al., 1982; Fuerstenau and Kapur, 2004). In general, disappearances of the one-size-fraction quartz feeds follow the first-order grinding kinetics for all the size and grinding media conditions. However, the disappearance of coarsest size (-3.35+2.36 mm) shows non-linearity at the initial stage where abnormal breakage occurs due to insufficient breakage action, so the weaker particles are easily broken while the stronger ones resist as Austin et al. (1984) mentioned. The relatively smaller sizes show linear disappearance proving that the breakage rates are independent of time. Efficiency of grinding media varies at different feed sizes.

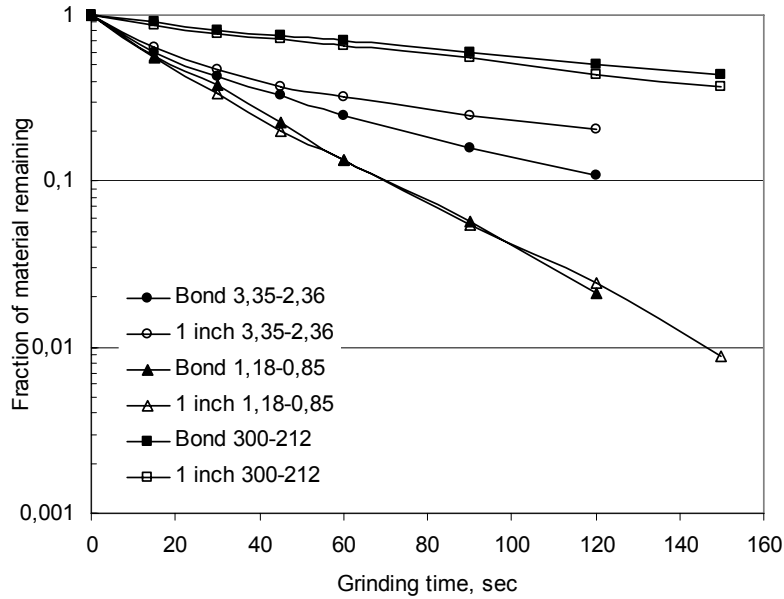
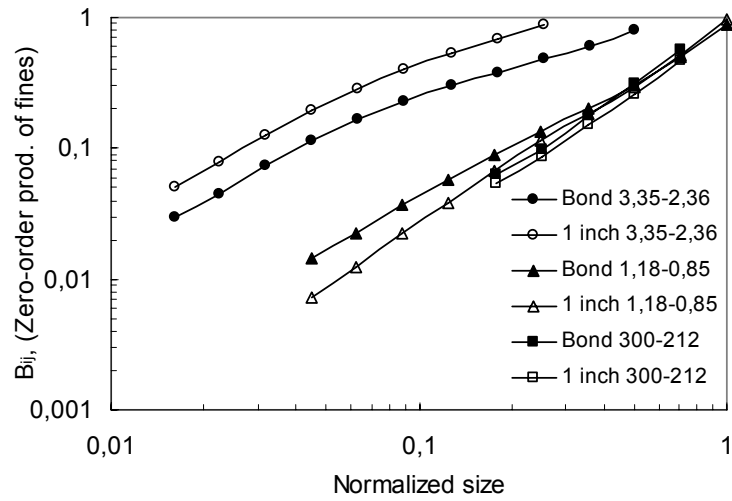


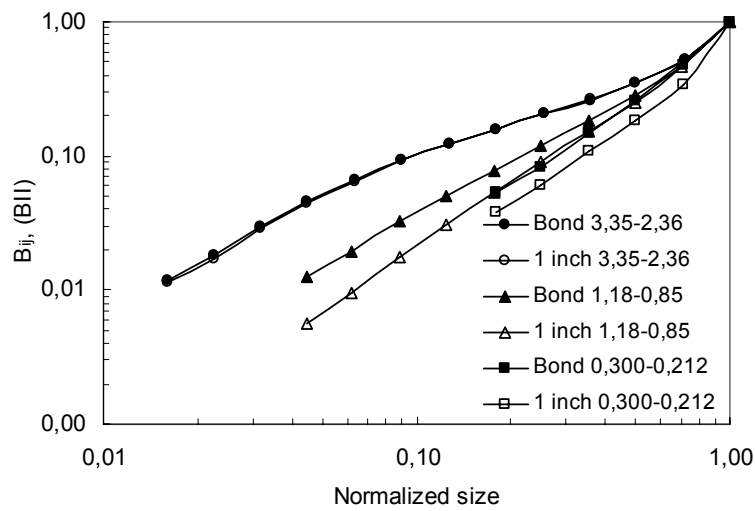
**Figure 5.1.** The disappearance of one-size-fraction quartz feeds ground with 1 inch and Bond ball charges

The cumulative breakage distribution function data of the three samples were plotted against normalized size according to zero-order production of fines, BII and G-H methods in order to compare these three methods and also evaluate the effect of particle size on  $B_{ij}$ . As it is seen from the Figure 5.2 (a), (b) and (c),  $B_{ij}$  values are not normalizable; that is, the breakage distribution functions of feed material changes with the size of feed. In addition, size distribution of grinding media seems to be effective on the  $B_{ij}$  values except for the coarsest size fraction (-3.35+2.36 mm) plotted by BII and G-H methods. Zero-order method of Herbst and Fuerstenau (1968) gives improper results for this size fraction. The reason is that the evaluation of  $B_{ij}$  from short-time grinding data needs breakage rate function to be determined. However, since abnormal breakage occurs at this size fraction (see Figure 5.1), there are actually two different breakage rate, initial one is fast and the latter is relatively slow. The breakage rate function that were used in the evaluation of  $B_{ij}$  at -3.35+2.36 size fraction is the latter one which does not actually belong to initial grinding time which the method utilizes.

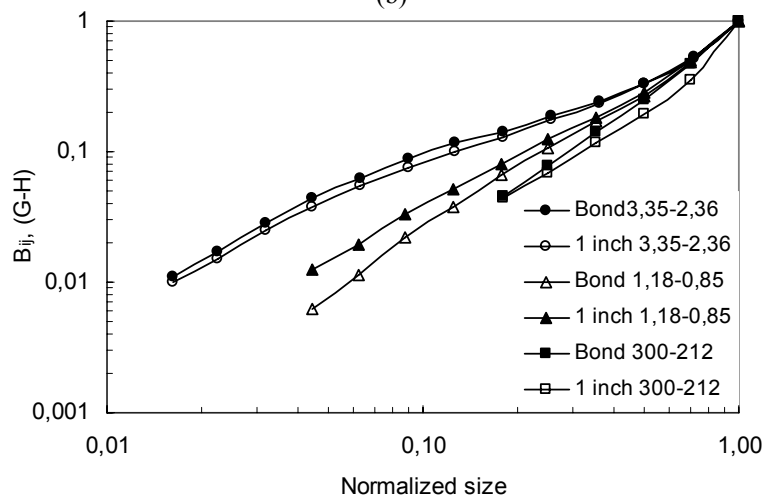
The breakage distribution function of three different feed sizes that were ground with Bond ball charge were plotted by the use of three  $B_{ij}$  estimation methods in Figure 5.3 in order to illustrate if these methods yield any significant differences.



(a)

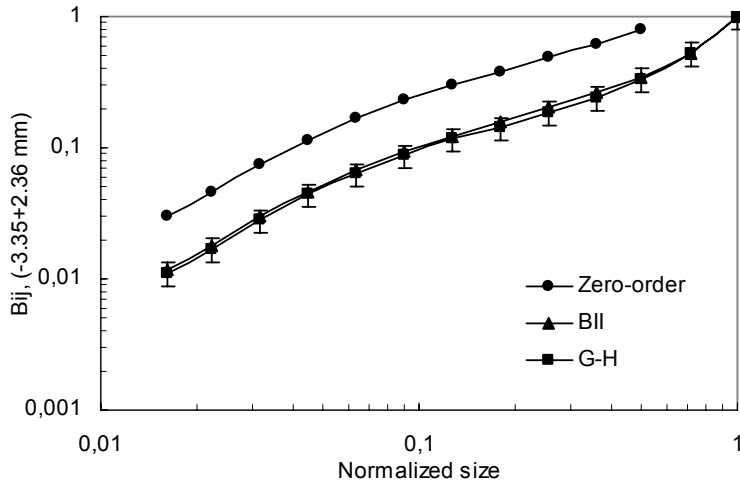


(b)

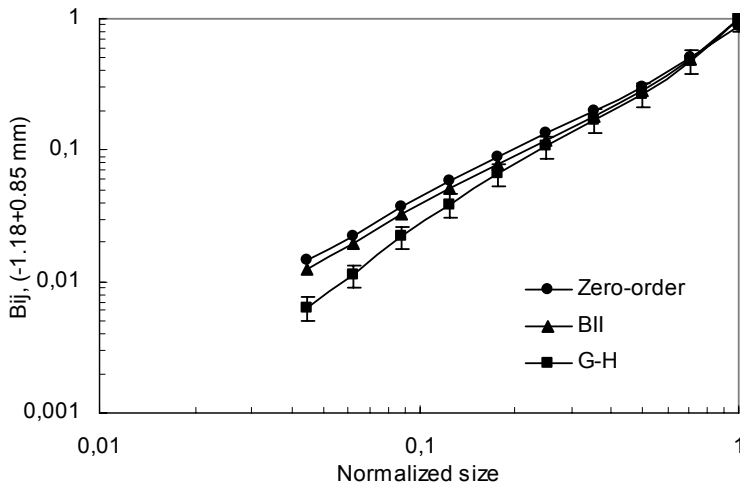


(c)

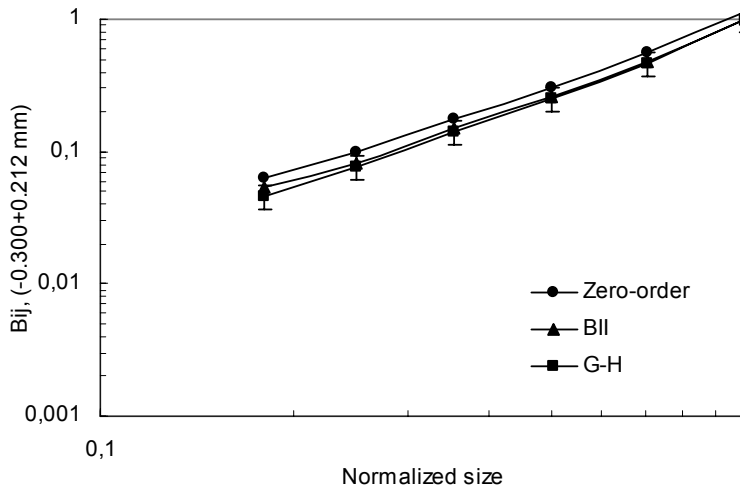
**Figure 5.2.** Cumulative breakage distribution functions of one-size-fraction quartz feeds plotted by (a) Zero-order, (b) BII and (c) G-H methods



(a)



(b)



(c)

**Figure 5.3.** Comparison of  $B_{ij}$  values plotted by three different estimation methods on different size of feeds (a)  $-3.35+2.36$  mm, (b)  $-1.18+0.85$  mm, (c)  $-0.300+0.212$  mm, ground with Bond ball charge

The three  $B_{ij}$  estimation methods, except for the coarsest size fraction where zero-order method fails to give reasonable values, follow the same trend although they show slight deviations. The results of G-H and BII methods almost coincide with each other at the coarsest and finest feed sizes within  $\pm 10\%$  significance level. However, deviations occur at the lower size fractions for G-H method at  $-1.18+0.85$  mm feed size. It can be concluded that the methods show dissimilarities at different feed sizes which may lead to disagreements on the evaluation of grinding behavior of the feed material.

### 5.3. Concluding Remarks

Three breakage distribution functions estimation methods, zero-order production of fines, BII and G-H, were compared and evaluated by plotting the  $B_{ij}$ 's of three one-size-fraction quartz feeds ground with both 1 inch and Bond ball charges. Time and breakage rate function restricted Zero-order production of fines gives close values to others at fine feed size fractions. However, this method fails at coarse sizes where abnormal breakage occurs. Moreover, it is difficult to determine the  $F_i$  values of zero-order method since the time that should be used in calculations is not exact for all the particle sizes. BII and G-H methods showed very close results to each other at the coarsest and finest feed sizes although BII method is considered to be time restricted special case of G-H method (Kapur, 1982). The  $B_{ij}$  estimation methods show dissimilarities in behavior at different feed sizes. This occurrence may be one of the reasons for the disagreements in the literature on the grinding kinetics of the feed material. On the other hand, all the  $B_{ij}$  estimation methods pointed out that  $B_{ij}$  of feed material depends on particle size and grinding media charge.

G-H method was proved to give reasonable estimations in any tested conditions. It provides quite similar results with the BII method. Unlikely, G-H method is not time restricted so it was stated to be the improved version of other methods. Therefore, G-H method was decided to utilize for the determination of breakage parameters in Chapter-6 as it provides more reliable data for wide range of operating conditions.



## CHAPTER 6

### PARTICLE BREAKAGE PARAMETERS IN LOCKED-CYCLE BALL MILLING

Determination of breakage parameters under the conditions which closely resemble the industrial milling operations helps understanding and modeling the grinding kinetics. There are many investigations in the literature on determination of breakage parameters and their dependence on grinding environment (Shoji et al., 1982; Austin et al., 1982; Fuerstenau and Abouzeid, 1991; Rajamani and Guo, 1992; Verma and Rajamani, 1992; Fuerstenau et al., 2010). However, representativeness of these studies is questionable since the conditions in industrial mills were not fully satisfied.

In this study, the variation of breakage parameters with milling environment has been investigated with steady state grinding environment in Bond ball mill with the intention of obtaining more representative results by combining the traditional Bond method with the simulation approach using population balance models. In order to carry out mathematical analysis of the grinding kinetics of materials, size-discretized/time-continuous population balance model (eq. 2.21) (Fuerstenau and Abouzeid, 1991) and linearized form of batch grinding equation (eq. 2.25) have been used. Kapur's G-H method which is an approximate solution for the graphical determination of  $B_{ij}$  has been utilized. The derivation of this method was given in Chapter 5. Assuming first order kinetics, the breakage rates of the top size fractions were obtained by evaluating the slope of semi-log plots of the fraction retained versus time which generally shows straight line (eq. 2.22) (Sand and Subasinghe, 2004). The breakage rates for the lower sizes were determined by using eq. 2.23.

#### 6.1. The Effect of Material Size Distribution on the Breakage Parameters of Coarse Particles

Fuerstenau and Abouzeid (1991), Fuerstenau et al. (2010), Fuerstenau et al. (2011) studied the materials having artificially generated size distributions in order to determine the effects of fines on the breakage rate. However, there is evidence in the recent literature that the size distribution of the mill contents affects these parameters (Zhang and Kavetsky, 1993; Rajamani and Guo, 1992; Hoşten and Avşar, 2004). Gupta noted that the size distributions generated by grinding one-size-fraction feeds are not representative of those obtained under industrial milling conditions, and the size distribution range considered in numerous investigations corresponds to very small volume of the wide size distribution normally dealt within an industrial grinding operation. He also reported that the top size fraction in a natural size-distribution environment is ground at rates different from those observed for a one-size-fraction feed charge (cited in Fuerstenau and Abouzeid, 1991).

The objective of this investigation is to determine the effect of fines on the breakage kinetics in a steady state milling environment which closely resembles the industrial milling operations. In industrial ball milling operations, material is generally fed to the mill after consecutive crushing stages. Therefore, mill feed attains a characteristic size distribution. Ball mills are generally closed by a classifier in which fines are separated and coarse ones are sent back to the mill, which is called circulating load. Then, the circulating load is mixed with the fresh feed for regrinding. After a certain time of operation, the percent of circulating load to the feed becomes constant. That is called 'steady-state condition' at which the amount of product is equal to the amount of fresh feed. After achieving this condition, assuming it to be perfectly mixed, the size distribution of mill content does not change significantly. On the other hand, according to the multi-compartment (n-mixers in series) approach,

the material characteristics show dissimilarities in each compartment but they do not alter significantly within each compartment at steady state operating conditions.

In order to simulate industrial grinding environment, Bond grindability tests were applied to -6 mesh (-3.35  $\mu\text{m}$ ) quartz and calcite by using 75, 106, 150, 212, 300  $\mu\text{m}$  closing screens. Steady state mill hold-up materials were obtained in each Bond Grindability Test. The obtained size distributions were modified because of the fine removal and fresh feed addition. The size distribution near the feed inlet and near the discharge end of the industrial mill may differ from each other in that the former one is relatively coarser because of the addition of fresh feed. Figure 6.1 shows the size distribution of the steady state mill hold-up before screening for different closing screens. After achieving steady state conditions, product was scalped by a screen and the size distributions in Figure 6.2 were achieved. After the addition of fresh feed to the materials in Figure 6.2, the combined feeds that were used for kinetic tests were obtained (Figure 6.3). The material flow through the mill is usually described by an *n*-mixers-in series model, dispersion model or a single perfect mixer model depending on the operating conditions of the mill (Lynch, 1977). According to the *n*-mixers-in series model Figure 6.1 and Figure 6.3 can be considered as the material size distributions near the discharge end of the mill and near the feed inlet, respectively. The size distributions in Figure 6.2 represent the circulating loads. In this study, the mill content material with which the kinetic grinding tests were carried out was perfectly mixed since the tests were performed in a batch ball mill.

By the use of different size of test sieves, different size distributions were obtained for quartz and calcite materials which had certain coarse/fine ratios. The materials with the size distributions shown in Figure 6.3 were exposed to short-time grinding tests for the determination of grinding kinetics of the coarsest fraction 6x8 mesh (-3.35+2.36 mm). It was intended that, considering the industrial ball milling operations, the investigation of effects of size distribution of the mill hold-up on the grinding kinetics of coarse particles by using these kinds of naturally occurred size distributions would result in more realistic parameter estimations. The changes in size distribution of combined feeds during the short-time grinding tests are shown in Figure 6.4.

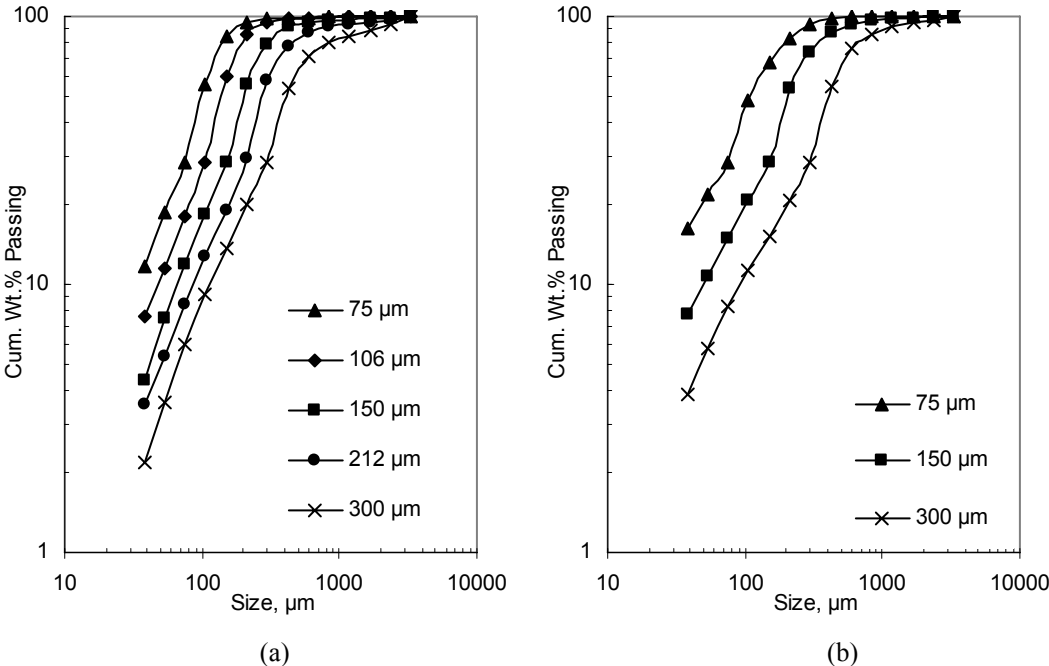


**Figure 6.1.** Cumulative size distribution of steady state mill hold-up of quartz (a) and calcite (b) before screening with different closing screens

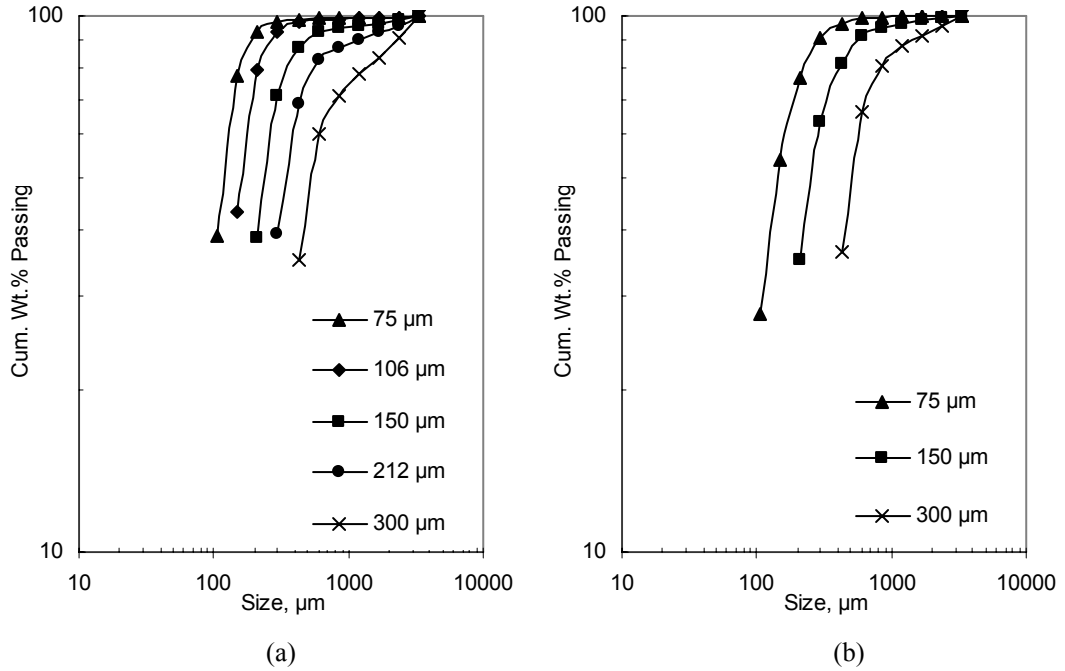


**Figure 6.2.** Cumulative size distribution of steady state mill hold-up of quartz (a) and calcite (b) after screening with different closing screens

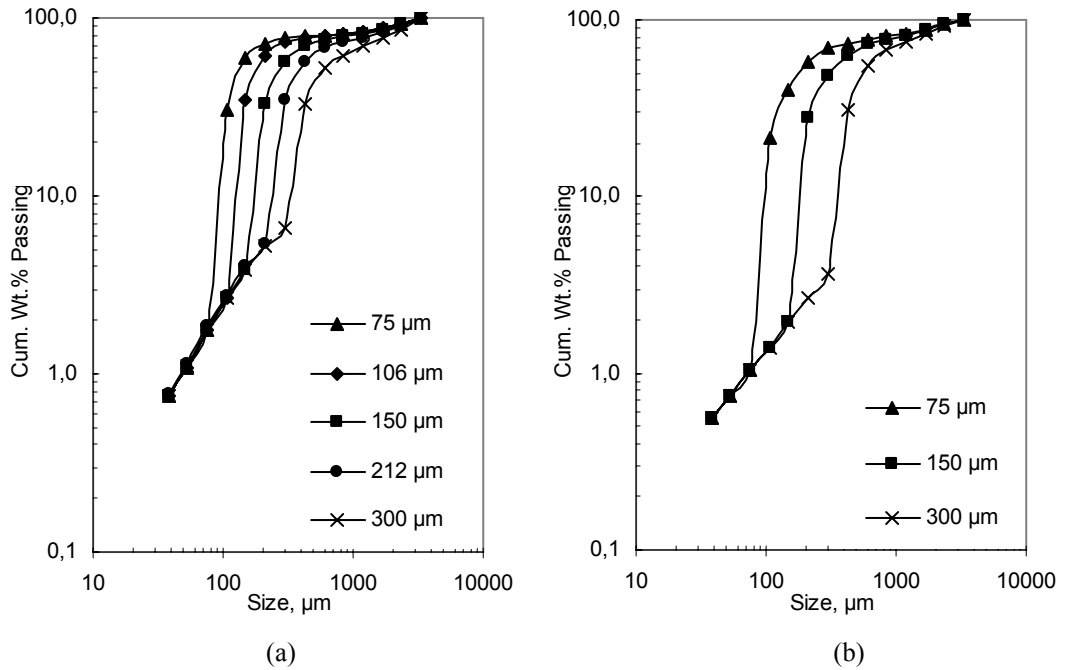


**Figure 6.3.** Cumulative size distributions of combined feeds quartz (a) and calcite (b) after screening of mill contents and addition of fresh feeds

In order to get rid of the sharp and random fluctuations, the experimental cumulative size distribution data were smoothed by using MATLAB-Curve Fitting Toolbox, ‘moving average method’ ( $yy=smooth(y,moving)$ ).

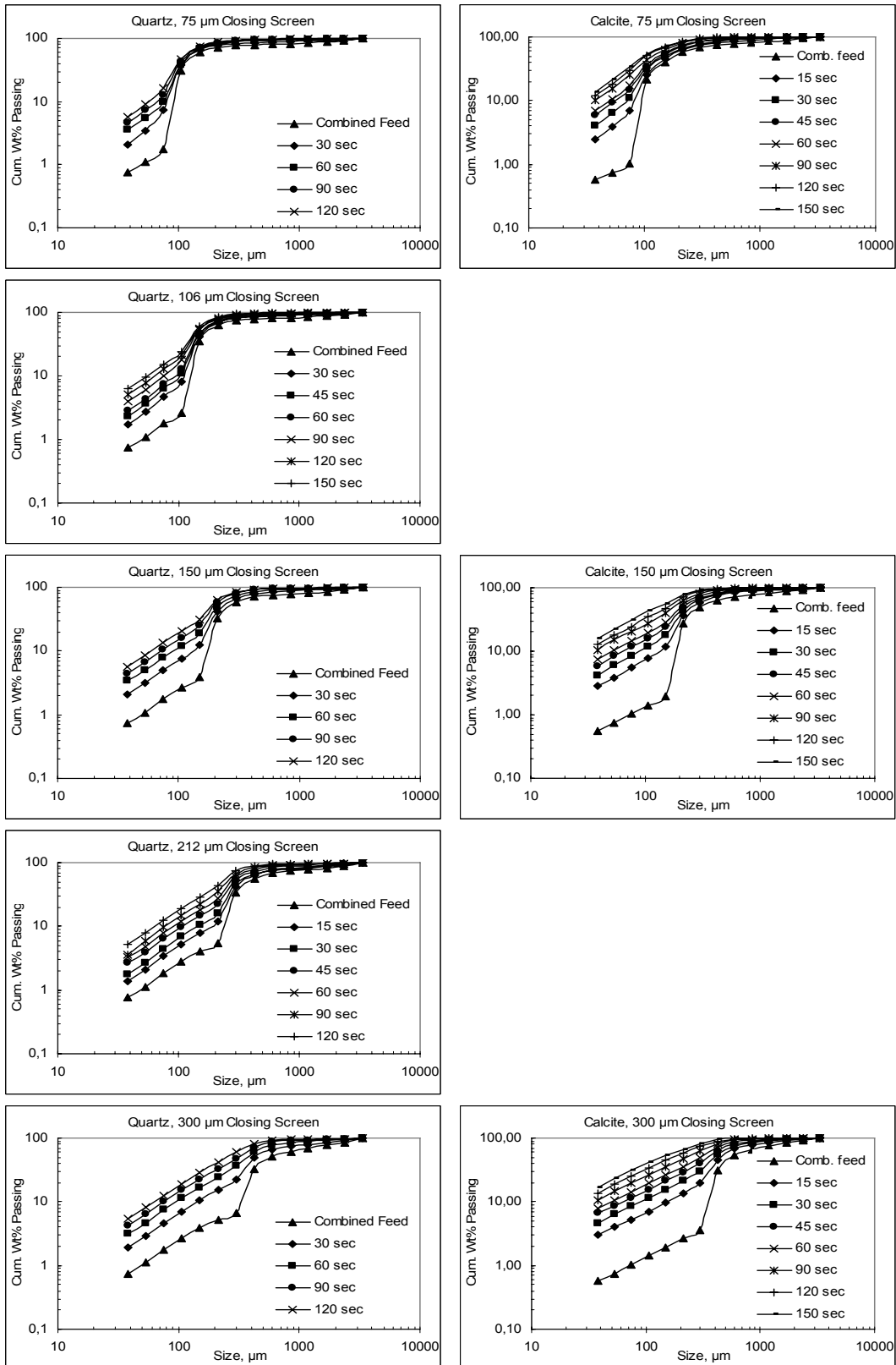


**Figure 6.4.** The change in size distribution of steady state mill feeds quartz (left) and calcite (right) during short-time grinding tests

In Figure 6.4, the general behavior of the curves is that the amount of material just above the closing screen size is relatively higher at the beginning. Then, it gradually decreases by grinding, and a naturally broken material size distribution is achieved. Figure 6.5 and Figure 6.6 generated by eq. 2.22 show the rate of disappearance of 6x8 mesh quartz and calcite in different size distributions given in Figure 6.4, as a function of time. 6x8 mesh material is the coarsest fraction in the fresh feed and has the highest proportion with 24.39% for quartz, and 19.15% for calcite. In the feeds to the mill, the proportion of 6x8 mesh fraction changes between 7.35–13.65% for quartz and between 5.56-8.46% for calcite. This variation in the proportion of the 6x8 mesh material had negligible effect on the breakage rates.

Typical experimental results of short-time grinding tests are presented in Figures 6.5 and 6.6. For different grinding environments generated by several test sieves, the fraction of top size material (6x8 mesh) remaining in the original size range by grinding time could be well described by first-order grinding kinetics. For both materials tested, the rate of grinding of coarsest fraction increases as the closing screen aperture becomes smaller, and, accordingly, the proportion of fine fraction in the mill increases. This result complies with the previous studies carried out by Fuerstenau and Abouzeid (1991), Fuerstenau et al. (2010), Fuerstenau et al. (2011) who stated that the presence of fines enhances the breakage of coarse particles.

Figure 6.7 shows the change of the breakage rate of 6x8 mesh materials with respect to the closing screen aperture. There is a sharp increase in breakage rate below 150  $\mu\text{m}$  closing screen. The change in breakage rate decreases beyond that point. Fuerstenau and Abouzeid (1991) concluded that the breakage rate of coarse fraction decreases more than 50% when the proportion of that size of particles increases from 15% to 100%. This result had been observed by the use of artificially blended mixture of fine and coarse particles. However, by using naturally generated mill hold-up compositions, it can be seen in Figure 6.7 that the decrease in breakage rates is not as dramatic as their study since all the feed compositions include certain amount of fine particles unless narrow size feed is used.

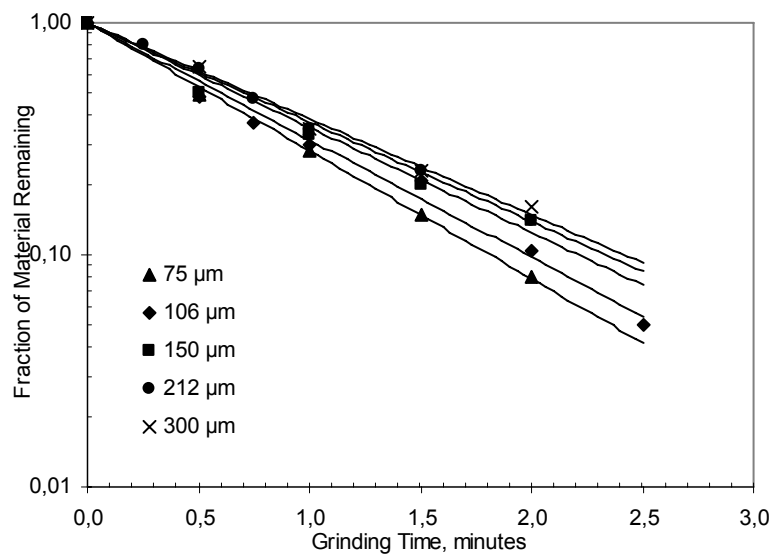


**Figure 6.5.** The disappearance of coarsest fraction (6x8 mesh) of quartz feed at steady state generated by different closing screens

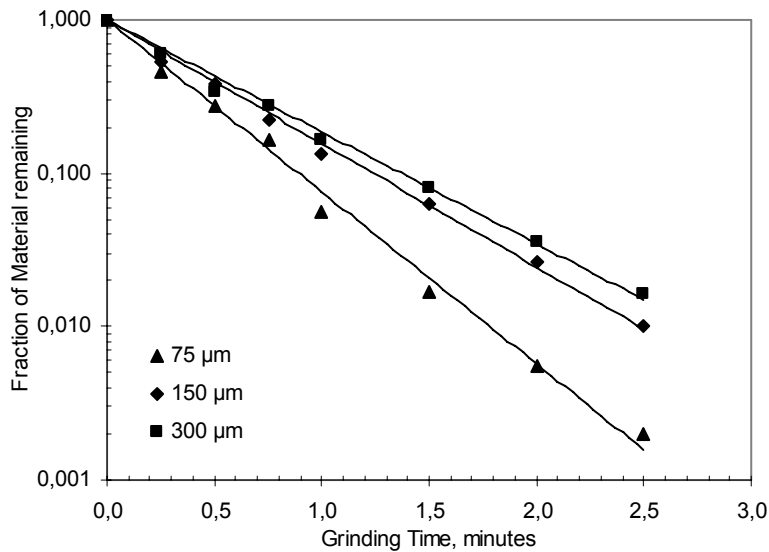


**Figure 6.6.** The disappearance of coarsest fraction (6x8 mesh) of calcite feed at steady state generated by different closing screens

By the use of different size of closing screens from 75 µm to 300 µm, the increase in breakage rate due to the increase of fine particle proportion reached to 35% for both quartz and calcite material. The most of that increase occurred between 75-150 µm closing screen apertures.

Fuerstenau and Abouzeid (1991), Fuerstenau et al. (2010), Fuerstenau et al. (2011) stated that fine particles have little resistance to the falling balls at the grinding zone. Then, the energy associated with the falling ball is mostly consumed in the breakage of coarse particle. They also concluded by using energy split factor that the specific energy consumed by the coarse particle increases as the initial fraction of coarse material in the feed decreases. This is the main reason for the increase in rate of breakage with decreasing amount of coarse material in the feed.

The fine particles cannot resist to the falling balls since they escape from pressure zone like a fluid. Quartz and calcite fines surrounding the coarse particles may show different kind of resistances to the falling ball because of the differences in their hygroscopic properties. Unlike quartz, calcite is a hygroscopic mineral which means that its fines easily adsorb moisture in the air so they form larger lumps or coat any surface such as ball, mill shell, and coarse particles. This property of calcite may prevent fines from escaping so they share the impact energy of the falling balls. Still, the change in breakage rates for both mineral show similar trends meaning that the effect of hygroscopic property of calcite is not significant.

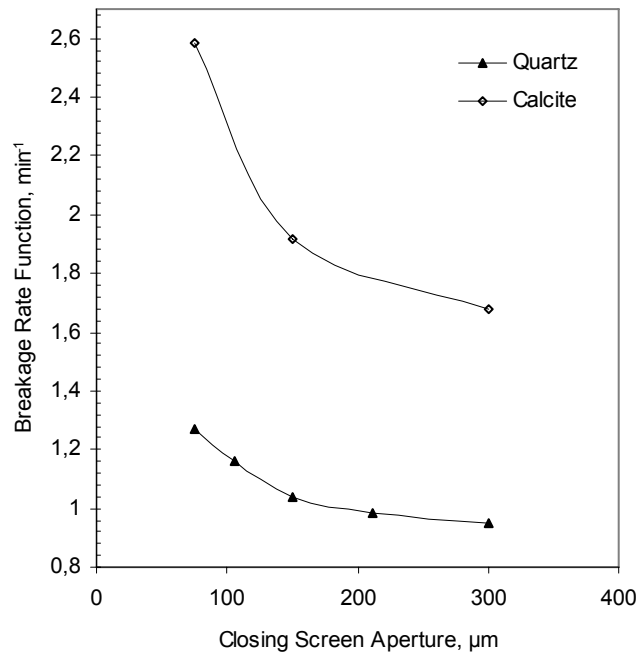


**Figure 6.7.** The change of the breakage rate of coarsest fraction (6x8 mesh) of quartz and calcite feeds at steady state generated by different closing screens

The observations on the effect of grinding environment on breakage rates of particles are supported by Figure 6.8 which compares the disappearance of 6x8 mesh quartz ground as one-size-fraction feed, and ground in a steady state mill content generated by 75  $\mu\text{m}$  test sieve. It is identified that the disappearance of 6x8 mesh material deviates from the linearity when it is ground alone. This result had been observed by other investigators (Austin et al., 1982; Tavares and Carvalho, 2009). They concluded that it was encountered for sizes above those corresponding to the maximum breakage rate. This was named as ‘abnormal breakage region’ by Austin (1982). Austin and Bagga (1981) and Austin et al. (1981) stated that this can be due to a general slowing down of all grinding rates as fines accumulate in the charge for dry grinding. However, this was disproved by Figure 6.5 and Figure 6.6 as fines enhance grinding of coarse particles. Austin et al. (1982) explained this phenomena as the coarse particles are too large to be properly nipped by grinding media. In this case, the material behaves as if some particles are stronger than the others. Actually, during the very first stage of tumbling, coarse particles are rather fresh and comprise more flaws. As they are tumbled, weaker particles having more flaws and the corners of irregularly shaped particles are broken faster even if they are not properly nipped by grinding. As the tumbling proceeds, the remaining particles, especially the ones with lower flaws are rounded so they are broken relatively slower because of insufficient impact energy of grinding balls. It is anticipated that the use of larger balls in a mill with larger diameter would increase impact energy to a sufficient level for the first order breakage of coarse particles. Another statement presented in Figure 6.8. is that, after the initial stage, the disappearance of 6x8 mesh quartz feed is faster within the presence of fines, which is consistent with the previous observations.

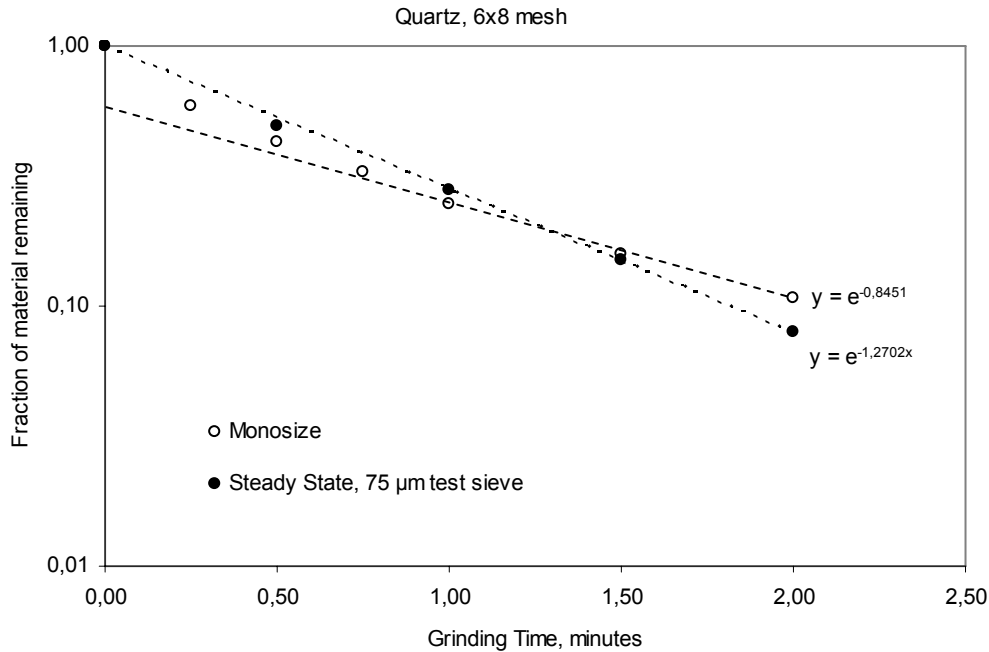


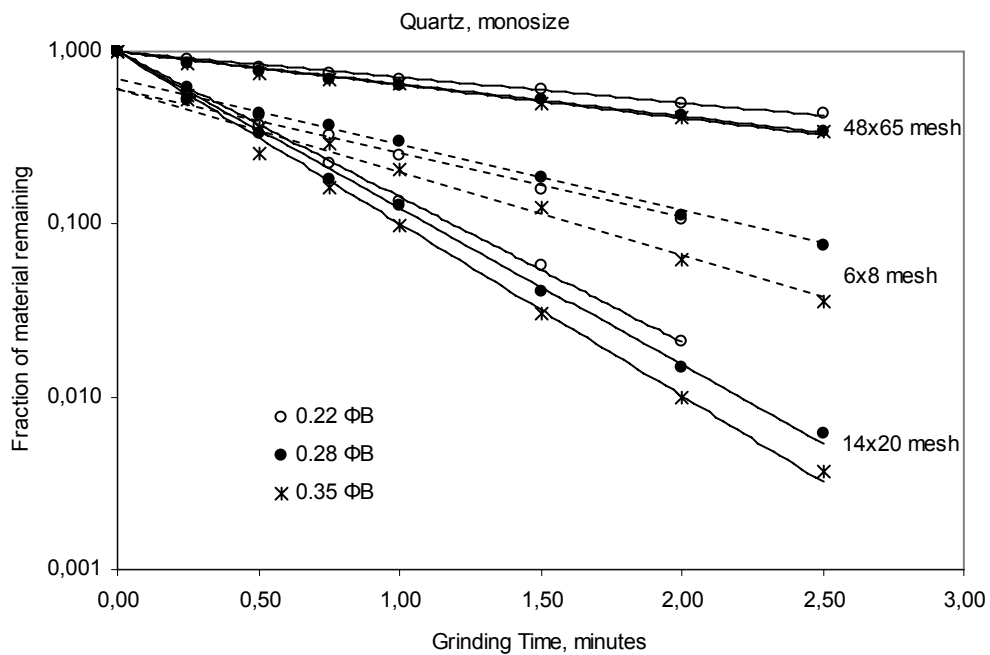
**Figure 6.8.** The disappearance of 6x8 mesh quartz as one-size-fraction feed and steady state mill content generated by 75 μm test sieve

For feeds having a distribution of particle sizes, breakage rate and distribution functions can be obtained experimentally by monitoring the breakage of individual fractions with radioactive tracers. However, the test setup required is so extensive that such models cannot be used in many laboratories despite the advantages they offer (Herbst and Fuerstenau, 1968). Another method for such feeds is replacing lower fractions with a secondary mineral like calcite ( $\text{CaCO}_3$ ), which dissolves in acidic solution. The procedure for such a test is rather difficult. Moreover, the contribution of secondary mineral with different mechanical characteristics into the breakage zone as surrounding environment may affect the breakage parameters of primary mineral. In light of the foregoing, in this study, the breakage distribution functions of materials were determined using one-size-fraction feeds assuming them to be independent of grinding environment. Then, the reliability of this assumption was checked in Section 6.2.4 by comparing the attained product size distributions.

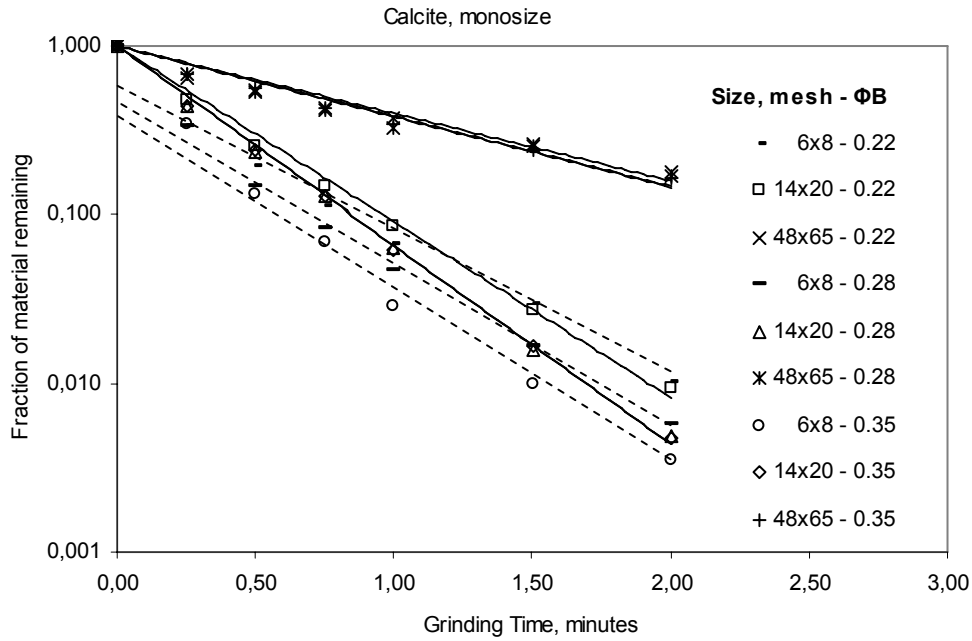
### 6.2.1. The effect of Fractional Ball Charges on the Particle Breakage Parameters

Austin et al. (1984) studied the effect of operating variables on breakage parameters and provided empirical equations related to them, which were mentioned in Chapter 2. However, the operating variables of batch ball mills are not independent so changing one of them would manipulate one another making it difficult to evaluate their effects independently. In order to evaluate the specific energy relationship of  $K_i$  and  $B_{ij}$  in grinding mill, tests should be carried out at different specific grinding energy values keeping all the conditions, such as number of impact per unit weight of material, type of media motion and ball size distribution, same. For example, modifying the mill speed would change the specific grinding energy but the cascading or cataracting motion of charge would also change. Similarly, change in  $\Phi_M$  or  $\Phi_B$  would change the number of impact per unit weight of material. Therefore, it was intended that using different values of  $\Phi_B$  at constant  $\Phi_M$  would change specific grinding energy without affecting any other variables significantly which could make it possible to evaluate the specific energy relationship of breakage parameters under milling environment.

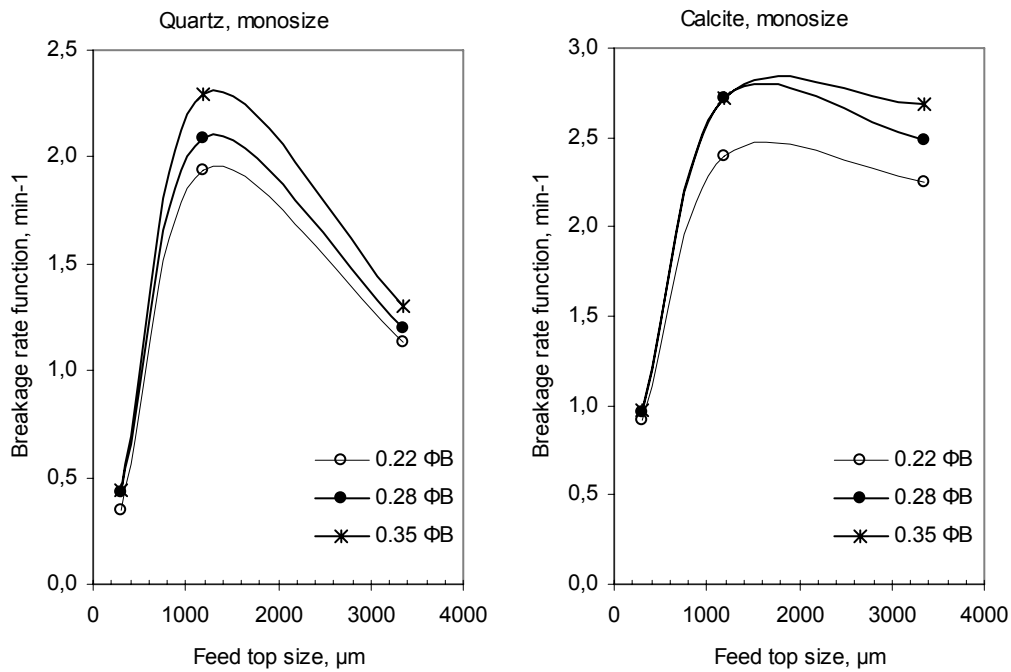
The one-size-fraction grinding tests were carried out using three different fractional ball charges  $\Phi_B$ , 0.22, 0.28, 0.35. The quartz and calcite feeds were prepared as three different narrow-sizes, 6x8 mesh, 14x20 mesh, and 48x65 mesh, which can be considered as coarse, medium and fine feeds, respectively. The  $\Phi_B$  value for tests was limited by 0.35 since the grinding regime changes significantly above that point for laboratory scale Bond Ball Mill as observed in power measurements via torque transducer. The disappearance rates of the one-size-fraction feeds were plotted in Figure 6.9 and Figure 6.10. For both minerals, the fastest disappearance rates belong to the medium size feeds (14x20 mesh) for all tested  $\Phi_B$  values. As it was expected by the nature of size reduction-energy relationship, fine materials (48x65 mesh) have the lowest disappearance rates. For the coarse material (6x8 mesh), which is the top size fraction of Bond Ball Mill Grindability Test, the disappearance rates deviate from linearity according to the first order grinding kinetics. The reason was already explained in the previous part (6.1) as ‘abnormal breakage region’. According to the theory, there may be two different disappearance rates (initial fast rate and slow rate) for the coarse materials because of insufficient impact energy of grinding media, and cracks existing in coarse particles. In general, the initial fast disappearance rates last less than half a minute. Therefore, the contiguous slow rates should be considered to be the actual disappearance rates of coarse materials, which are presented with dashed lines. Then, it can be stated that the disappearance rate of the coarsest fraction is less than the medium size feed. This means that the 6x8 mesh particles are not broken efficiently because of insufficient impact energy in the Bond Ball Mill. As presented in Figure 6.11, the decrease in the rate of breakage of 6x8 mesh calcite particles is not as dramatic as it is for the same size of quartz particles since calcite is relatively easier to break although the impact energy is not sufficient. According to Figure 6.11, generally the disappearance rates are increasing with increasing ball charge up to 0.35  $\Phi_B$  although the specific grinding energy is reduced (see Figure 4.10). The reason may be that, at lower  $\Phi_B$  values, the particles cannot be nipped efficiently because of less crowd in the mill so the number of ball-to-ball and ball-to-mill surface collisions, which end without breakage, is relatively higher.



**Figure 6.9.** The disappearance of one-size-fraction quartz feeds at different ball charges ( $\Phi_B$ ), ( $\Phi_M=0.35$ )



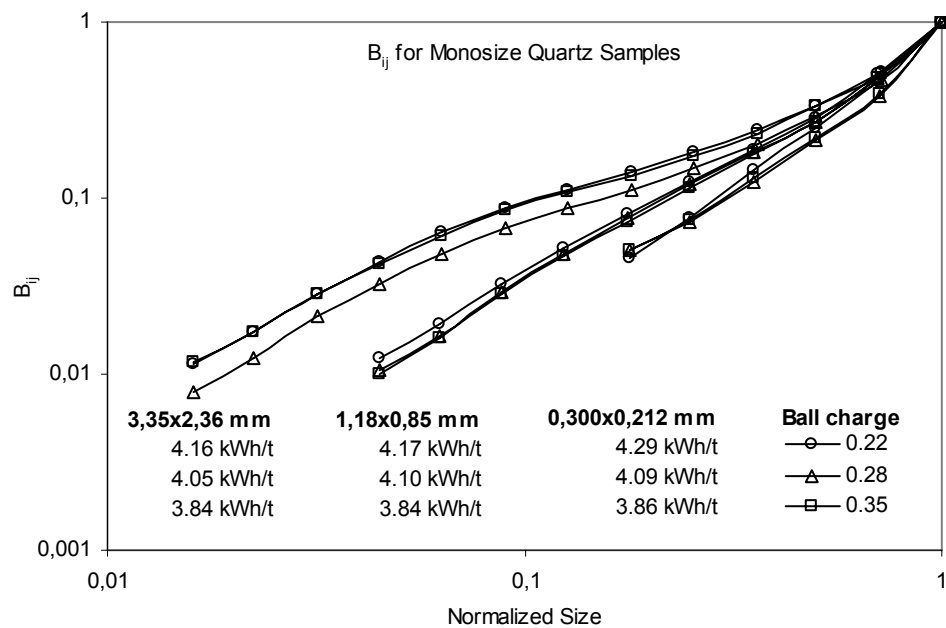
**Figure 6.10.** The disappearance of one-size-fraction calcite feeds at different ball charges ( $\Phi_B$ ), ( $\Phi_M=0.35$ )



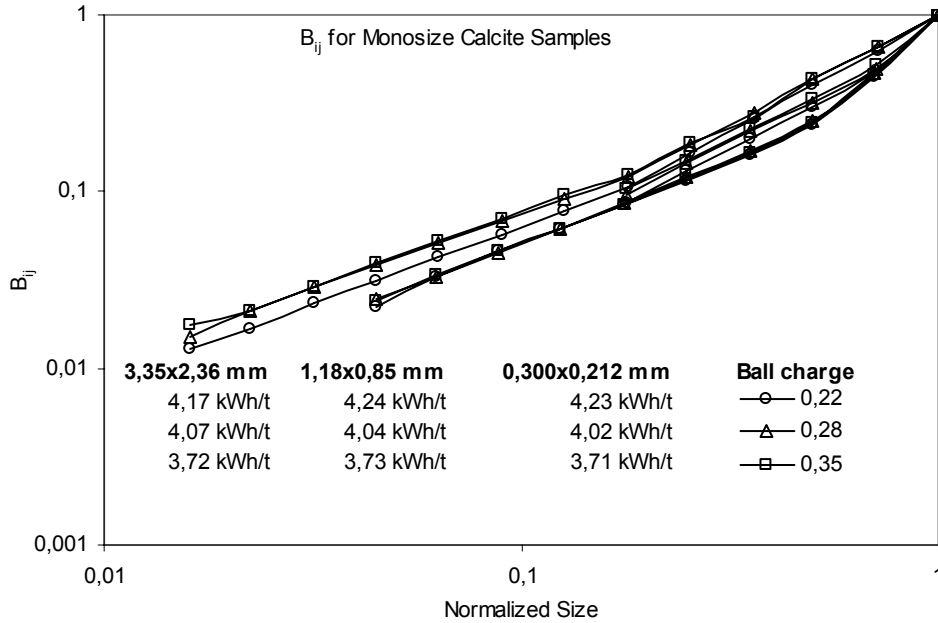
**Figure 6.11.** The change of the breakage rate of 6x8, 14x20, 48x65 mesh quartz and calcite feeds at different ball charges ( $\Phi_B$ ), ( $\Phi_M=0.35$ )

Figure 6.12 and Figure 6.13 present the cumulative breakage distribution functions ( $B_{ij}$ ) of 3 different one-size-fraction quartz and calcite feeds, respectively, with specific energy values at different ball charges ( $\Phi_B$ ). The fractional material filling  $\Phi_M$  was kept constant at 0.35 for all experiments. The plots delineate that the  $B_{ij}$  values for different one-size-fraction feeds plotted versus normalized size do not coincide. This means that  $B_{ij}$ s are not normalizable by size for the studied minerals. Moreover, for quartz mineral, size distribution of progeny particles becomes finer as the feed size increases. The similar phenomenon was observed for calcite mineral as well but the variation is relatively lower.

The specific grinding energy- $B_{ij}$  relationship was also observed. As it was presented in Figure 6.12 and Figure 6.13, only around 10% increase in specific grinding energy was achieved by increasing  $\Phi_B$  from 0.22 to 0.35 with 0.35  $\Phi_M$ . Higher  $\Phi_B$  values could not be tested since grinding regime changes above 0.35 (see Figure 4.8), and  $\Phi_B$  values lower than 0.22 were thought to be meaningless. According to the plots, the results do not provide any significant difference in specific grinding energy to determine its effect on breakage distribution functions.



**Figure 6.12.** The cumulative breakage distribution function ( $B_{ij}$ ) of 3 different one-size-fraction quartz feeds with specific energy values at different ball charges ( $\Phi_B$ ), ( $\Phi_M=0.35$ )



**Figure 6.13.** The cumulative breakage distribution function ( $B_{ij}$ ) of 3 different one-size-fraction calcite feeds with specific energy values at different ball charges ( $\Phi_B$ ), ( $\Phi_M=0.35$ )

### 6.2.2. The effect of Ball Size on Particle Breakage Parameters

The 6x8 mesh, 14x20 mesh and 48x65 mesh one-size-fraction quartz feeds were exposed to short-time grinding tests with standard Bond ball charge and 1-inch ball charge. The results presented in Figure 6.14 show abnormal breakage for 6x8 mesh material for both of the grinding media. For the first 30 seconds of grinding, the initial disappearance rates of particles, which are relatively fast, are quite similar for both grinding media. In this region, although the impact energy of grinding media is not sufficient, the weak and fresh feed comprising considerably more flaws can not resist even poor impacts so they are broken quite fast. Then, the remaining rounded particles are broken with a slow rate depending on the grinding media. For the region where the disappearance rate of particles is small, the grinding kinetics is first order. In this region, standard Bond Ball Charge seems to be more efficient than 1 inch ball charge.

For 14x20 mesh and 48x65 mesh quartz feeds, there is no significant difference in disappearance rates with respect to ball size within the  $\pm 10\%$  significance level (Figure 6.15 and Figure 6.16). According to Figure 5.2 (c) in the previous chapter, the  $B_{ij}$  shows a finer size distribution for Bond ball charge than that for 1 inch ball charge for all the one-size-fraction quartz feeds studied. Therefore, with the combination of these two parameters, it is expected that the product size distributions of quartz feeds must be slightly finer for Bond ball charge after a certain time of grinding. The experimental results of particle size distribution for 120 seconds of grinding meet this expectation in Figure 6.17.

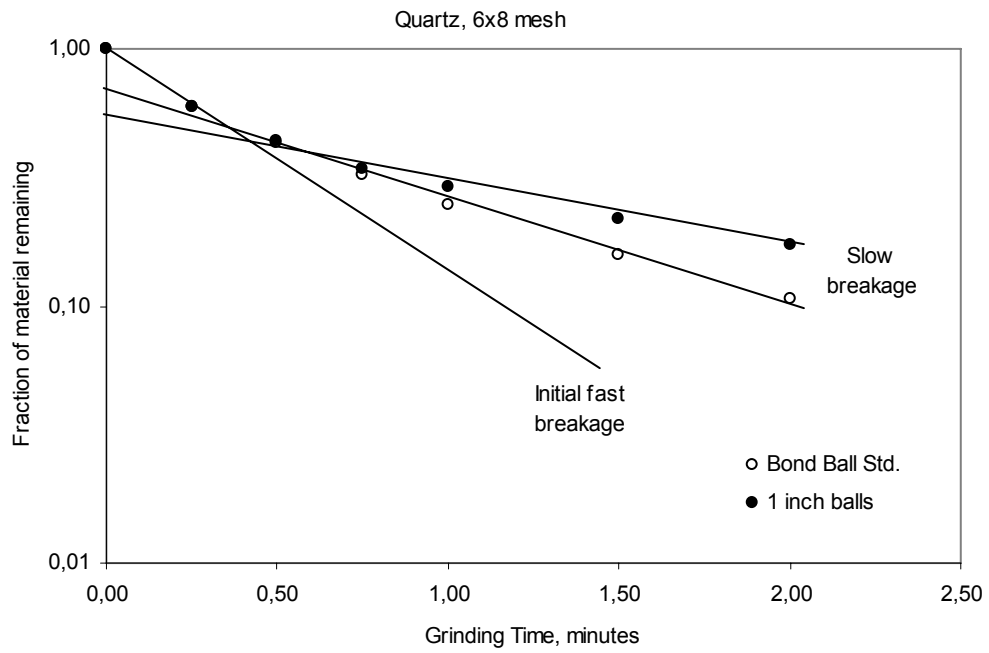


Figure 6.14. The disappearance of 6x8 mesh quartz using Bond ball charge and 1 inch ball charge

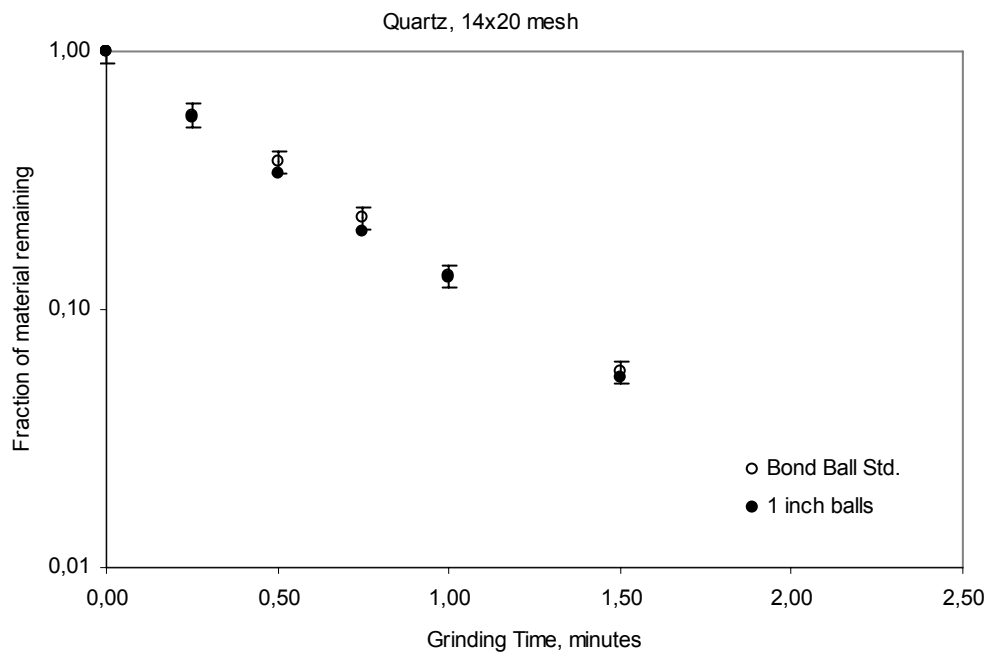
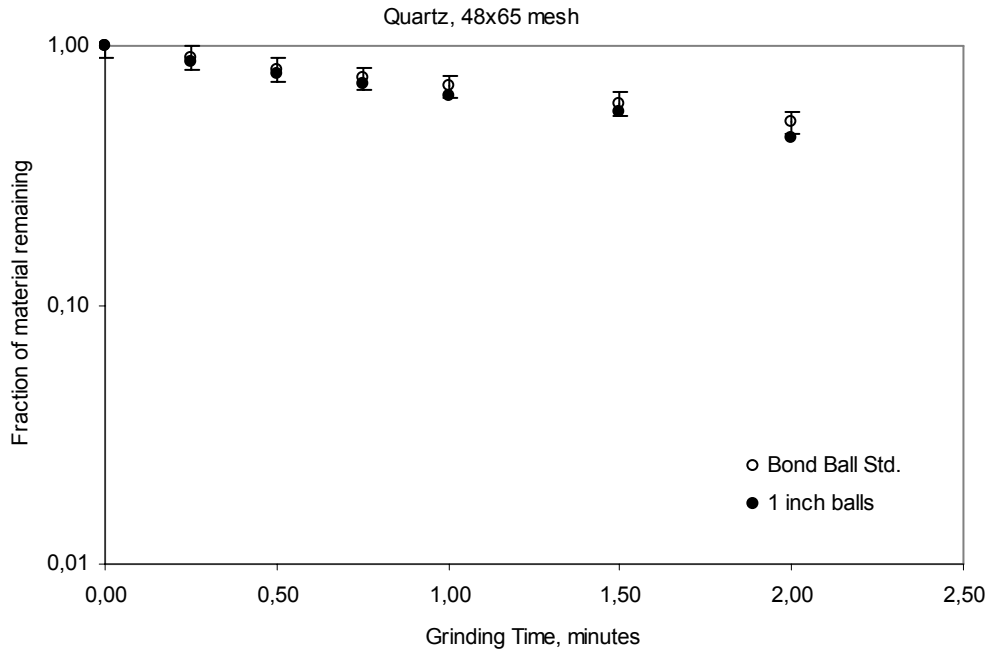
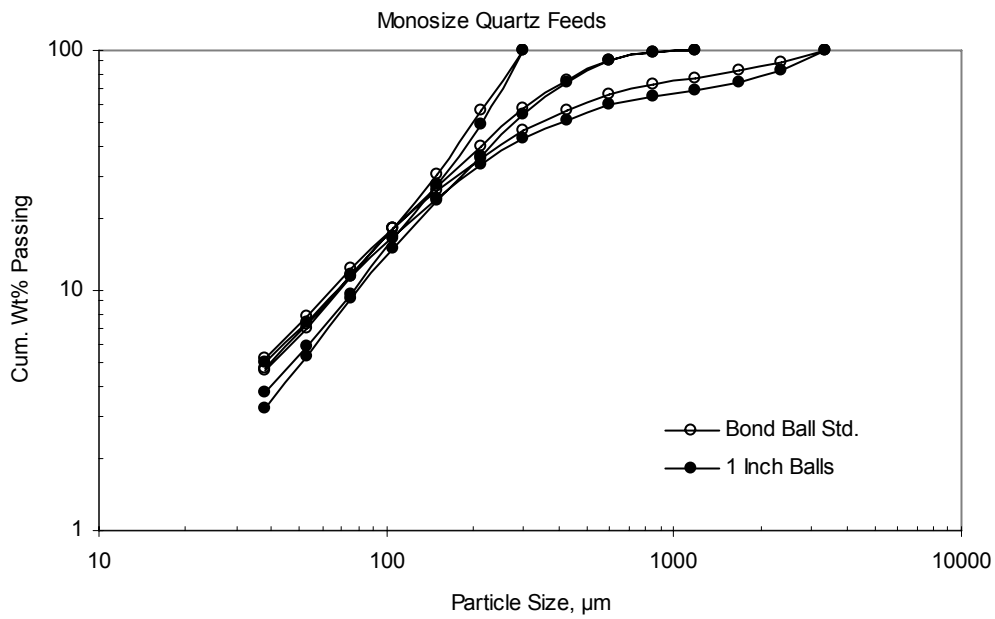


Figure 6.15. The disappearance of 14x20 mesh quartz using Bond ball charge and 1 inch ball charge



**Figure 6.16.** The disappearance of 48x65 mesh quartz using Bond ball charge and 1 inch ball charge



**Figure 6.17.** The particle size distribution of 6x8 mesh, 14x20 mesh and 48x65 mesh quartz feeds after being ground with Bond Ball Charge and 1 inch ball charge

### 6.2.3. The effect of Percent Circulating Load on the Particle Breakage Parameters

The percentage of fresh feed to the material returned to the crushing unit by the classifier is described as circulating load (C.L.). Wills and Napier-Munn (2006) stated that the useful capacity of the mill increases with increasing circulating load within limits. They also stated that the optimum circulating load for a particular circuit depends on the classifier capacity and the cost of transporting the load to the mill. The circulating load is generally in the range of 100-350%, although it can be as high as 600% (Wills and Napier-Munn, 2006). One thing they did not consider is whether any variation in circulating load causes the size distribution of mill hold-up to alter, which may lead to a change in breakage parameters and may result in a significant change in the mill capacity. Aforementioned phenomenon was also investigated in this study by using steady state mill hold-up materials at different circulating loads.

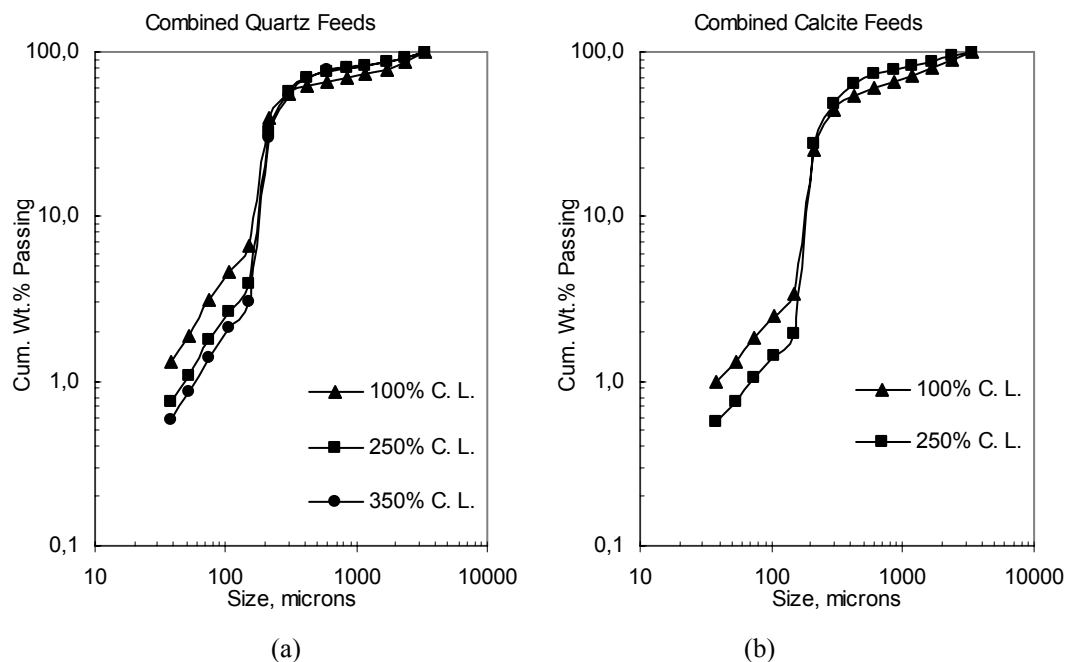


**Figure 6.18.** Size distributions of quartz (a) and calcite (b) feeds at different percent of circulating loads generated by 150 µm closing screen

The standard Bond Grindability Test is carried out at 250% circulating load. Besides, the separate quartz and calcite feeds were prepared by Bond Grindability Test procedure using 150 microns closing screen at 100% and 350% circulating loads, too. The plots in Figure 6.18 represent the distributions near the feed-inlet of the mill at different circulating loads. There is no significant difference between the size distributions of feeds prepared at 250% and 350% C. L., while the ratio of +300 µm particles, which is a relatively coarse fraction, is slightly higher in the feed prepared at 100% circulating load compared to others. The difference in the size distribution of -150 µm material is due to the addition of different amounts of fresh feed and it is not that significant as it comprises less than 5% of the total feed. Therefore, it can be stated that the size distribution of material, so the coarse-fine ratio, in the closed circuit mills changes to a certain extent within the industrial operating range, which is 100-350%. In order to evaluate its effect on the breakage rates, feeds were exposed to short-time grinding test up to about 150 seconds. The disappearance of coarsest fraction (6x8 mesh) in the generated feeds were plotted by time for both materials in Figure 6.19. They were also compared with -6 mesh feeds in the same figure. The breakage rates do not change significantly for the circulating load range of 100-350%. The reason must be that the difference in particle size distributions is not that significant to alter the breakage mechanisms during grinding. Moreover, taking the energy split factor introduced by Kapur and, Fuerstenau (1988), which is the ratio of energy expended when the unit

mass of a mineral is ground in a mixture environment (mixture of two different materials or mixture of coarse and fine particles) and ground alone for the same interval, the amount of 6x8 mesh material is very close in tested range so the specific impact energy is quite similar in both conditions. However, in -6 mesh material, amount of 6x8 mesh material is considerably higher compared to the steady-state mill hold-ups as it is shown in Table 6.1. This leads the impact energy to be shared by the neighboring coarse particles in the breakage zone causing some of particles remain unbroken which result in decrease in breakage rate. Considering the less than 1% random error in breakage rates in the repeated tests (Figure 6.74), the difference in the breakage rates between these two cases is quite significant.

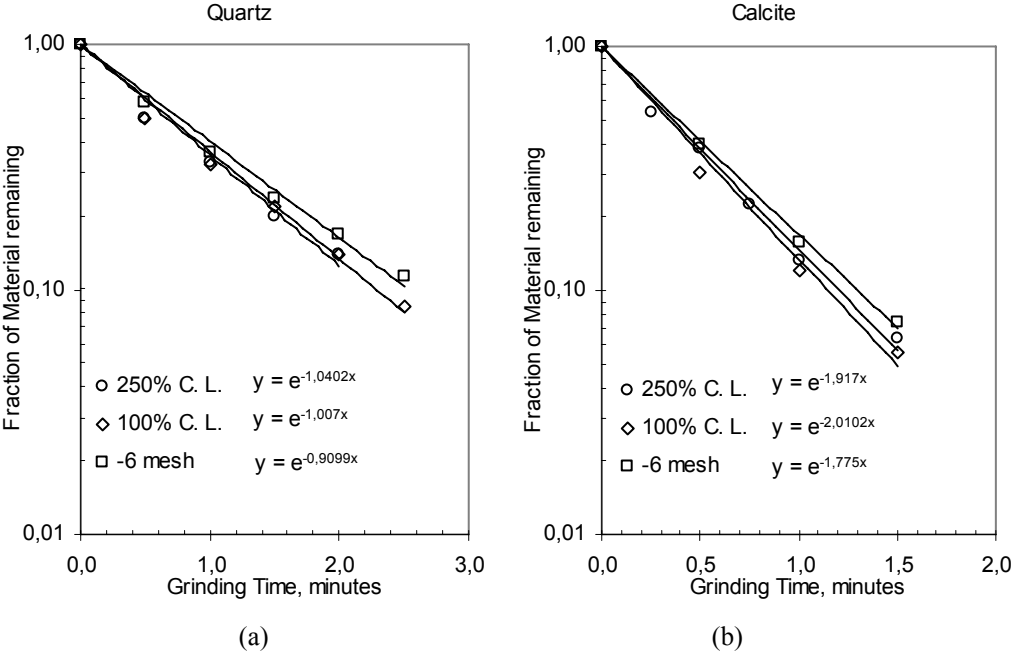


**Figure 6.19.** The disappearance of 6x8 mesh size fractions of quartz (a) and calcite (b) in -6 mesh feed and steady state mill feeds generated by 150 μm closing screen at 100% and 250% circulating loads

**Table 6.1.** The percent amount of 6x8 mesh material in different mill hold-ups, and -6 mesh feed.

Mill Hold-Up	% 6x8 Mesh Quartz	% 6x8 Mesh Calcite
250% C. L.	8.36	6.30
100% C. L.	12.56	9.78
-6 Mesh	40.55	19.15

**6.2.4. The effect of Grinding Environment on the Breakage Distribution Function**

The experimental results of one-size-fraction short-time grinding tests showed that the  $B_{ij}$  is particle size dependent so it is not normalizable by size for the tested minerals. This result was checked by comparing the experimental results of product size distributions with the PBM estimations in different grinding conditions using normalized  $B_{ij}$ . The particle breakage parameters obtained by G-H method were run in population balance model using a population balance model computing program -NLPBM Batch Mill Simulator – (Tuzcu, 2010). G-H method utilizes the size distribution data of short-time grinding tests for the prediction of  $B_{ij}$ . The pre-determined  $B_{ij}$  and experimentally found  $K_1$  values are used to calculate  $K_2, K_3, \dots K_n$ . This means that breakage rate functions of the materials finer than the

top size fraction is independent of breakage distribution functions according to G-H method. Moreover,  $K_n$  is independent of  $K_{n-1}$ . Therefore, if one of the  $B_{ij}$  and  $K_1$  values changes,  $K_2, K_3, \dots, K_n$  will change accordingly. As shown in the Figure 6.20., the PSD estimations for 90-seconds-ground 6x8 mesh calcite mineral using normalized  $B_{ij}$ s obtained via grinding of same size feed is very poor while quartz feed gives a reasonable fit. This may be because of the fact that the breakage rates of fine fractions are very slow for quartz mineral so the effect of their  $B_{ij}$  is negligible in the total feed. This is not the case for calcite mineral.

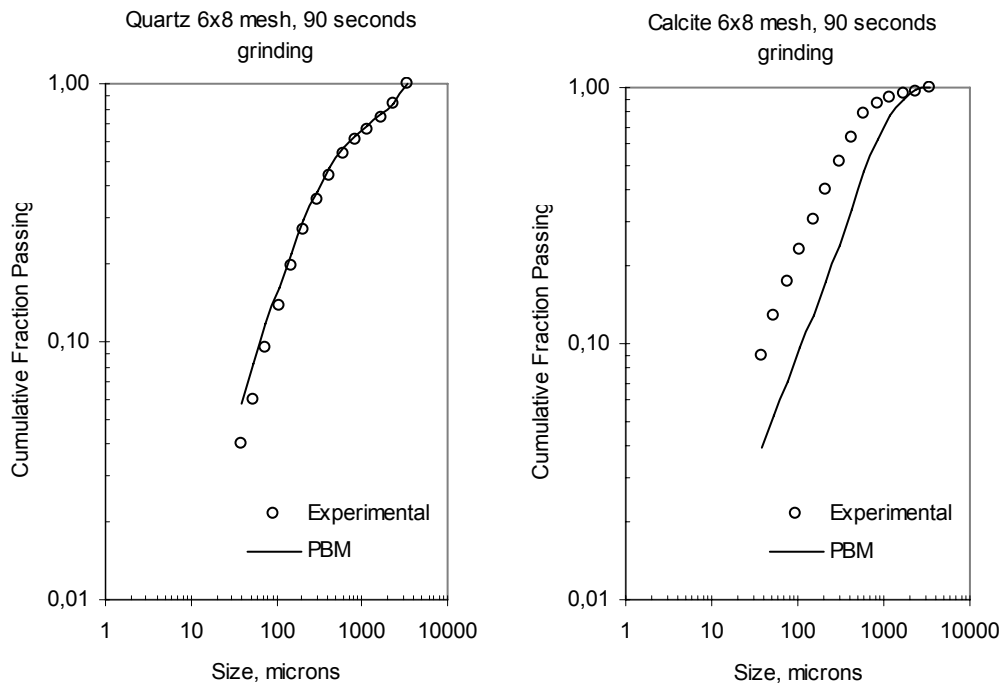


**Figure 6.20.** The experimental and predicted (PBM) size distributions for 6x8 mesh quartz and calcite products for 90 seconds grinding time at  $0.22 \Phi_B$

The reasonable estimation of quartz product size distribution shown in Figure 6.20 poses a question. Could the same  $B_{ij}$  be utilized for the quartz feeds having a size distribution? If so, a good estimation of product size distribution would mean that the  $B_{ij}$  was independent of milling environment. This was checked in Figure 6.21 by using the feeds generated by 75  $\mu\text{m}$  closing sieve. For 90 and 120 seconds of grinding, the estimation failed at the finer size fractions. This failure cannot be attributed only to  $K_i$  as it is determined via  $B_{ij}$ . This means that  $B_{ij}$  determined by grinding of one-size-fraction feed cannot be satisfactorily used for the same material ground in a different milling environment.

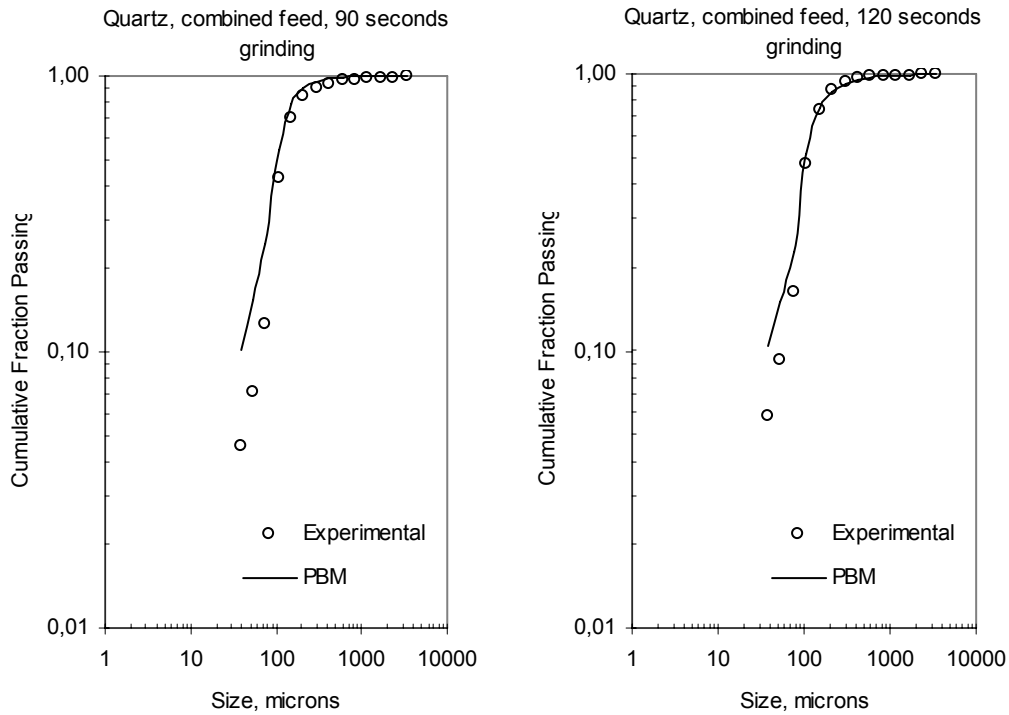


**Figure 6.21.** The experimental and predicted (PBM) size distributions for quartz products (75  $\mu\text{m}$  test sieve) for 90 and 120 seconds grinding time at 0.22  $\Phi_B$

The normalizability of  $B_{ij}$  was also tested for 14x20 and 48x65 mesh quartz and calcite feeds. Two different  $B_{ij}$  values were used for these tests.

- $B_{ij}$  of 6x8 mesh feeds and  $K_i$  calculated by G-H method.
- $B_{ij}$  of 14x20 mesh and 48x65 mesh, and  $K_i$  calculated by G-H method.

According to the Figures 6.22 and 6.23, the predictions using the  $B_{ij}$  values obtained by grinding of 14x20 and 48x65 mesh feeds are reasonable while the others failed for quartz mineral. These results prove that although  $B_{ij}$  is non-normalizable by size, the  $B_{ij}$  of fine sizes which have very slow  $K_i$  values may have negligible effect on the whole size distribution of feed. The change in  $K_i$  values was presented in Figures 6.24, 6.25 and 6.26 for different one-size-fraction feeds.

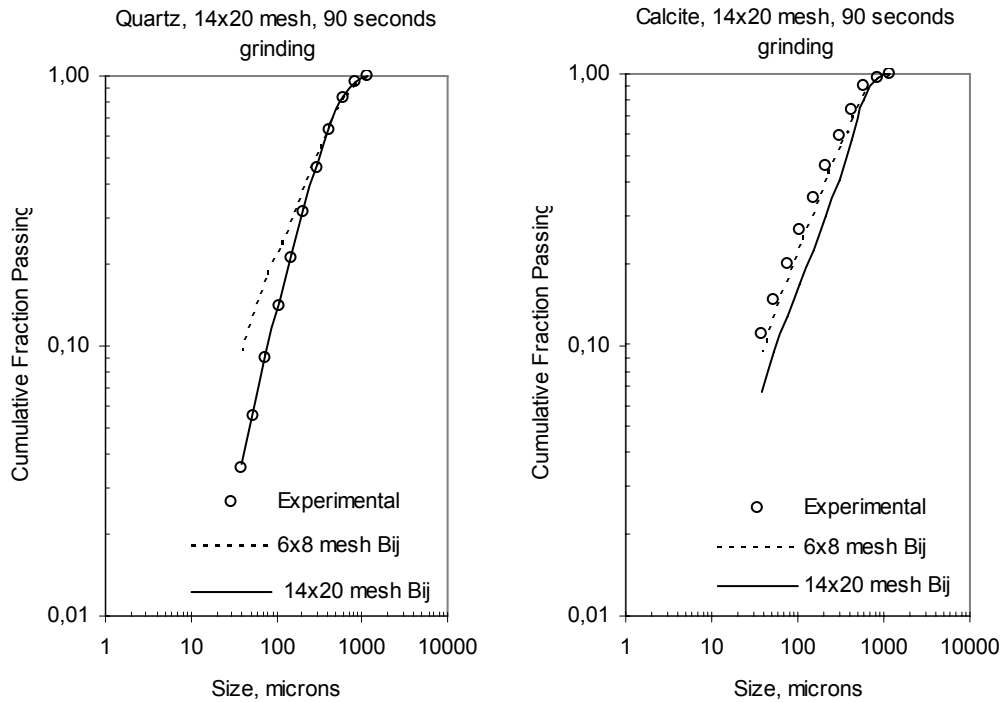


**Figure 6.22.** The experimental and predicted (PBM) size distributions for 14x20 mesh quartz and calcite products for 90 seconds grinding time at 0.22  $\Phi_B$  using  $B_{ij}$  of 6x8 mesh and 14x20 mesh feeds

Although the estimation for 6x8 mesh calcite mineral is poor in Figure 6.21, the use of  $B_{ij}$  values of 6x8 mesh feed provides better estimation for 14x20 mesh and 48x65 mesh feeds compared to the  $B_{ij}$  values belonging to those size fractions. This can be explained just by coincidence. Although both of the breakage parameters are not true, the combination of them could yield a reasonable estimation since they are not independent variables according to the G-H method. This poses another question. If breakage parameters are not independent, could they be combined in a single parameter representing both the rate and distribution functions? Then, instead of assuming  $B_{ij}$  to be independent of grinding environment and assigning all the variations to  $K_i$ , all the grinding behavior of minerals would be represented by a single parameter. This was evaluated in the following part by using linear form of batch grinding equation (eq. 2.25) assuming the grinding kinetics is first order.

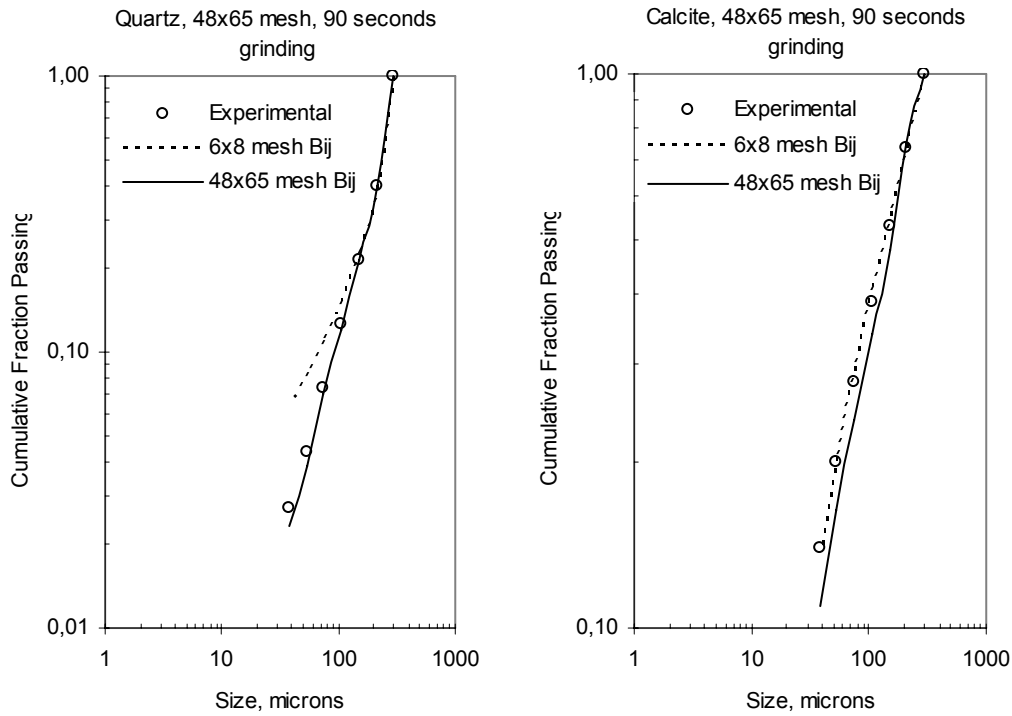


**Figure 6.23.** The experimental and predicted (PBM) size distributions for 48x65 mesh quartz and calcite products for 90 seconds grinding time at  $0.22 \Phi_B$  using  $B_{ij}$  of 6x8 mesh and 48x65 mesh feeds

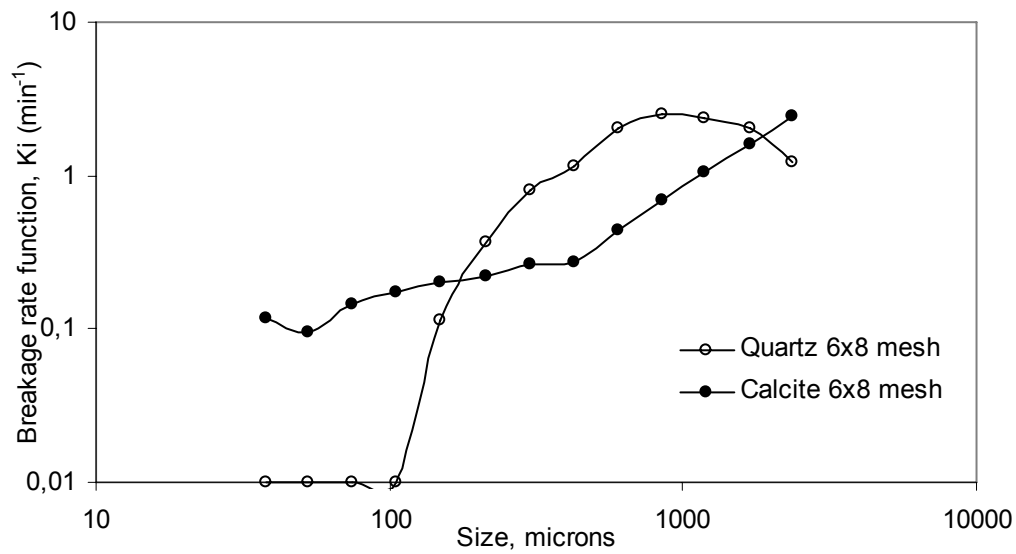


**Figure 6.24.** The variation of breakage rate functions by size for 6x8 mesh quartz and calcite minerals in narrow size 90 seconds of grinding

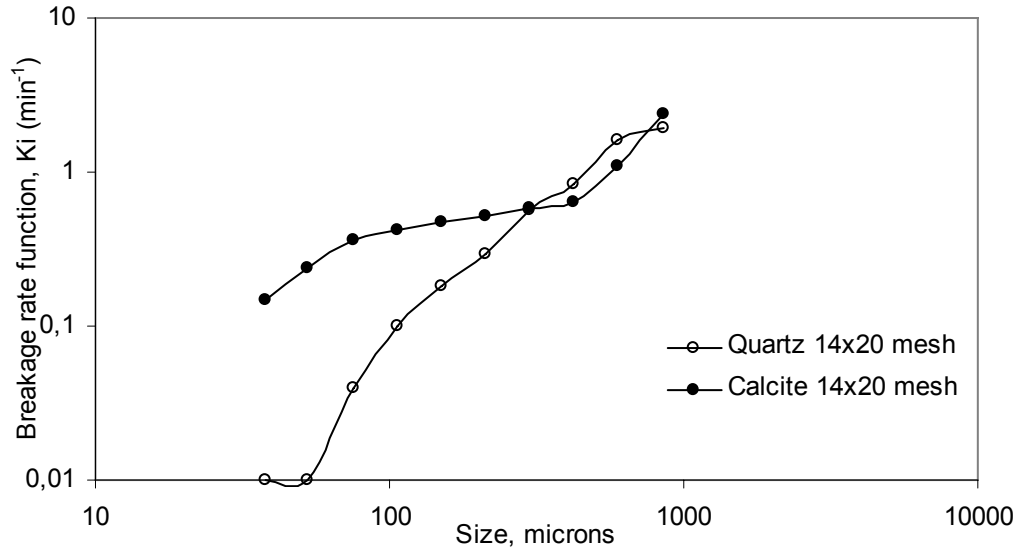


**Figure 6.25.** The variation of breakage rate functions by size for 14x20 mesh quartz and calcite minerals in narrow size 90 seconds of grinding

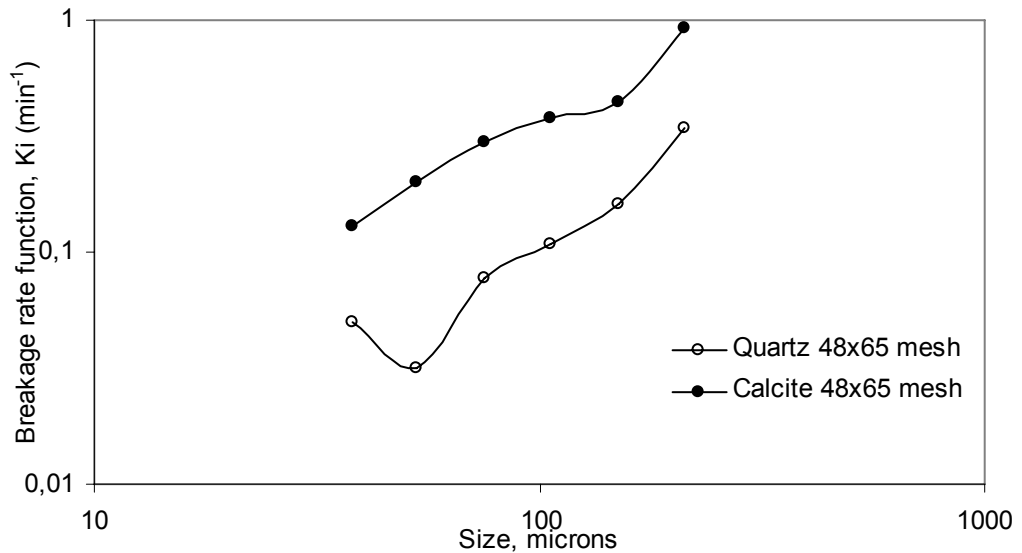


**Figure 6.26.** The variation of breakage rate functions by size for 48x65 mesh quartz and calcite minerals in narrow size 90 seconds of grinding

### 6.2.5. The Evaluation of Grinding Kinetics with the Linear Form of Batch Grinding Equation

According to G-H method,  $B_{ij}$  values are determined independent of time and breakage rate functions. However,  $K_i$  values are determined by substituting calculated  $B_{ij}$  and experimentally determined  $K_i$  in eq. 2.23. Therefore, except for the top size fraction,  $K_i$  values are not independent of  $B_{ij}$ . The variation of  $B_{ij}$  manipulates the  $K_i$  values, accordingly. Therefore, the use of a single parameter that combines the rate and distribution parameters, which represents grinding kinetics thoroughly, would be more practical. Ramirez-Castro and Finch (1980) utilized this assumption in linearized form of batch grinding equation (eq. 6.1) for simulation of a grinding circuit successfully. Austin et al. (1984) stated that the simplified form of linear batch grinding equation can represent grinding with a high accuracy. Laplante et al. (1987) simulated closed-circuit ball milling with the simple linear model, adequately.

In this part of the study, accuracy of linearized form of batch grinding equation was evaluated on the tested conditions.

$$R(x_i, t) = R(x_i, 0) \exp(-z_i t^{p_i}) \quad (6.1)$$

According to the equation, the plot of  $\ln[R(x_i, t)/R(x_i, 0)]$  versus grinding time should yield a straight line, of which the slope represents the cumulative breakage rate function,  $z_i$ .  $p_i$  was selected as 1.0 in order to simplify the equation. The graphs generated by using the data for all tested conditions generally present straight line. For the first fraction,  $z_i$  is equal to  $K_1$  since breakage distribution function is not present for the top sizes. Therefore, it is an expected situation that the top size fractions may deviate from linearity in some cases where the abnormal breakage occurs. Though, their lower fractions still follow a straight line.

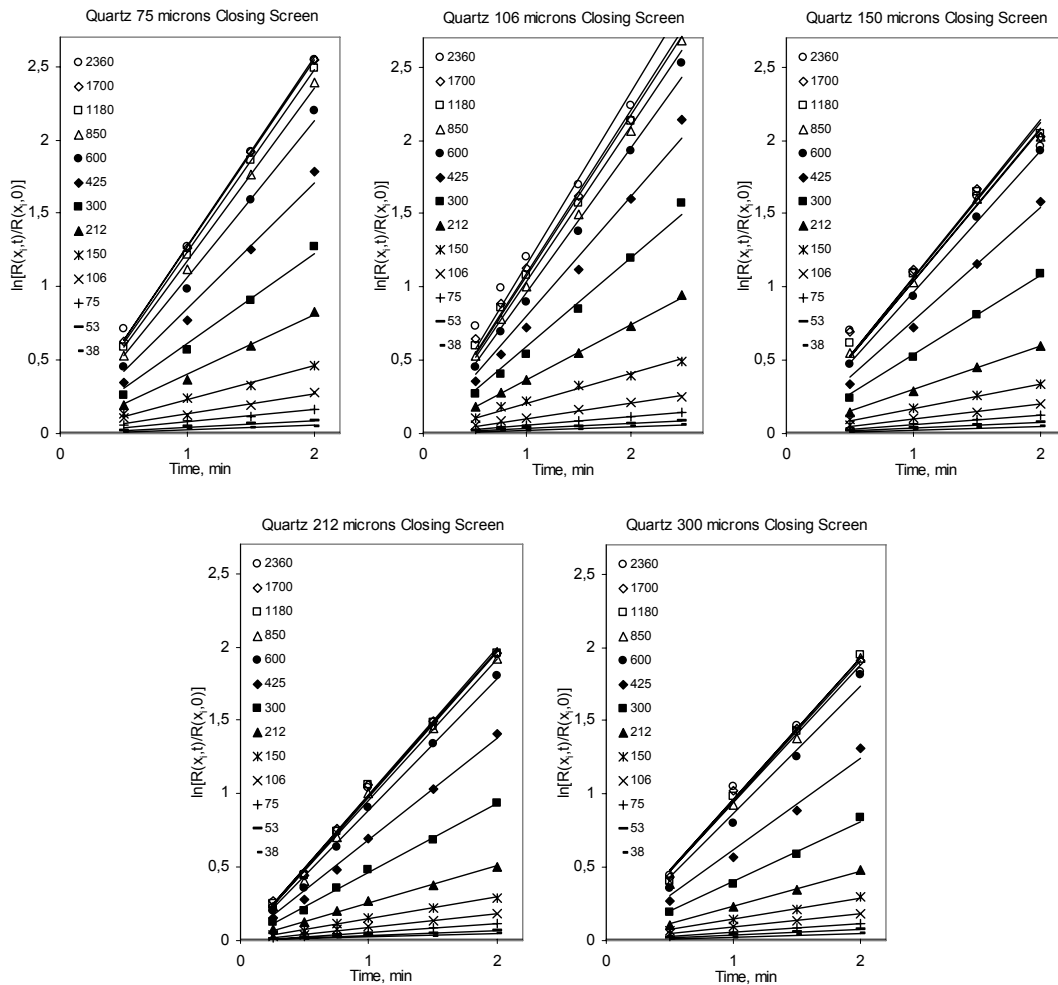


Figure 6.27. The linear batch grinding plots for quartz feeds at steady state generated by different closing screens

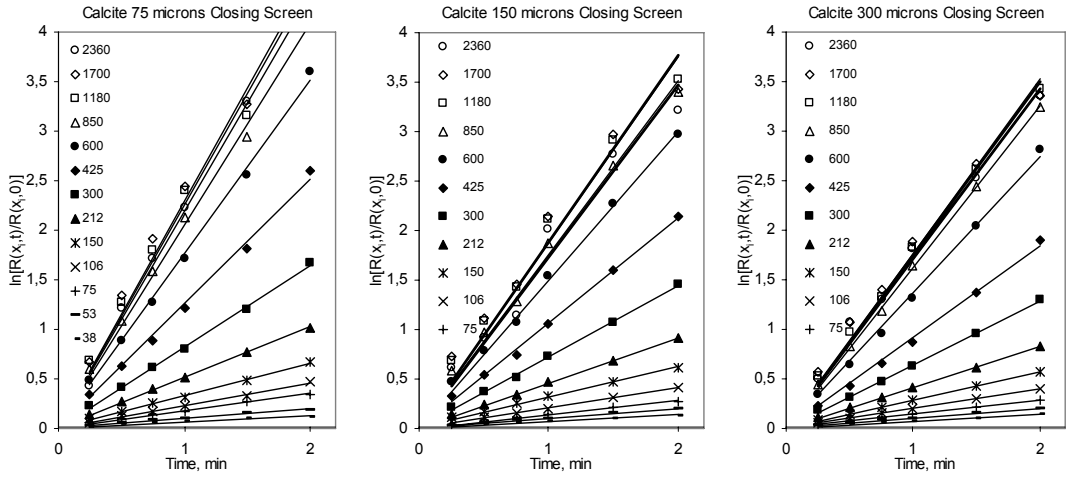


Figure 6.28. The linear batch grinding plots for calcite feeds at steady state generated by different closing screens

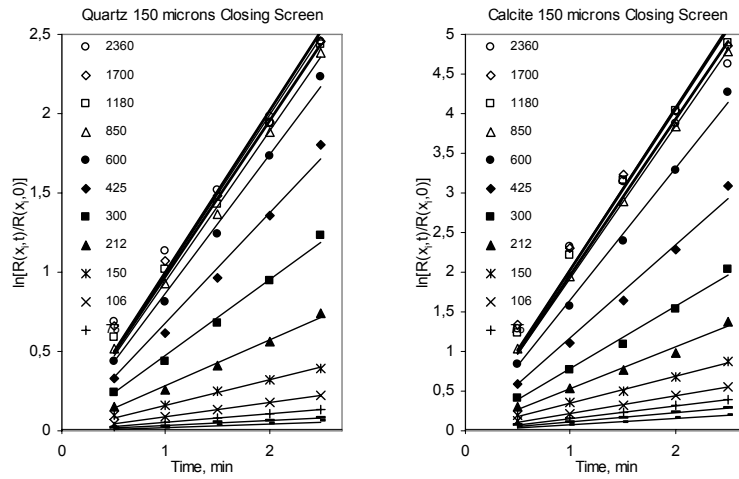


Figure 6.29. The linear batch grinding plots for quartz and calcite feeds at steady state generated 150  $\mu\text{m}$  closing screens at 100% Circulating Load

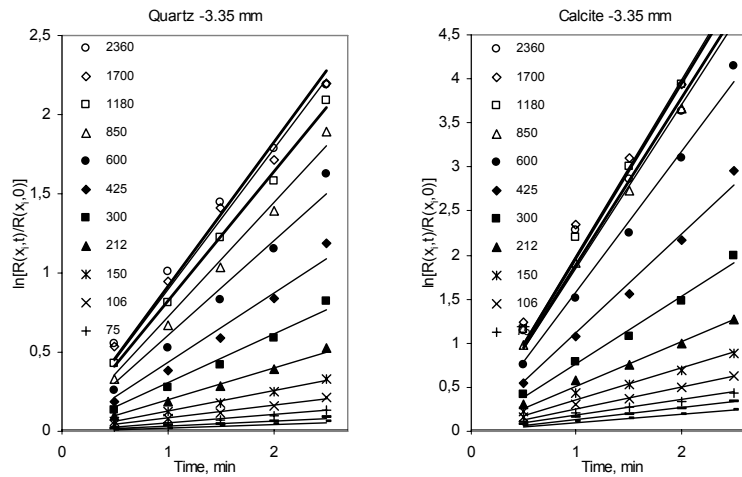


Figure 6.30. The linear batch grinding plots for -3.35 mm quartz and calcite feeds

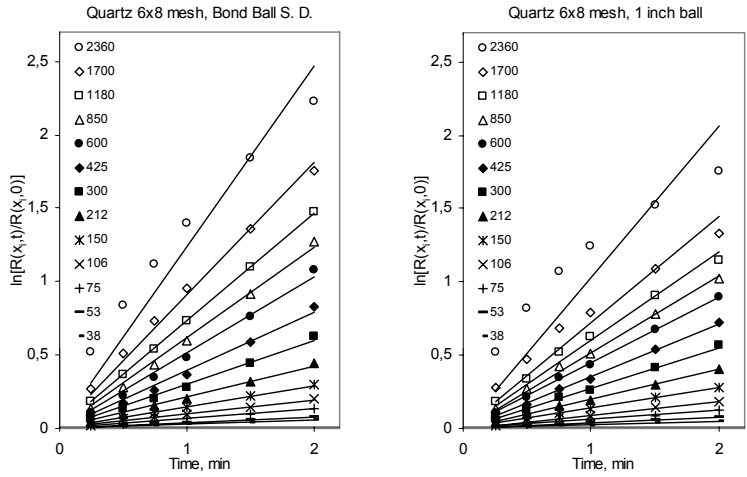


Figure 6.31. The linear batch grinding plots for -3.35+2.36 mm (6x8 mesh) quartz feed ground by Bond ball size distribution and 1 inch balls ( $\Phi_B$  0.22,  $\Phi_M$  0.35)

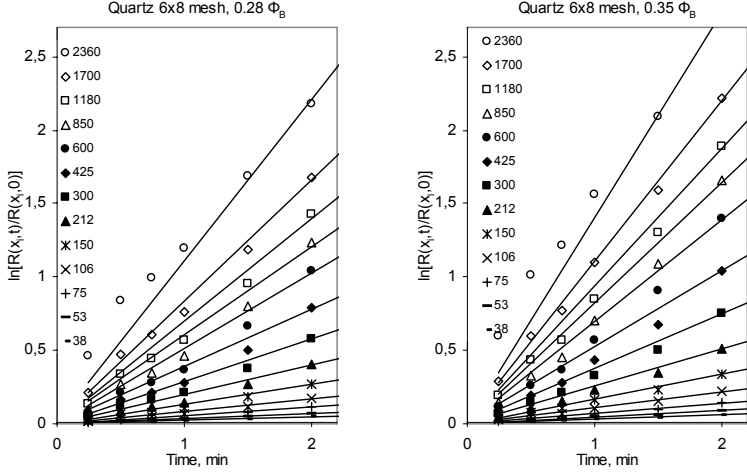


Figure 6.32. The linear batch grinding plots for -3.35+2.36 mm (6x8 mesh) quartz feed ground by Bond ball size distribution at  $\Phi_B$  0.28 and 0.35

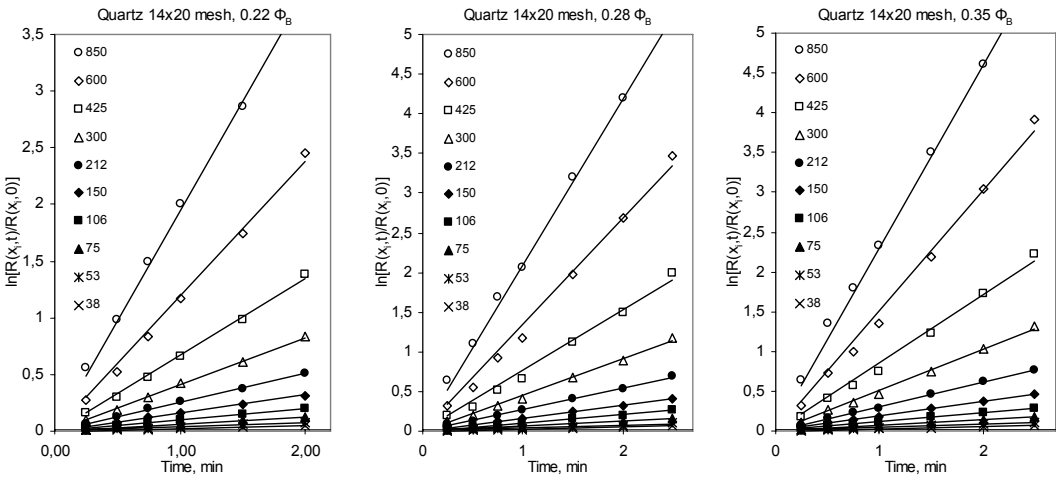
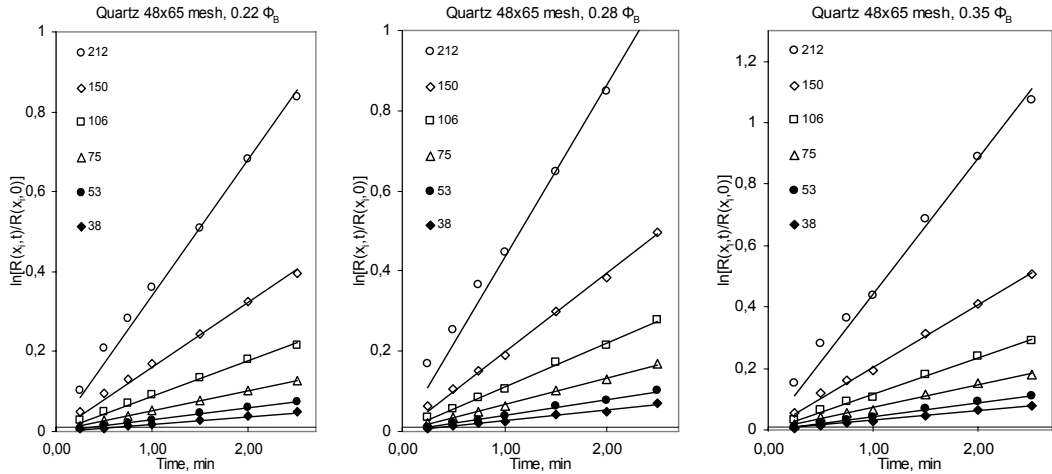
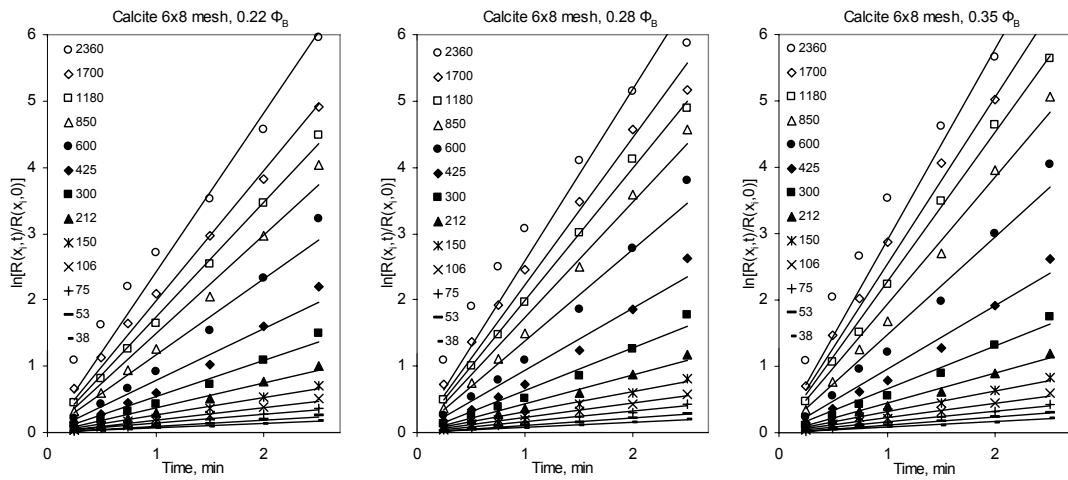


Figure 6.33. The linear batch grinding plots for -1.18+0.85 mm (14x20 mesh) quartz feed ground by Bond ball size distribution at  $\Phi_B$  0.22, 0.28 and 0.35



**Figure 6.34.** The linear batch grinding plots for -0.300+0.212 mm (48x65 mesh) quartz feed ground by Bond ball size distribution at  $\Phi_B$  0.22, 0.28 and 0.35



**Figure 6.35.** The linear batch grinding plots for -3.35+2.36 mm (6x8 mesh) calcite feed ground by Bond ball size distribution at  $\Phi_B$  0.22, 0.28 and 0.35

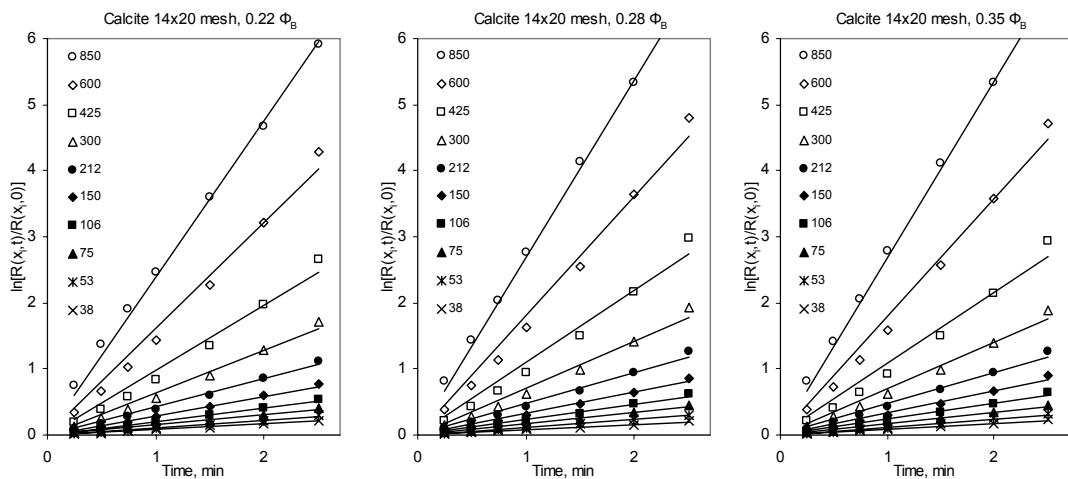


**Figure 6.36.** The linear batch grinding plots for -1.18+0.85 mm (14x20 mesh) calcite feed ground by Bond ball size distribution at  $\Phi_B$  0.22, 0.28 and 0.35

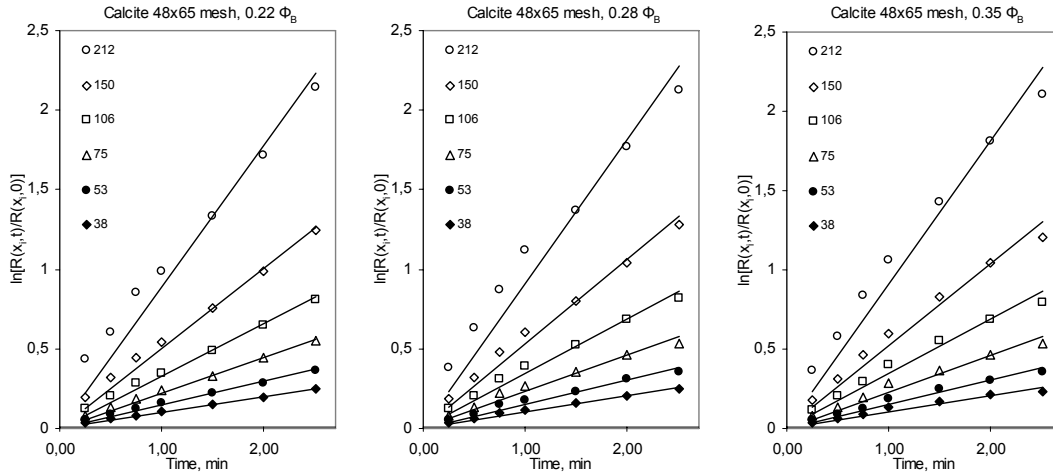


**Figure 6.37.** The linear batch grinding plots for  $-0.300+0.212$  mm (48x65 mesh) calcite feed ground by Bond ball size distribution at  $\Phi_B$  0.22, 0.28 and 0.35

Cumulative breakage rate functions for different grinding environments generated by different closing screens were plotted in Figure 6.38. and Figure 6.39 for both minerals. The effect of percent circulating load was also presented in the same graphs. Although  $-3.35$  mm ( $-6$  mesh) quartz feed shows slight deviation, the general trends are quite similar for all tests meaning that  $z_i$  is independent of grinding environment. On the other hand, it can be considered that the difference in feed size distributions may not be significant for the tested conditions to distinguish the effect of grinding environment. Anyway, as the tested conditions are quite similar to ones in industrial ball milling applications, it can be stated that the effect of grinding environment on the cumulative breakage rate functions is negligible for the wide range of operating conditions.

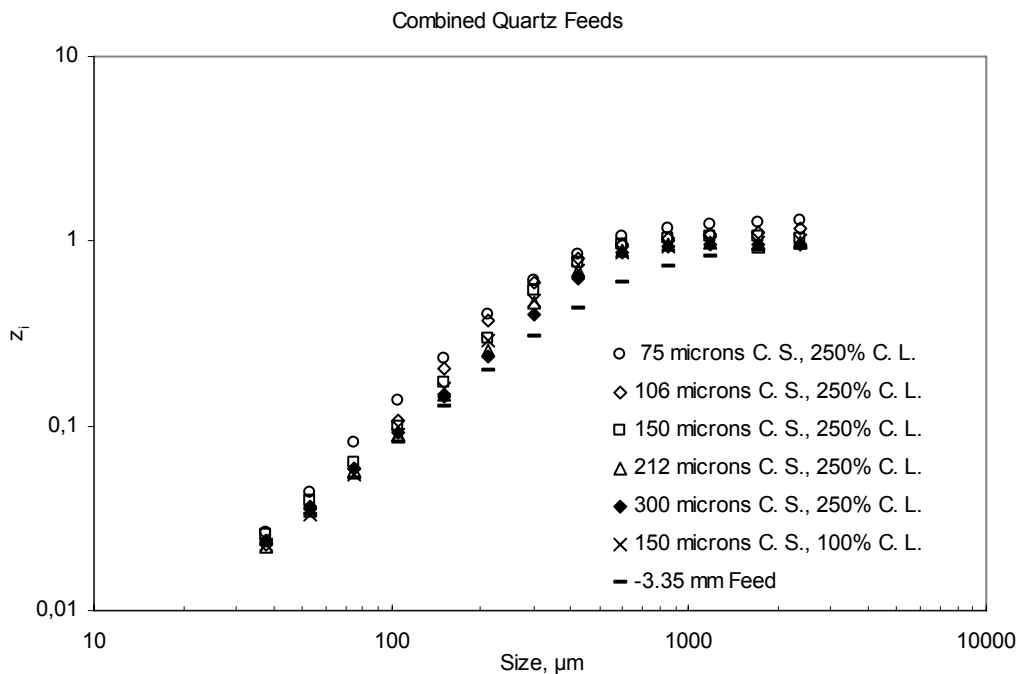


**Figure 6.38.** Cumulative breakage rate function for quartz feed at steady state generated by different closing screens

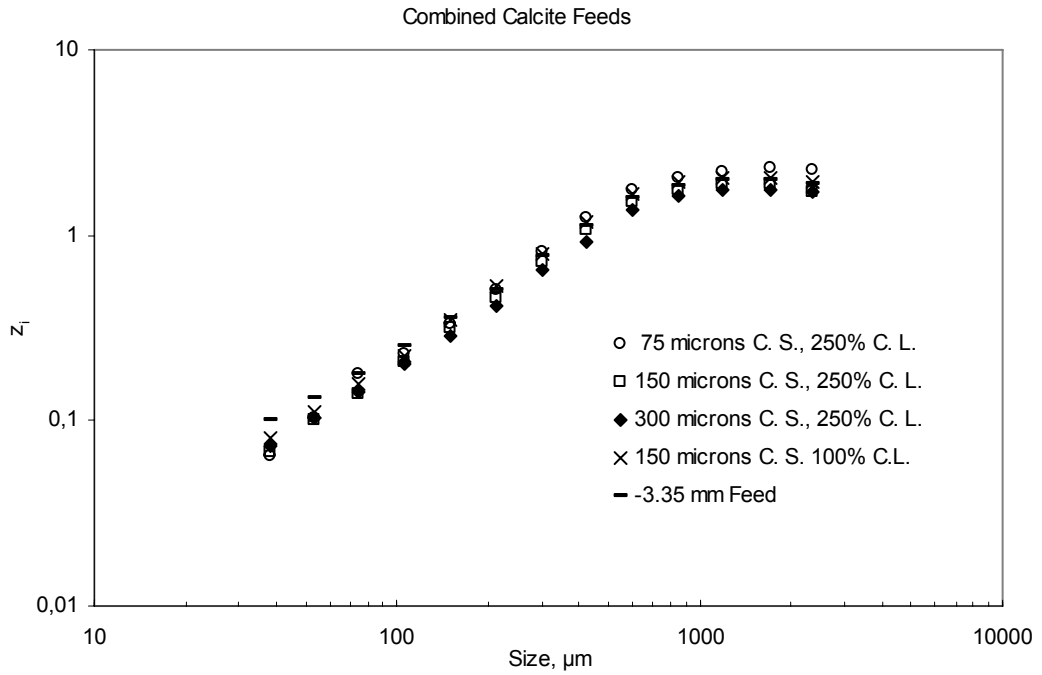


**Figure 6.39.** Cumulative breakage rate function for calcite feed at steady state generated by different closing screens

The cumulative breakage rate functions were compared by feed size and fractional ball charge in Figure 6.40. and Figure 6.41. They show that  $z_i$  is independent of  $\Phi_B$  for all tested feed sizes. In general,  $z_i$  is independent of particle size below about 1 mm. Above that point,  $z_i$  values of 6x8 mesh quartz, which presents abnormal breakage, deviates from the general trend.

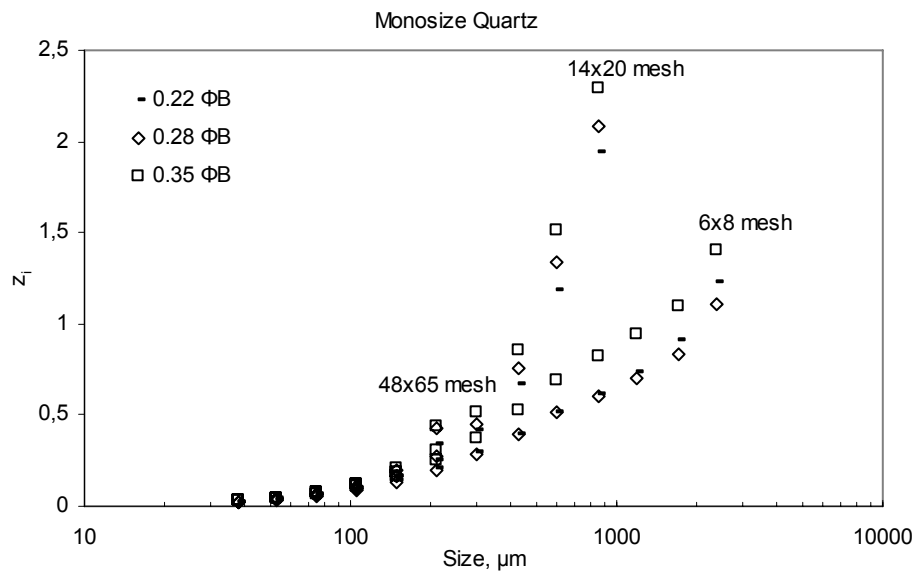


**Figure 6.40.** Cumulative breakage rate function for one-size-fraction 6x8, 14x20 and 48x65 mesh quartz feeds at different ball charges, plotted by normalized size ( $\Phi_M=0.35$ )

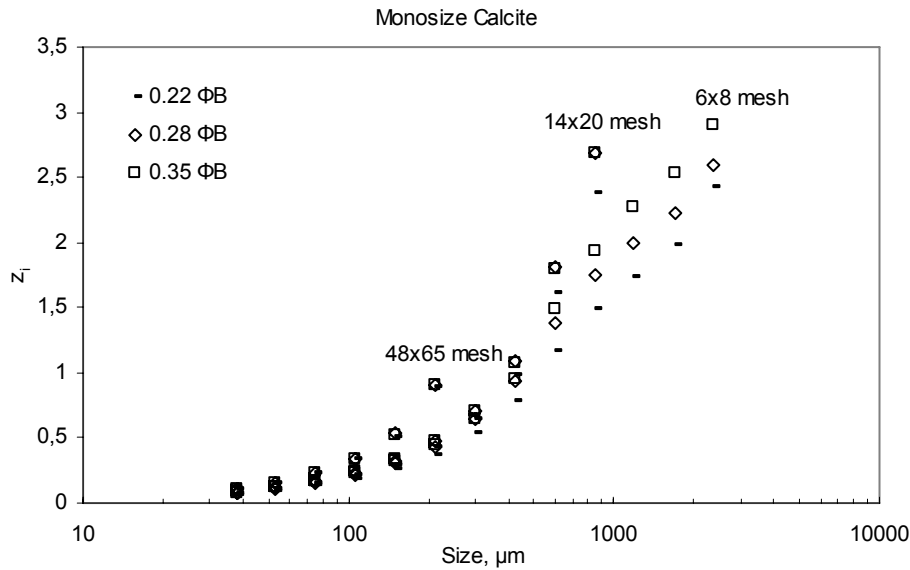


**Figure 6.41.** Cumulative breakage rate function for one-size-fraction 6x8, 14x20 and 48x65 mesh calcite feeds at different ball charges, plotted by normalized size ( $\Phi_M=0.35$ ).

The product size distributions were generated by substituting the calculated cumulative breakage rate functions in linear batch grinding equation (Figures 6.42 through 6.72). The predicted size distributions are quite successful in almost all tested conditions and grinding times up to 2.5 minutes including the tests at which abnormal breakage occurs. In a few tested conditions, the predictions are rather poor for the first 15 or 30 seconds (Figures 6.58, 6.66, 6.69, 6.70 and 6.72) but they achieve high accuracy as the grinding proceeds. The reason may be the abnormal breakage region and the unbalanced conditions during the initial time of grinding in the mill. This means that the abnormality in breakage rates during the first few seconds of grinding can be neglected and the grinding kinetics can be considered to be linear. Therefore, instead of determining two independent breakage parameters of population balance models, it is more practical to evaluate the grinding kinetics of materials by a single parameter of linear form of batch grinding equation. Another result that can be stated is that, for up to 2.5 minutes of grinding time, generally more than 50% of feeds are reduced to  $-100 \mu\text{m}$  even for quartz mineral, which has relatively higher work index ( $W_i$ ). Therefore, the residence time of material in the mill should not exceed a few minutes. This means that it is more convenient to limit the grinding time by a few minutes in the researches done for investigating the grinding kinetics of material rather than using long time of grinding data.

Finally, the predictions done by using two methods were compared for some of the tests in Figure 6.73. The results support that it is more convenient to evaluate the grinding kinetics of materials with a single parameter in linearized form of discrete size batch grinding equation. One of the short-time grinding tests was repeated (Figure 6.74) in order to check the reliability of the tests and determine the percent of random error. According to the results, there is no significant difference between the repeated tests in 5% significance level. The difference between the breakage rate functions of two repeated tests is less than 1%.

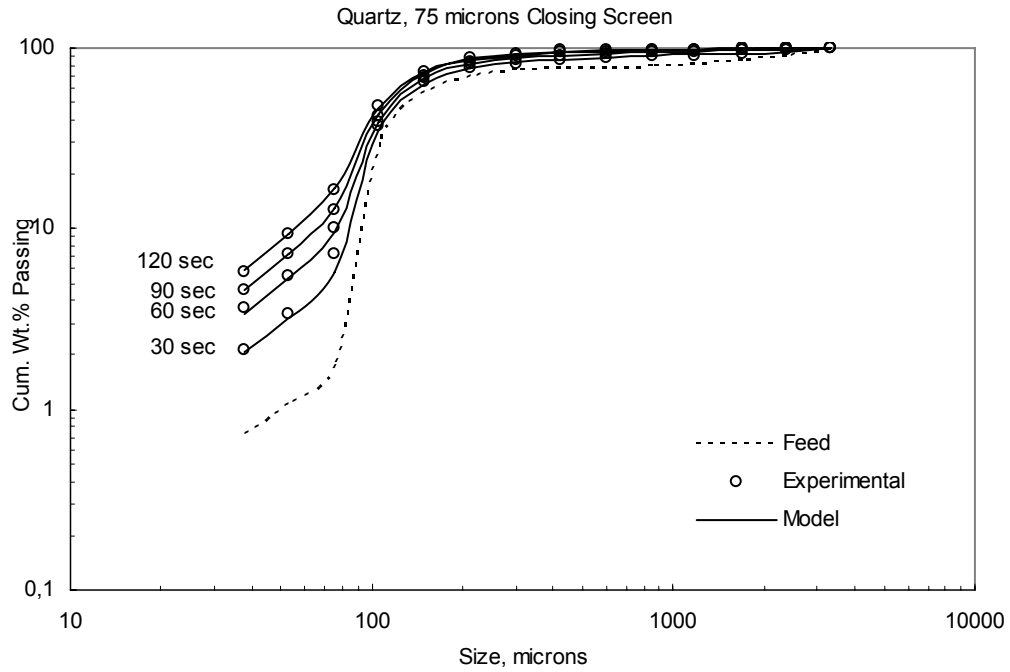


**Figure 6.42.** The experimental and predicted size distributions for quartz feed generated by 75  $\mu\text{m}$  closing screen, and its products for short grinding times

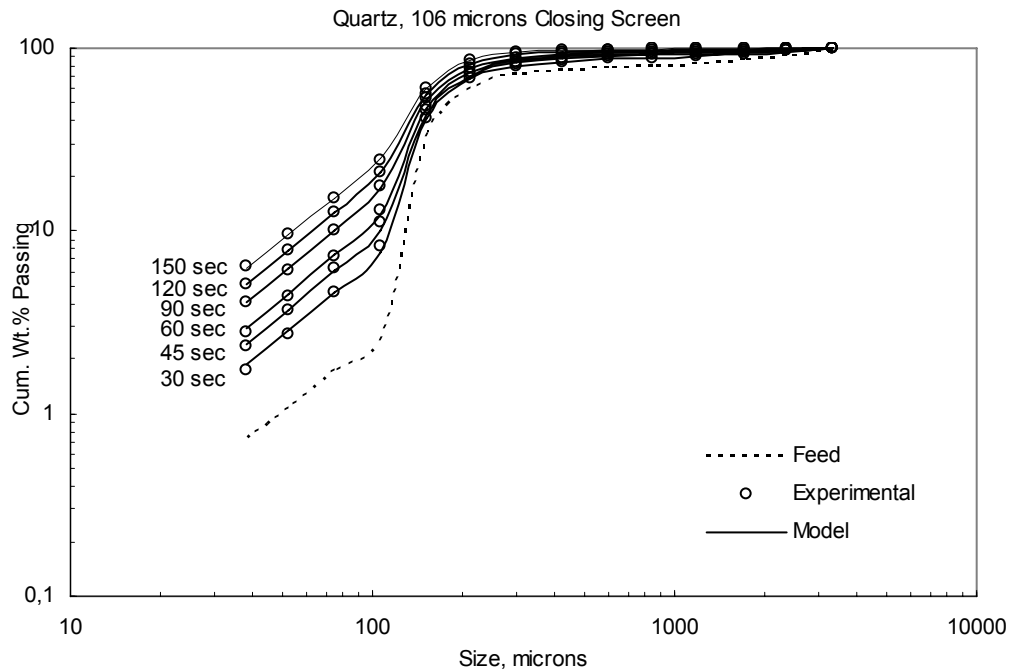


**Figure 6.43.** The experimental and predicted size distributions for quartz feed generated by 106  $\mu\text{m}$  closing screen, and its products for short grinding times

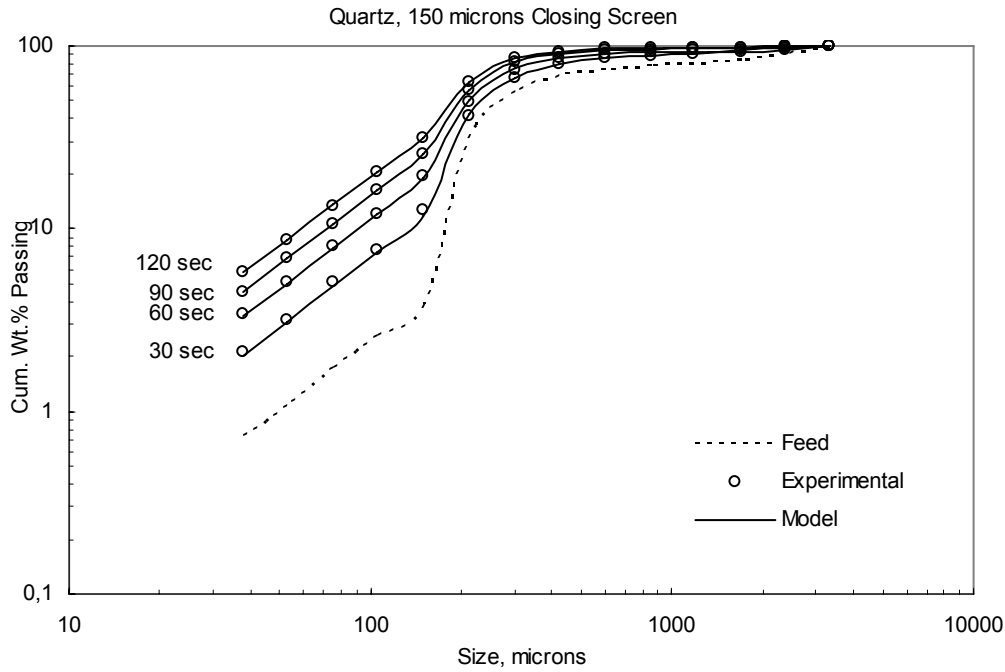


**Figure 6.44.** The experimental and predicted size distributions for quartz feed generated by 150  $\mu\text{m}$  closing screen, and its products for short grinding times

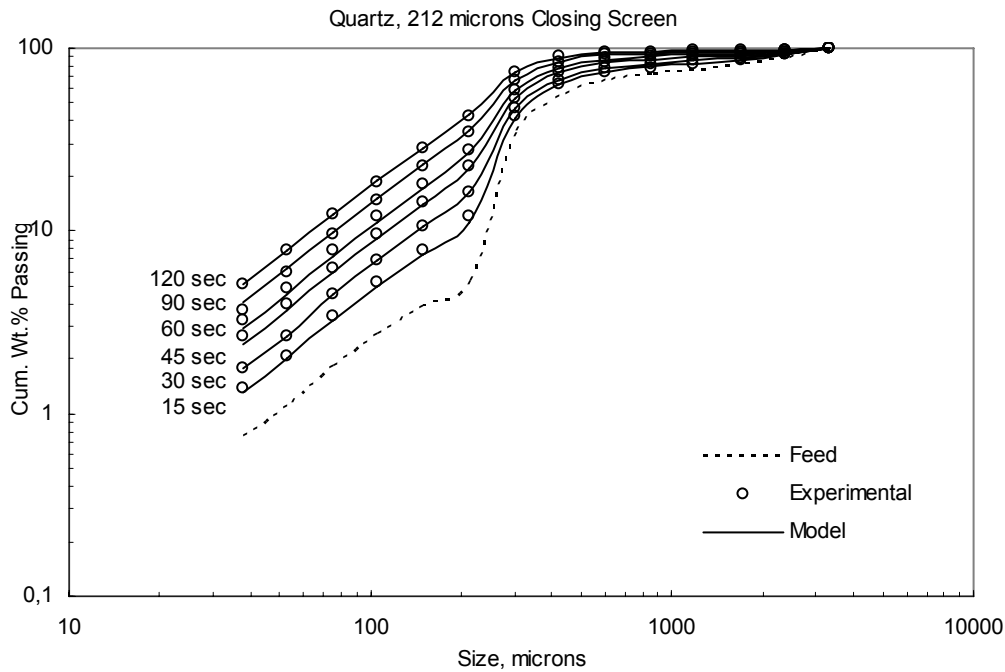


**Figure 6.45.** The experimental and predicted size distributions for quartz feed generated by 212  $\mu\text{m}$  closing screen, and its products for short grinding times

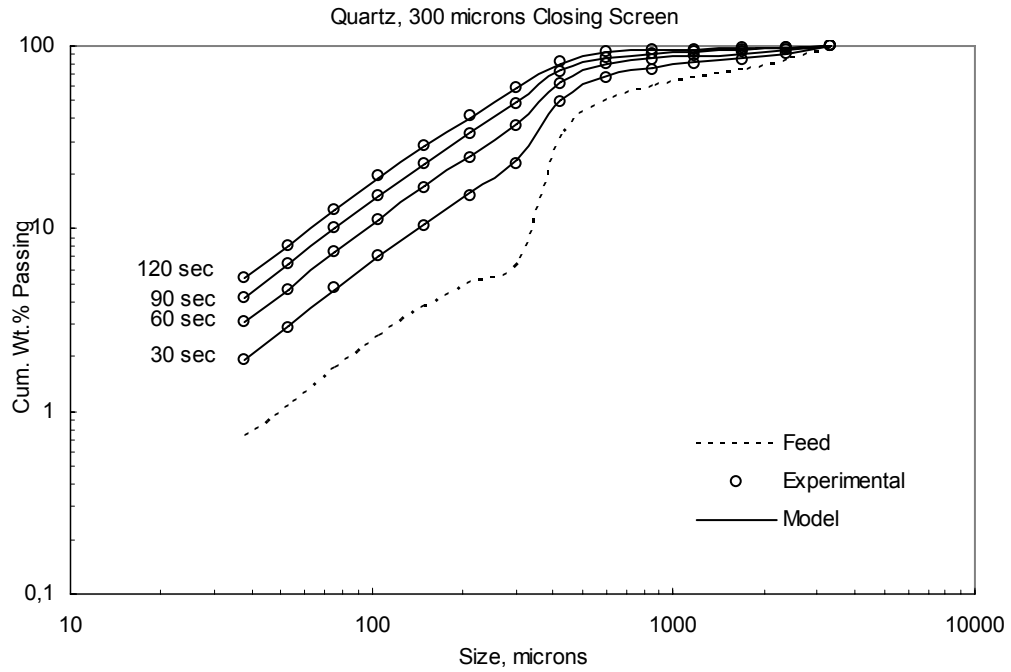


**Figure 6.46.** The experimental and predicted size distributions for quartz feed generated by 300  $\mu\text{m}$  closing screen, and its products for short grinding times

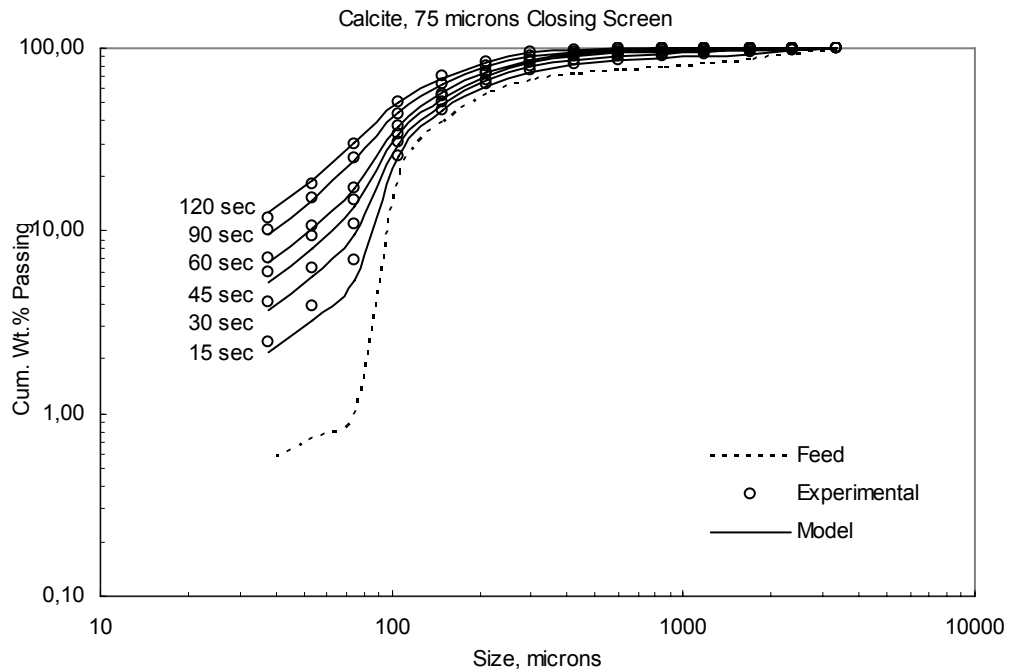


**Figure 6.47.** The experimental and predicted size distributions for calcite feed generated by 75  $\mu\text{m}$  closing screen, and its products for short grinding times

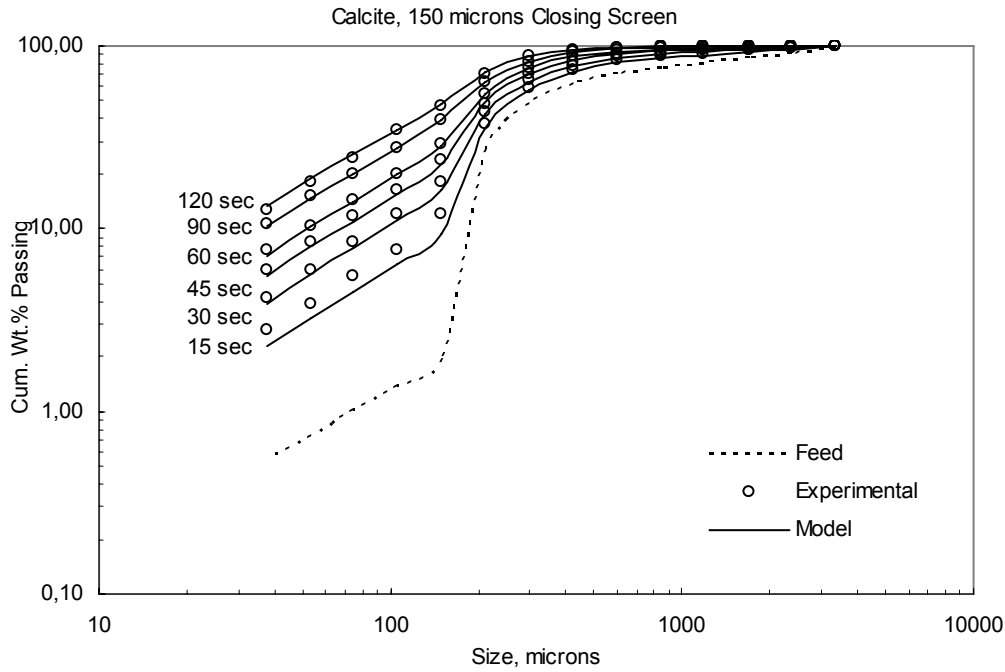


**Figure 6.48.** The experimental and predicted size distributions for calcite feed generated by 150  $\mu\text{m}$  closing screen, and its products for short grinding times

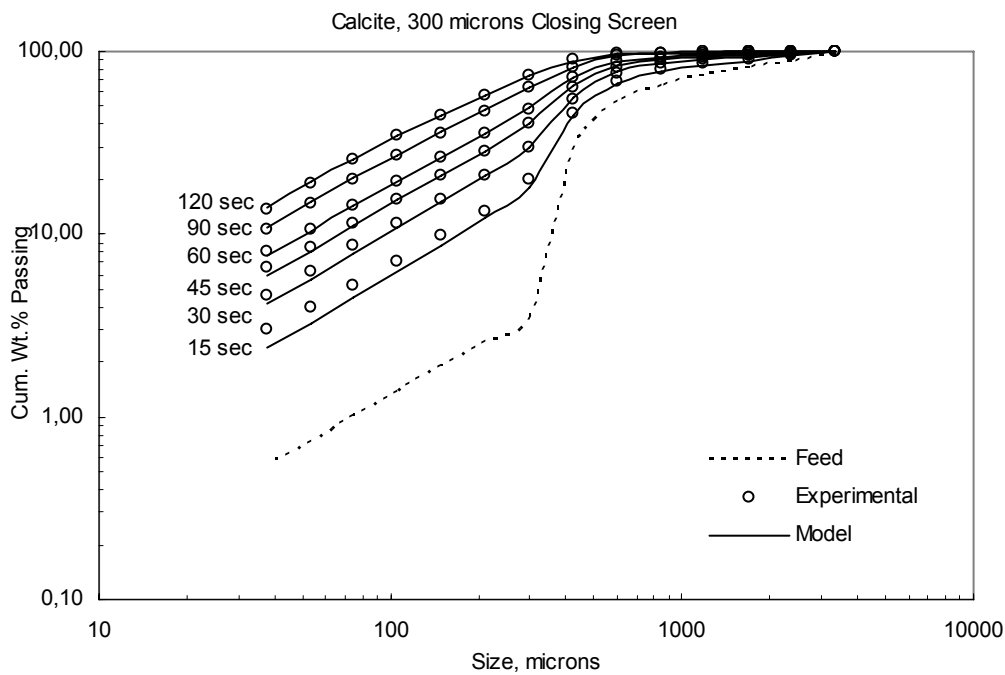


**Figure 6.49.** The experimental and predicted size distributions for calcite feed generated by 300  $\mu\text{m}$  closing screen, and its products for short grinding times

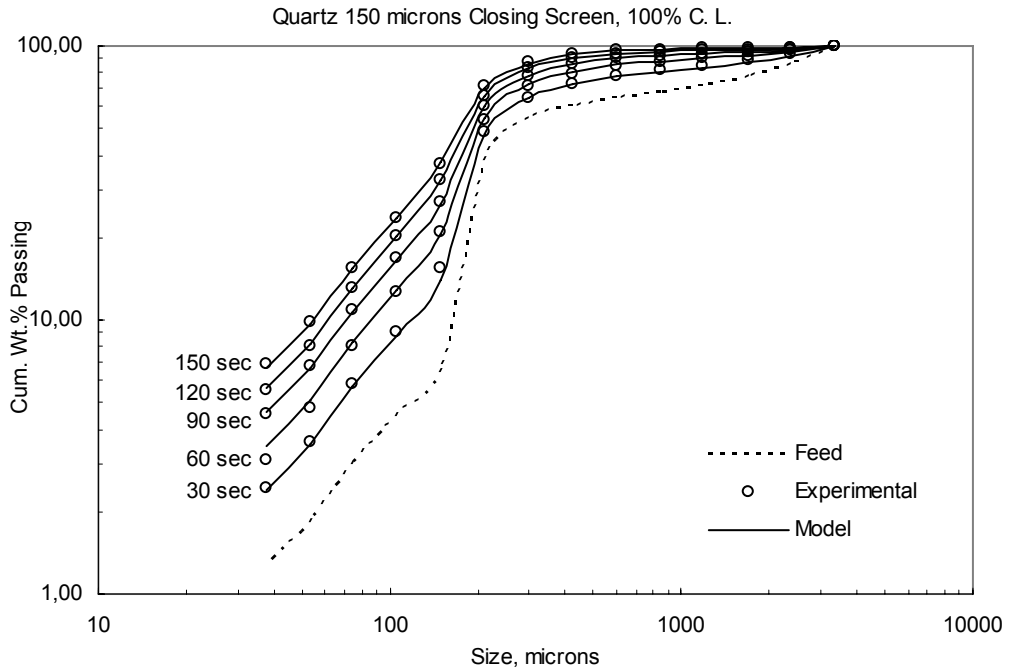


**Figure 6.50.** The experimental and predicted size distributions for quartz feed generated by 150  $\mu\text{m}$  closing screen at 100% circulating load, and its products for short grinding times

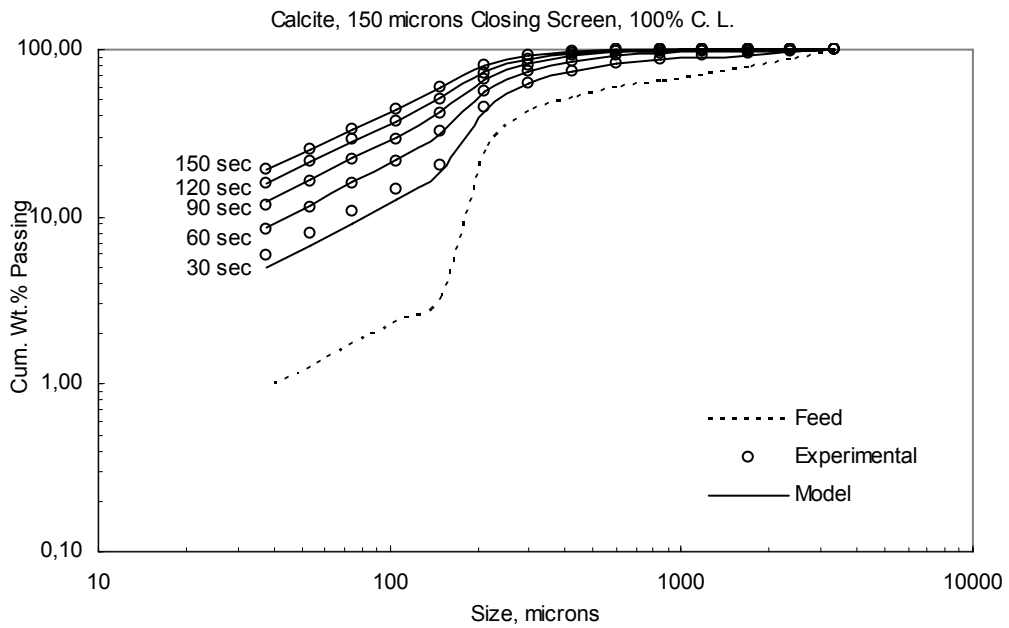


**Figure 6.51.** The experimental and predicted size distributions for calcite feed generated by 150  $\mu\text{m}$  closing screen at 100% circulating load, and its products for short grinding times

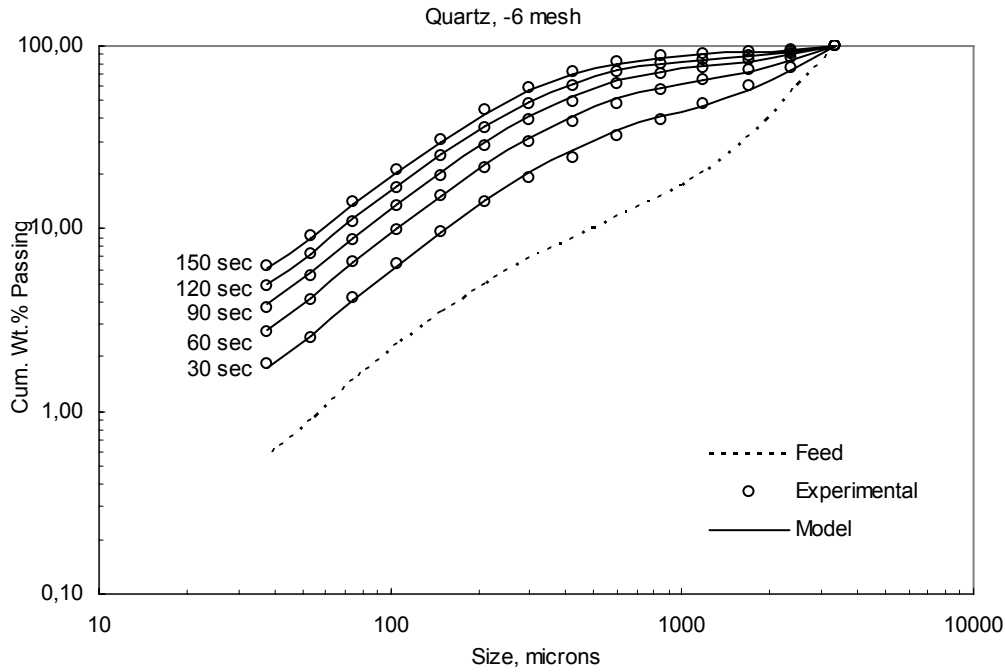


**Figure 6.52.** The experimental and predicted size distributions for -6 mesh quartz feed, and its products for short grinding times

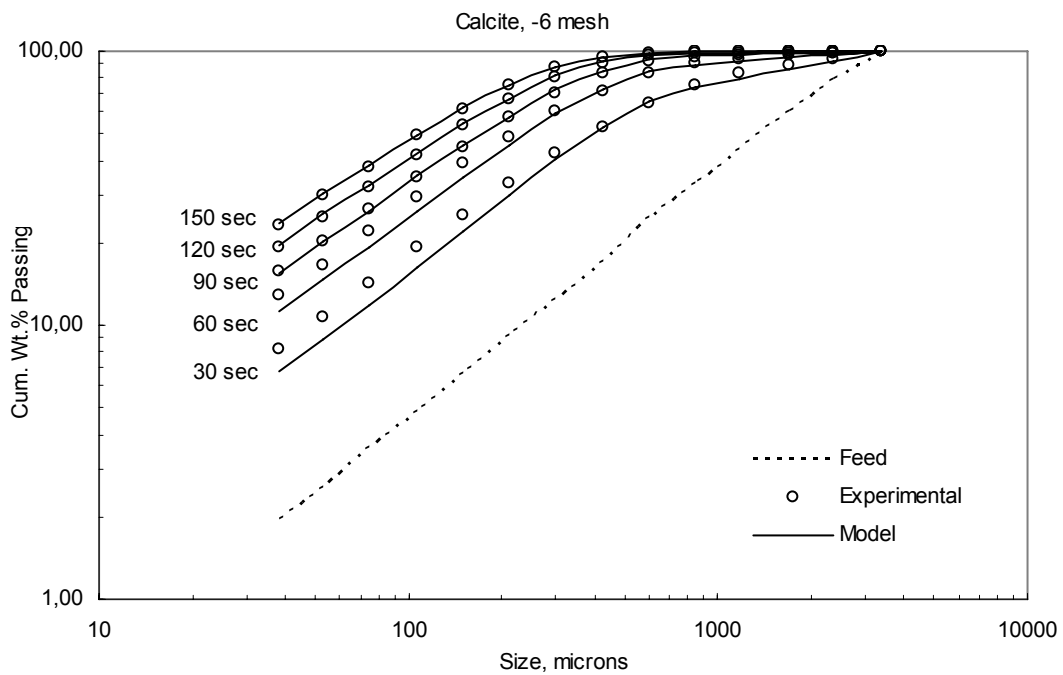


**Figure 6.53.** The experimental and predicted size distributions for -6 mesh calcite feed, and its products for short grinding times

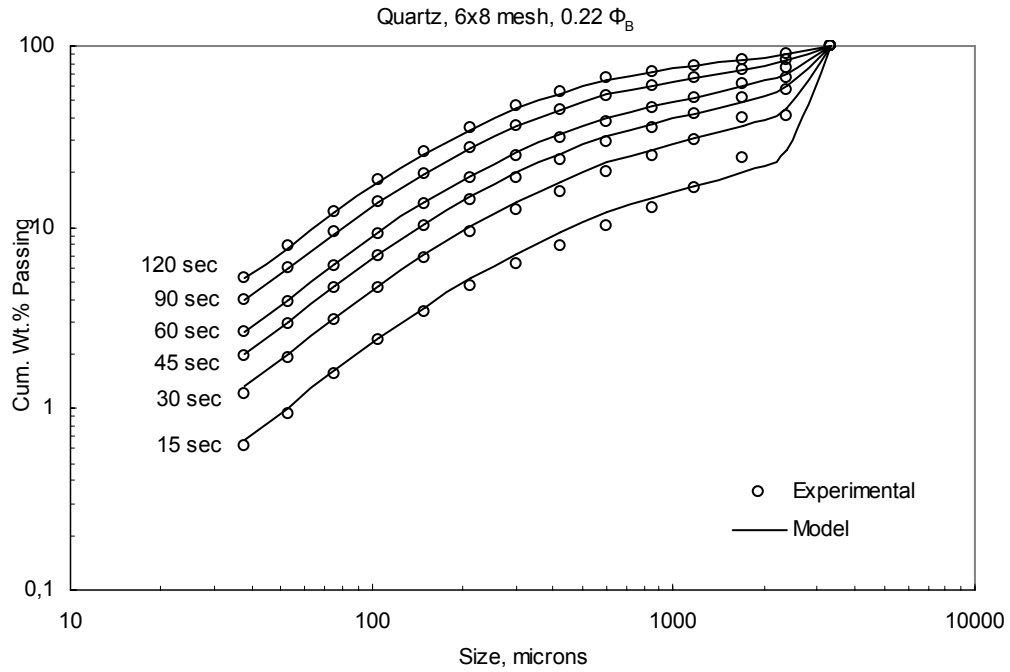


**Figure 6.54.** The experimental and predicted size distributions for 6x8 mesh quartz products for short grinding times at 0.22  $\Phi_B$

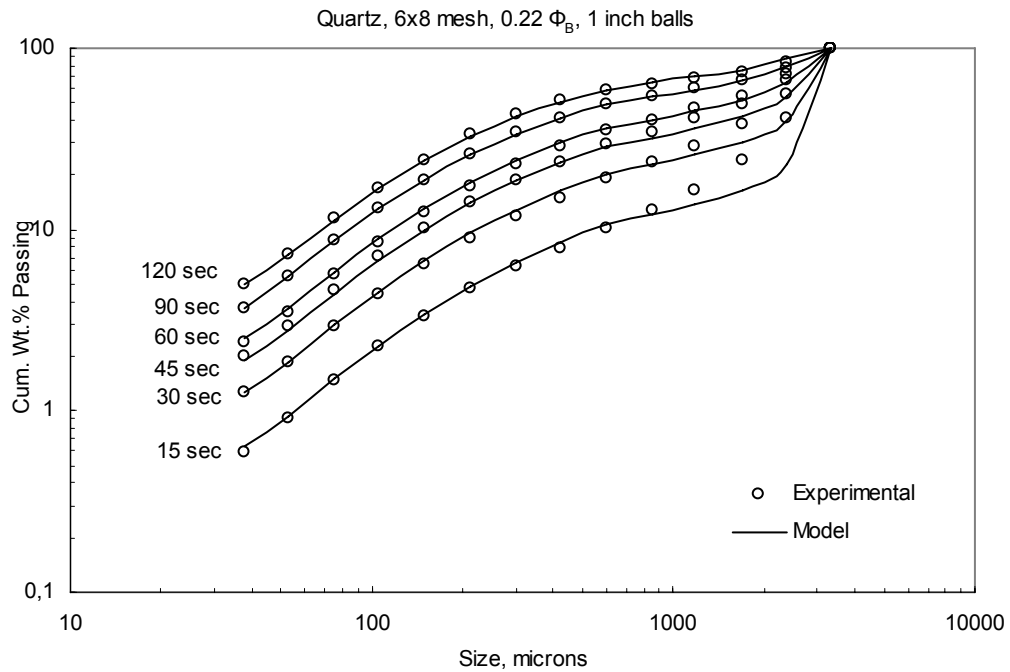


**Figure 6.55.** The experimental and predicted size distributions for 6x8 mesh quartz products for short grinding times at 0.22  $\Phi_B$ , 1 inch balls.

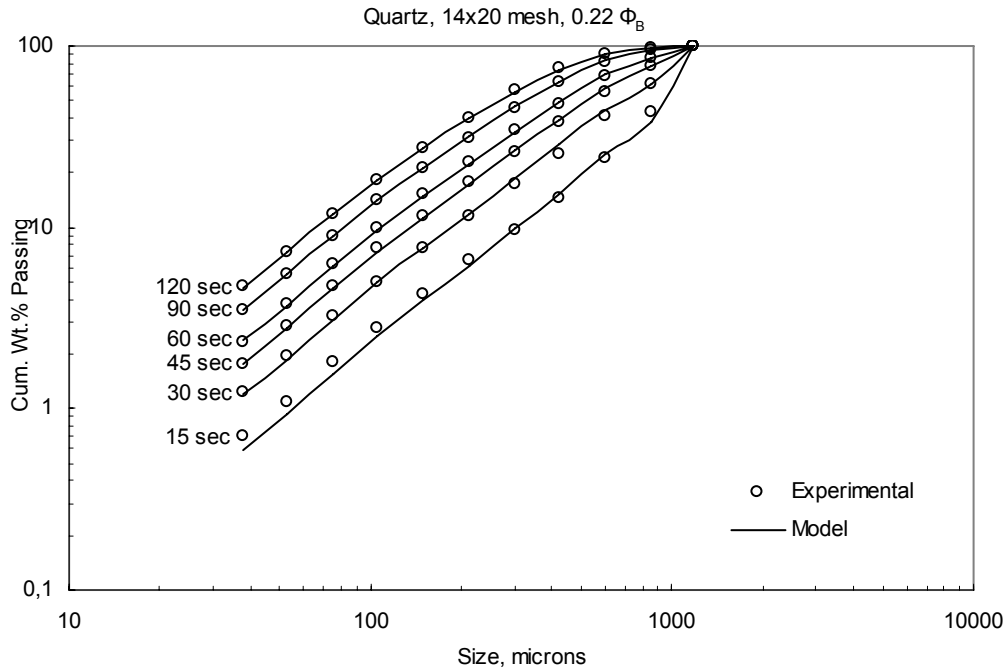


**Figure 6.56.** The experimental and predicted size distributions for 14x20 mesh quartz products for short grinding times at 0.22  $\Phi_B$

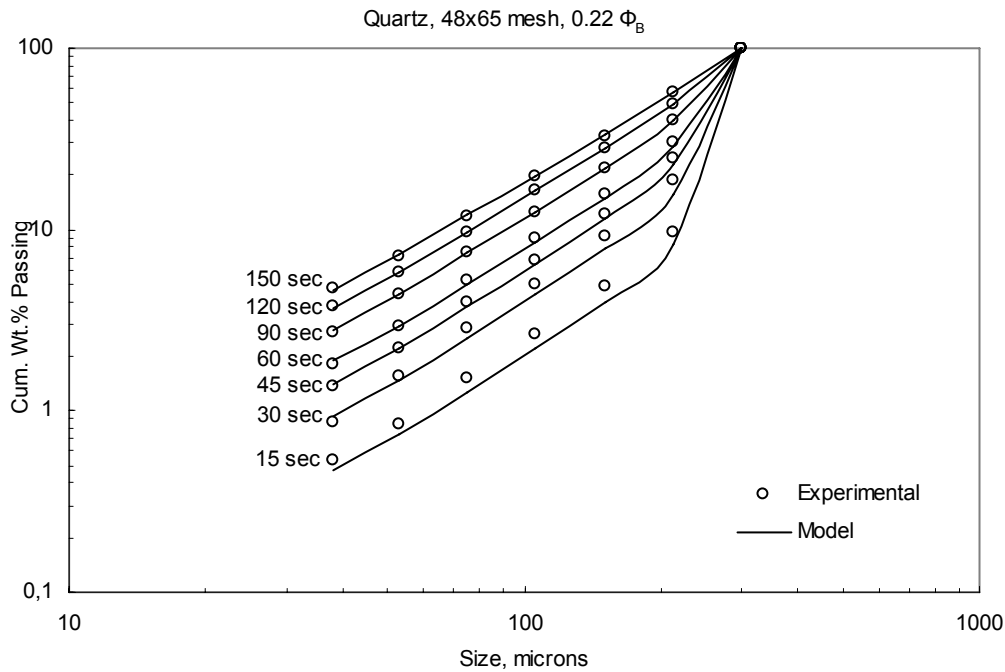


**Figure 6.57.** The experimental and predicted size distributions for 48x65 mesh quartz products for short grinding times at 0.22  $\Phi_B$

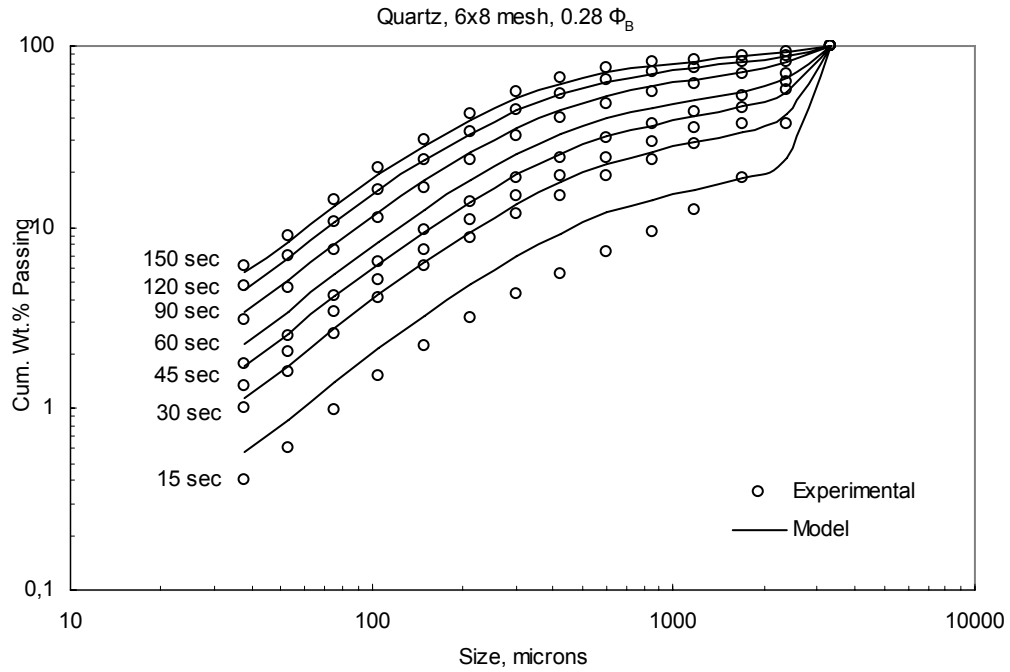


**Figure 6.58.** The experimental and predicted size distributions for 6x8 mesh quartz products for short grinding times at 0.28  $\Phi_B$

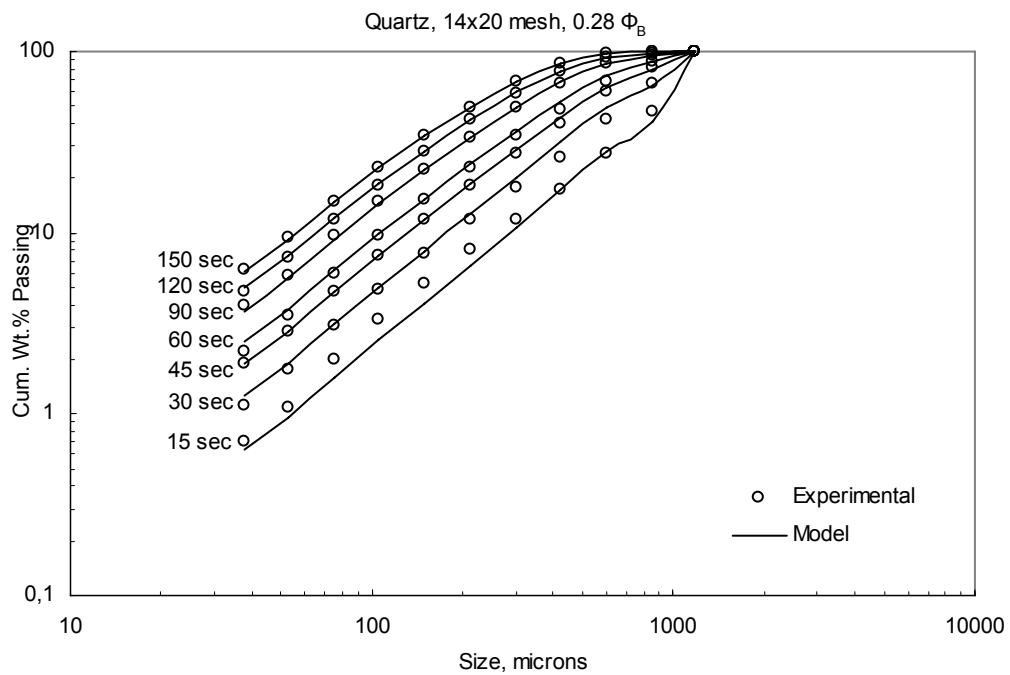


**Figure 6.59.** The experimental and predicted size distributions for 14x20 mesh quartz products for short grinding times at 0.28  $\Phi_B$

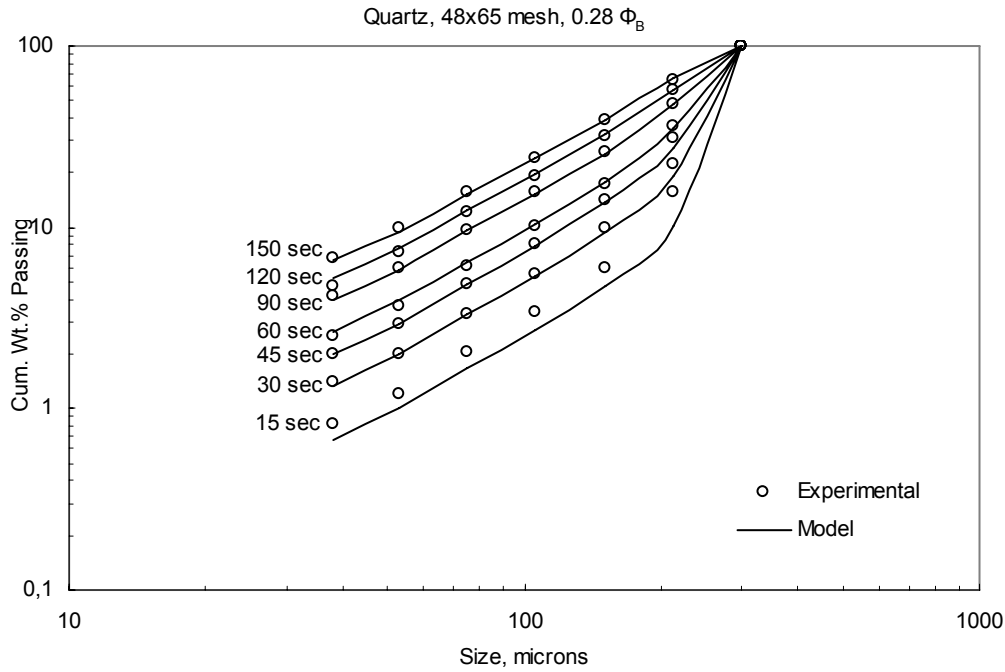


**Figure 6.60.** The experimental and predicted size distributions for 48x65 mesh quartz products for short grinding times at  $0.28 \Phi_B$

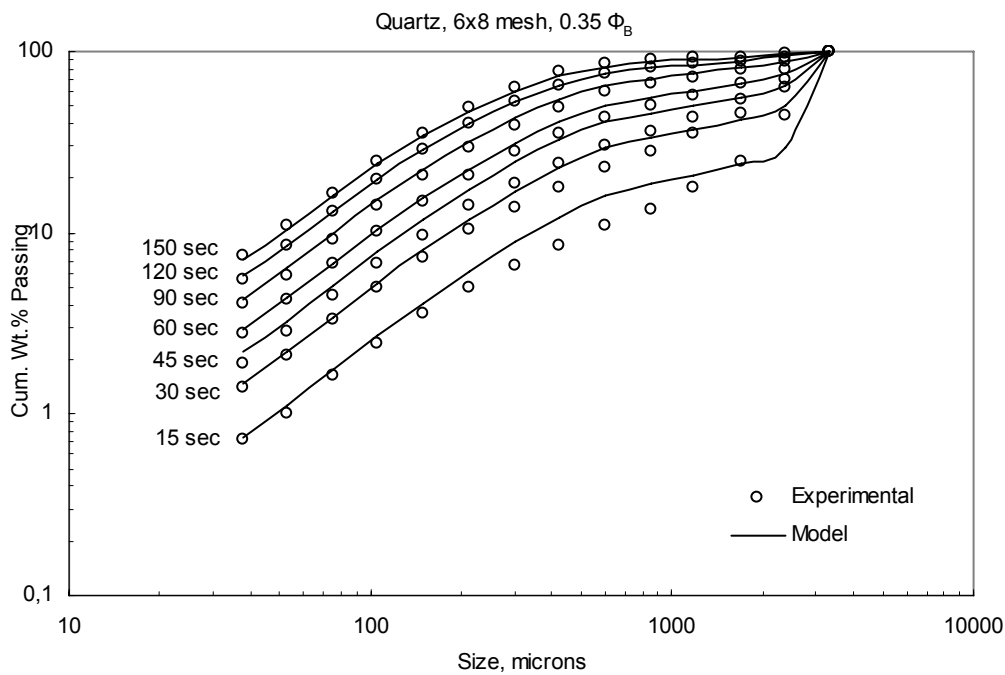


**Figure 6.61.** The experimental and predicted size distributions for 6x8 mesh quartz products for short grinding times at  $0.35 \Phi_B$

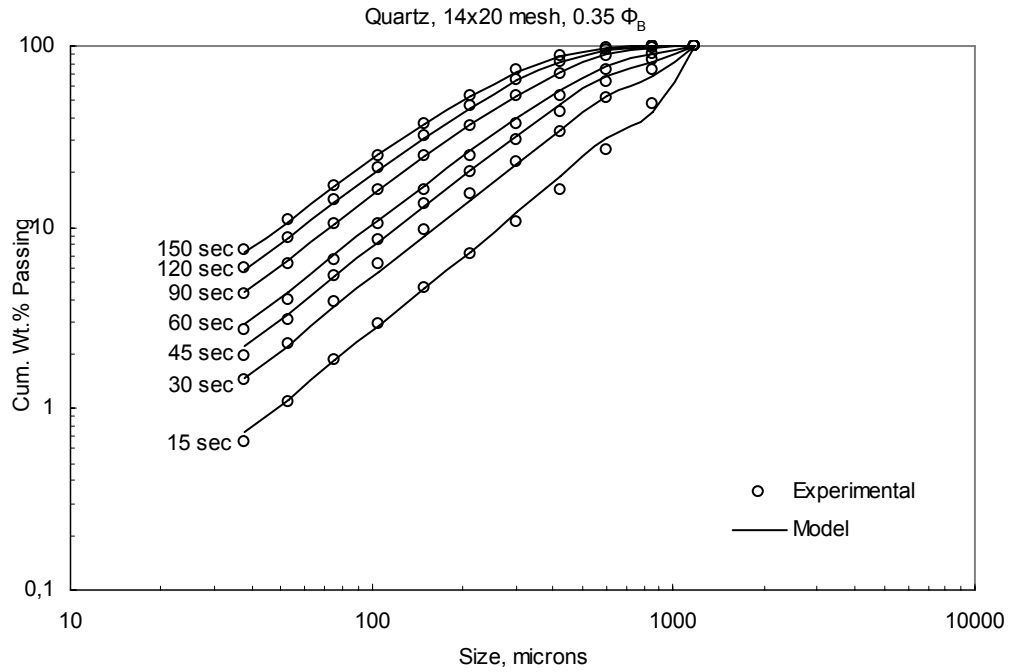


**Figure 6.62.** The experimental and predicted size distributions for 14x20 mesh quartz products for short grinding times at 0.35  $\Phi_B$

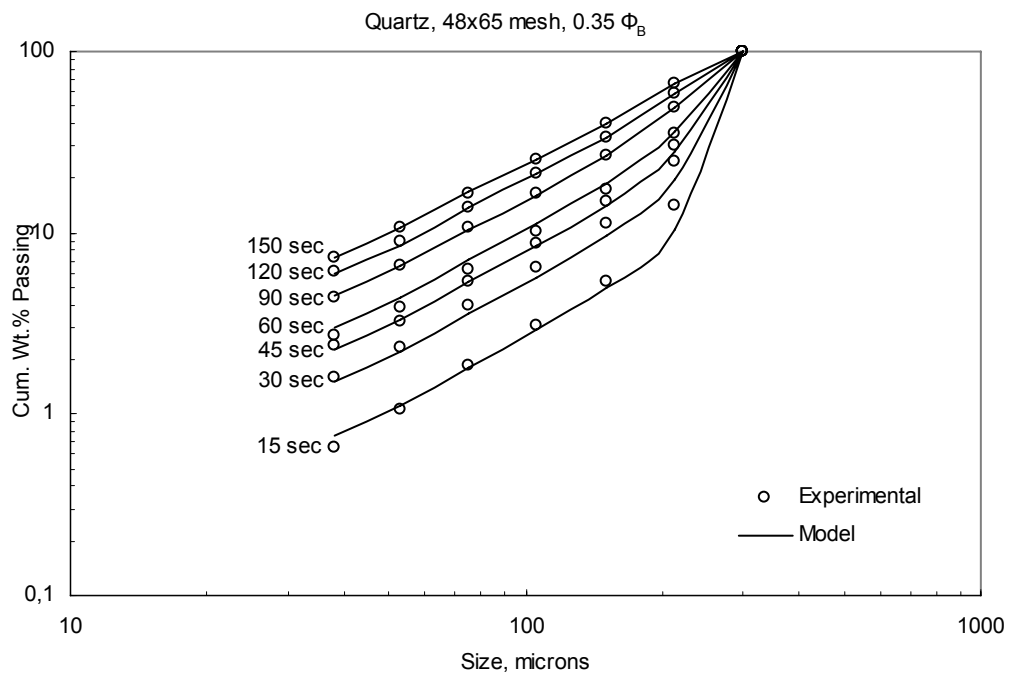


**Figure 6.63.** The experimental and predicted size distributions for 48x65 mesh quartz products for short grinding times at 0.35  $\Phi_B$

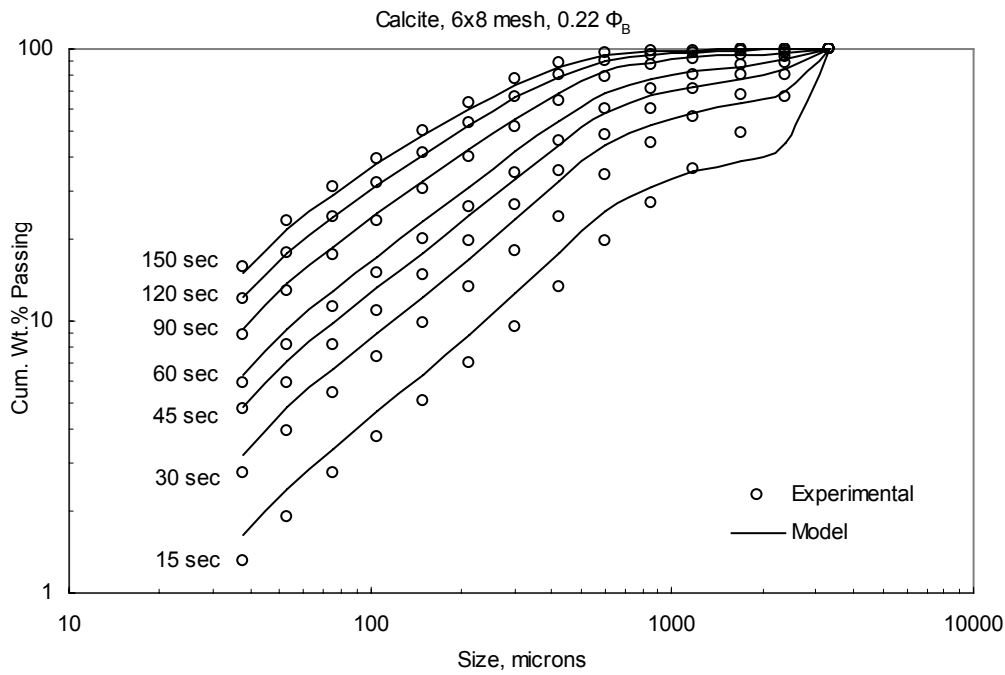


**Figure 6.64.** The experimental and predicted size distributions for 6x8 mesh calcite products for short grinding times at  $0.22 \Phi_B$

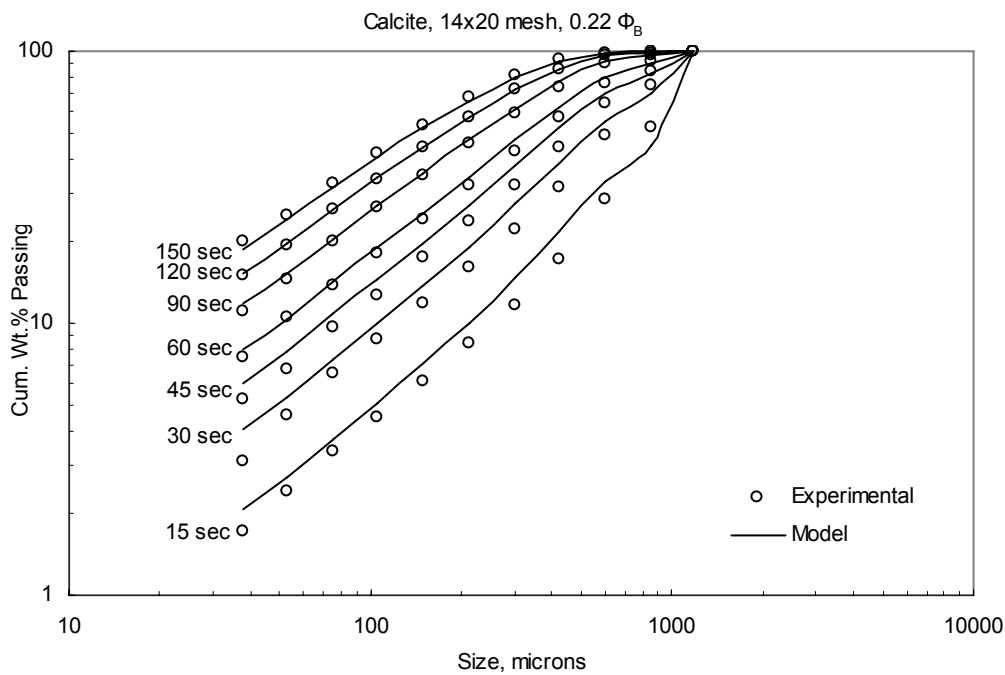


**Figure 6.65.** The experimental and predicted size distributions for 14x20 mesh calcite products for short grinding times at  $0.22 \Phi_B$

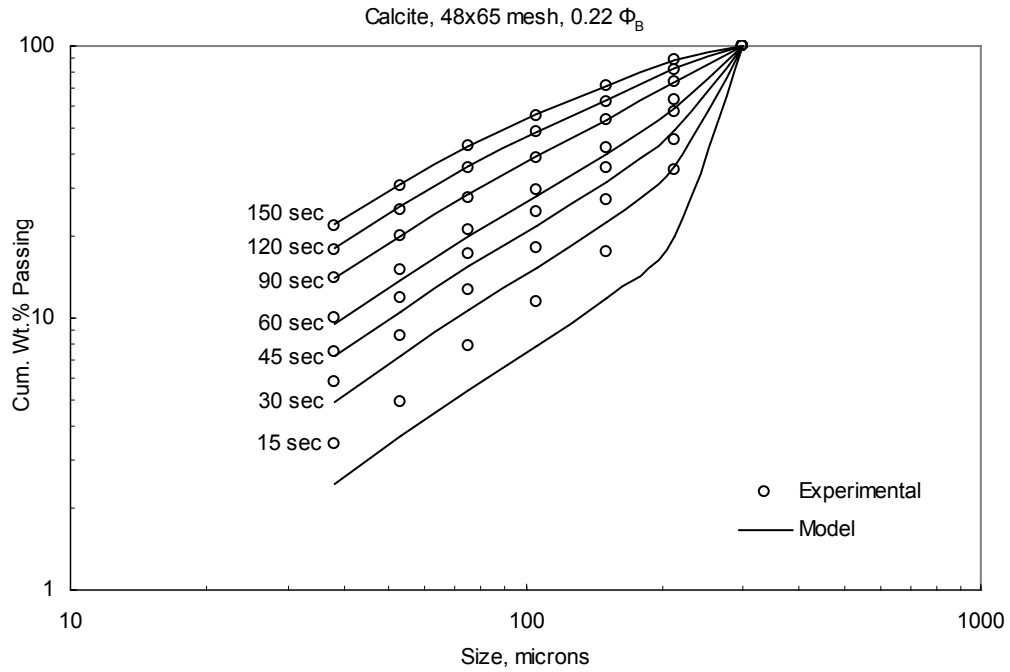


**Figure 6.66.** The experimental and predicted size distributions for 48x65 mesh calcite products for short grinding times at 0.22  $\Phi_B$

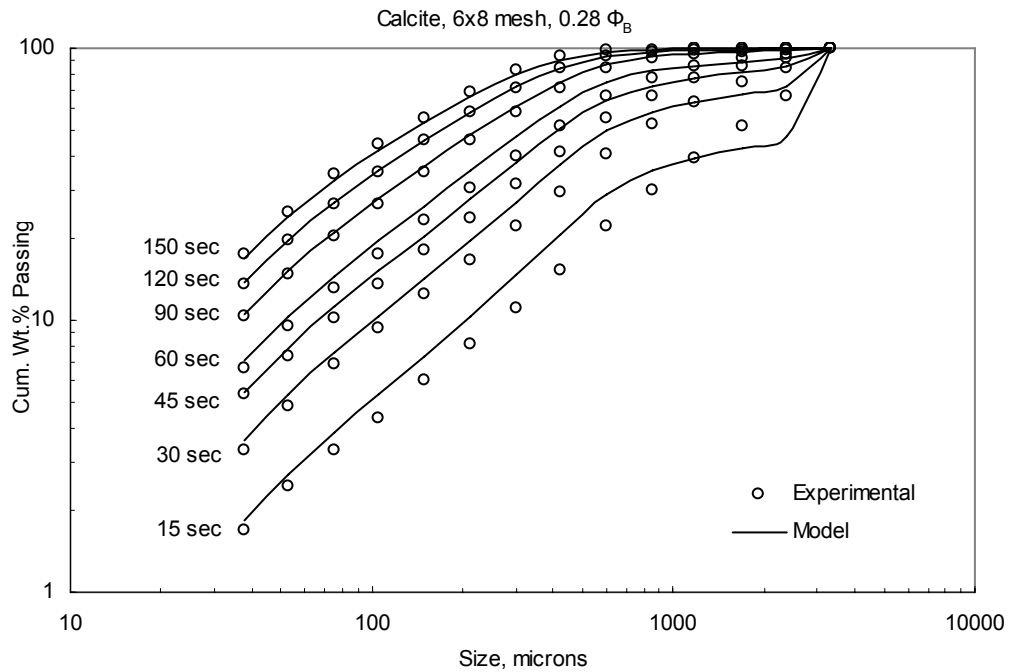


**Figure 6.67.** The experimental and predicted size distributions for 6x8 mesh calcite products for short grinding times at 0.28  $\Phi_B$

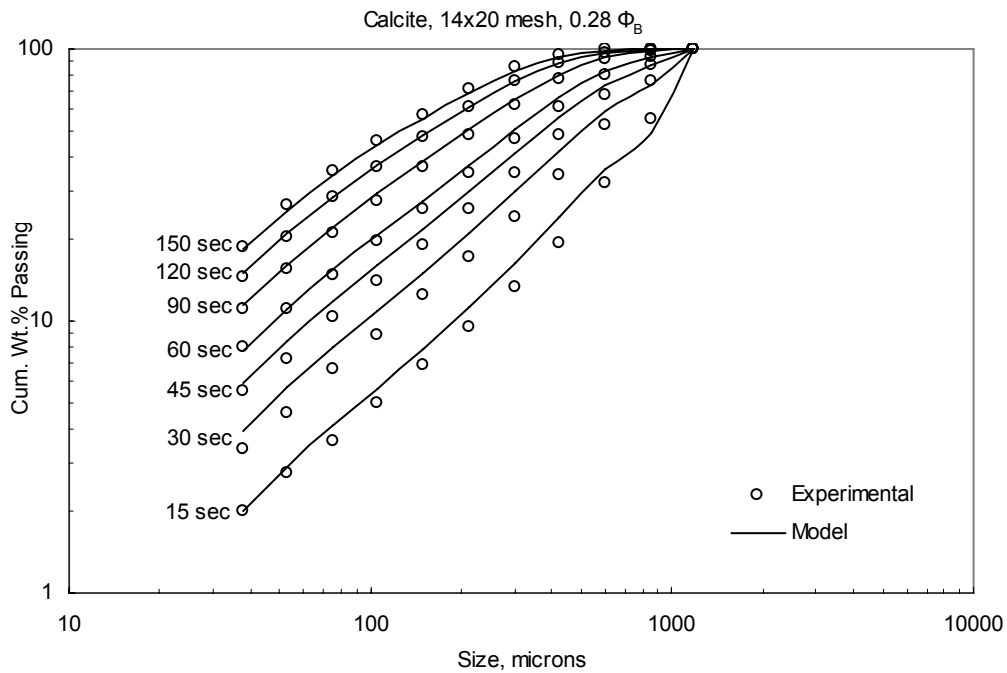


**Figure 6.68.** The experimental and predicted size distributions for 14x20 mesh calcite products for short grinding times at  $0.28 \Phi_B$

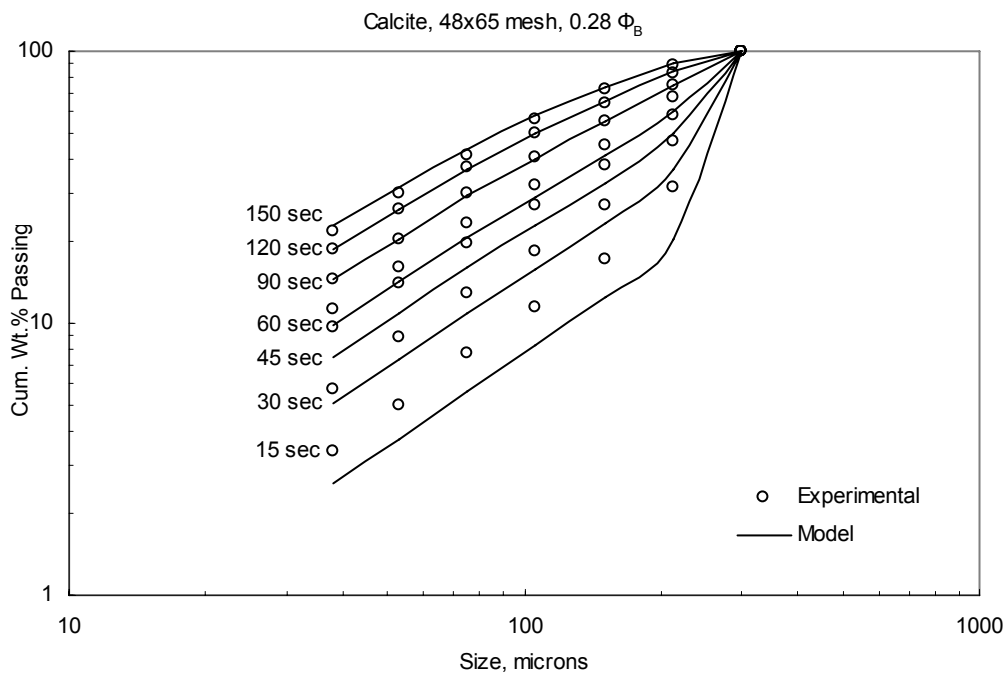


**Figure 6.69.** The experimental and predicted size distributions for 48x65 mesh calcite products for short grinding times at  $0.28 \Phi_B$

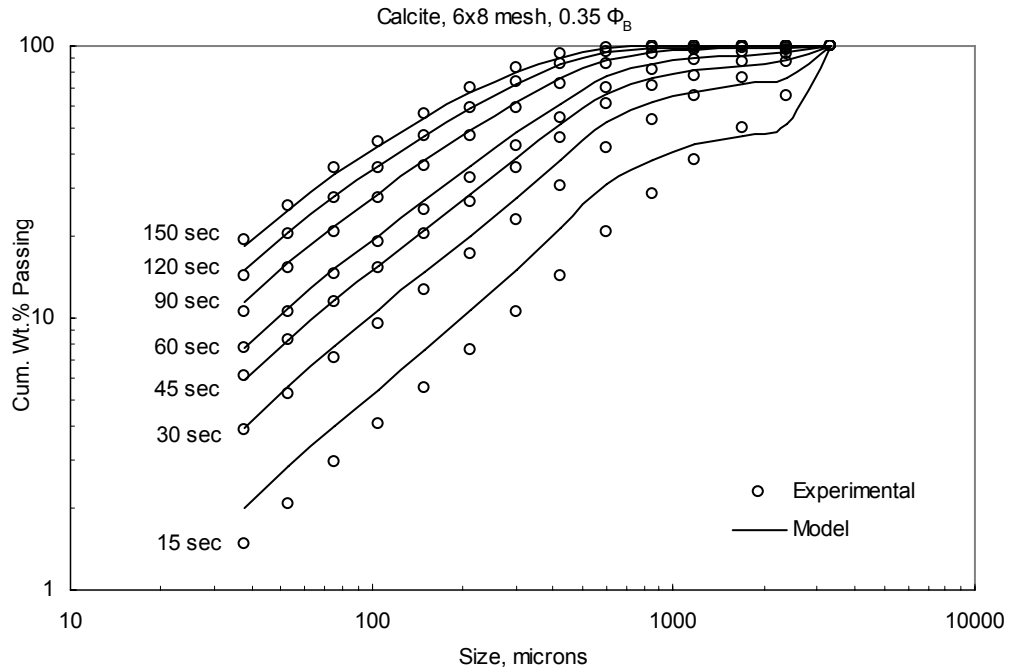


**Figure 6.70.** The experimental and predicted size distributions for 6x8 mesh calcite products for short grinding times at  $0.35 \Phi_B$

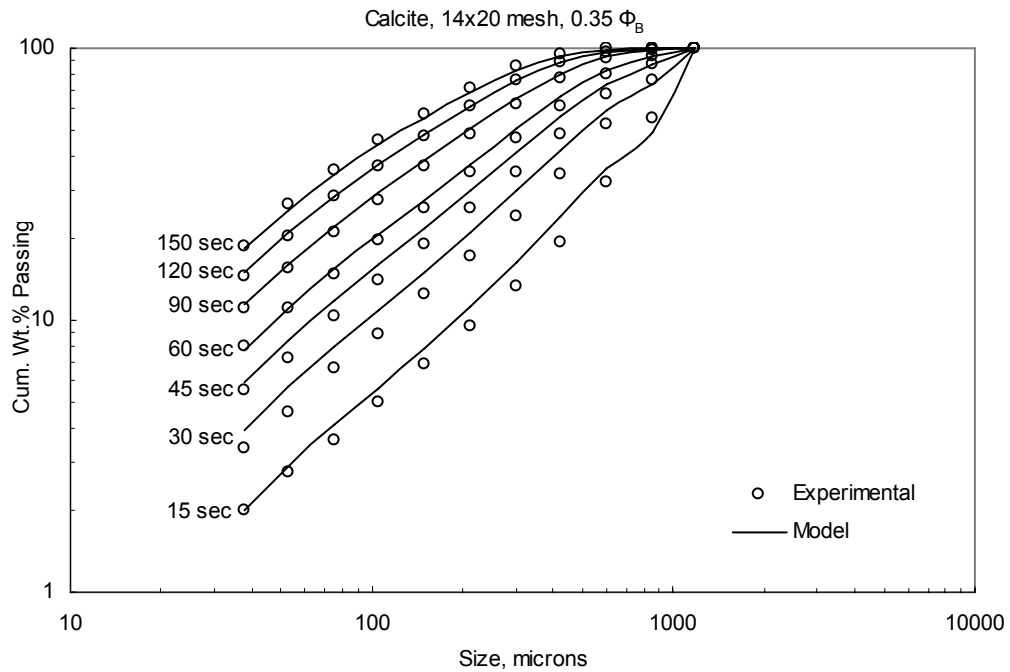


**Figure 6.71.** The experimental and predicted size distributions for 14x20 mesh calcite products for short grinding times at  $0.35 \Phi_B$

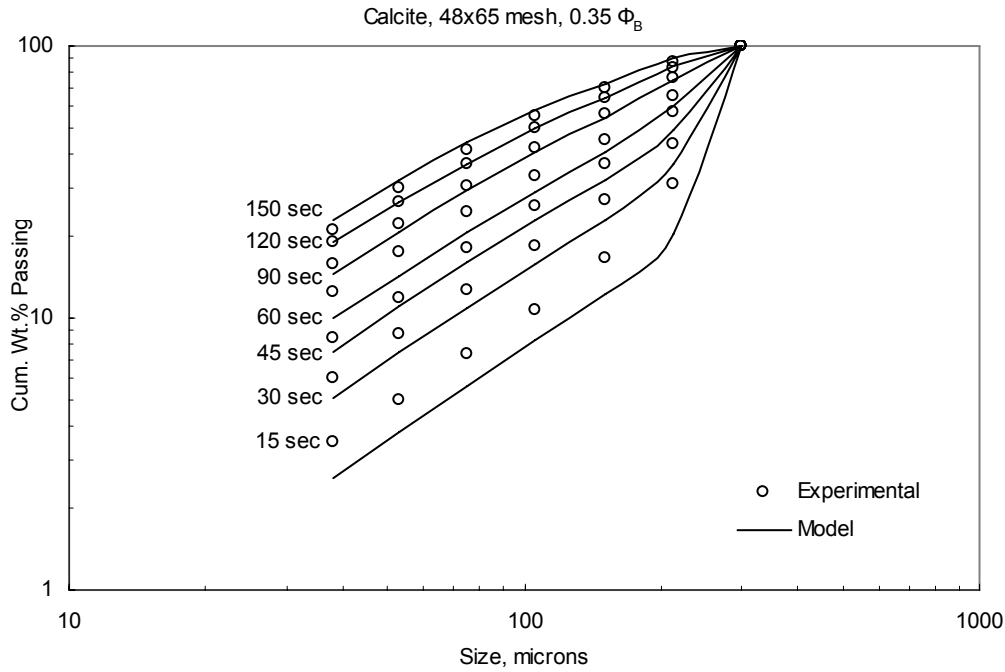


**Figure 6.72.** The experimental and predicted size distributions for 48x65 mesh calcite products for short grinding times at  $0.35 \Phi_B$

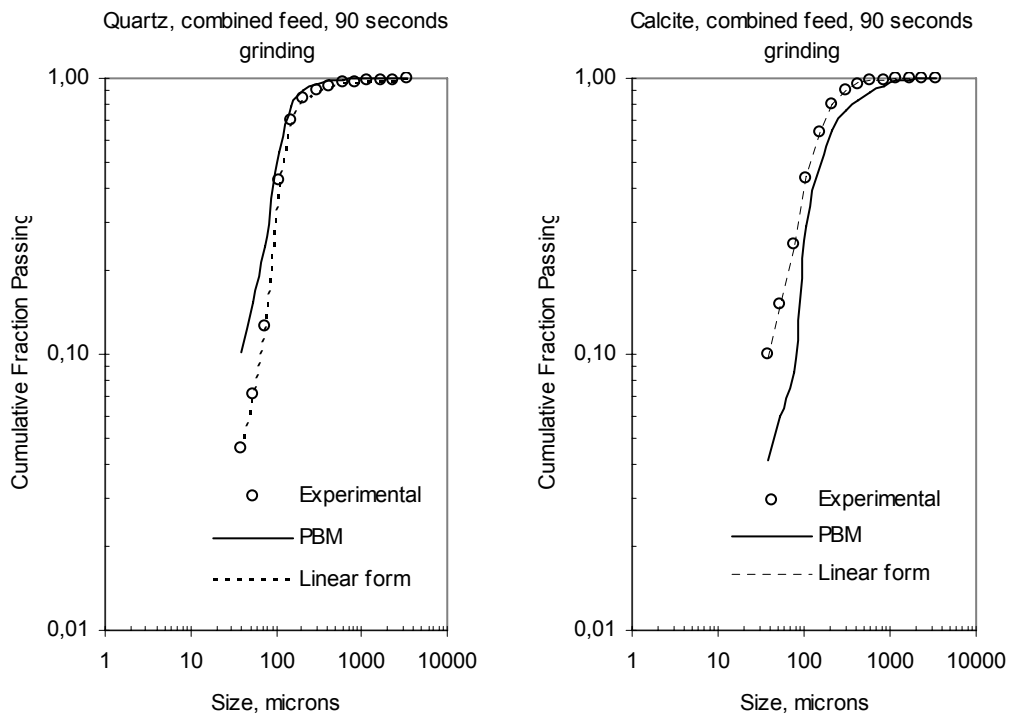


**Figure 6.73.** The experimental and predicted (PBM and Linear form) size distributions for 6x8 mesh quartz and calcite products for 90 seconds grinding time at  $0.22 \Phi_B$

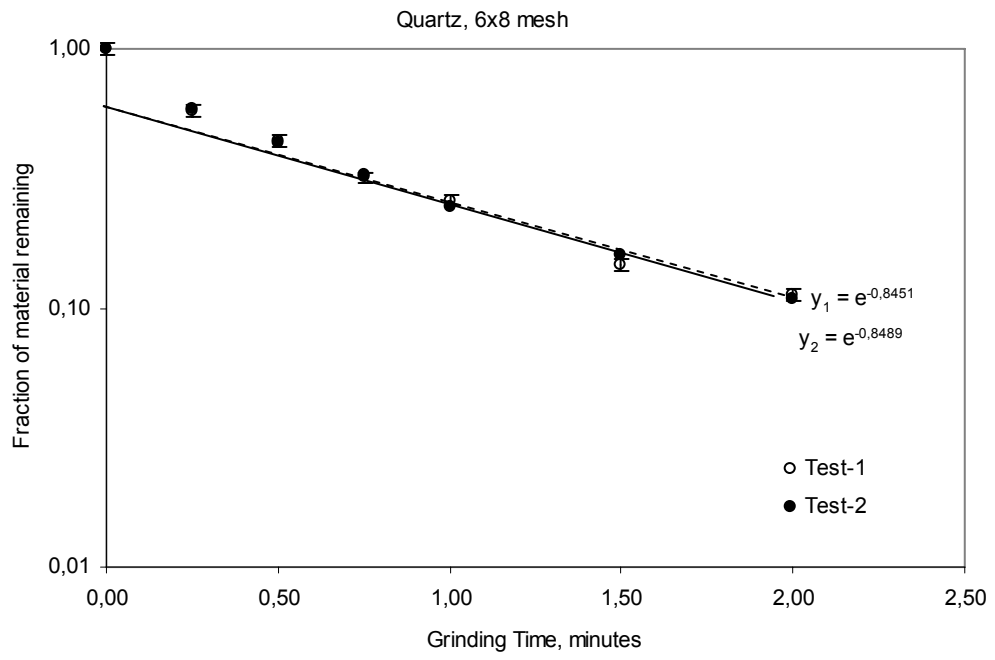


**Figure 6.74.** The repeatability of 6x8 mesh quartz short-time grinding test



## CHAPTER 7

### CONCLUSION

The particle breakage parameters of population balance model in closed-cycle ball milling were investigated in the Bond mill which was operated in different grinding conditions simulating the industrial milling applications. The reliability of the linear batch grinding model was evaluated. The power draw of the mill was measured during the experiments. The most appropriate breakage parameter estimation method for milling was determined. The major findings of the thesis are presented below:

The effects of grinding media and material charge dynamics on torque and power draw of the laboratory scale Bond ball mill were investigated under dry grinding conditions. Results showed that grinding media consisting of smaller balls drew more power because of higher friction. Similarly, aged balls drew more power than new ones because of the same reason. Mill speed did not affect the torque up to the critical speed, while it directly affected the power draw. At material fillings above 0.4, the mill torque decreased with increasing material filling for the ball loads of 30% and higher (up to 45%). The mill constant  $K$  of Morrell's empirical power equation was found to be 9.35 when no material was charged. However, the power equation is not valid for high material (above  $0.4 \Phi_M$ ) and high ball charges (above  $0.35 \Phi_B$ ). Fineness of the material affected the mill torque. At material fillings less than 0.4, the torque decreased with increasing grinding time (increasing fineness); but at higher material fillings, the torque decreased first and then increased again towards its steady value.

$\Phi_M = 0.40$  and  $\Phi_B = 0.30$  are the optimum operating conditions for the Bond ball mill. For different ball loadings, most efficient material filling conditions change between 0.40-0.60.

Three existing methods for the estimation of breakage distribution functions, namely, zero-order production of fines, BII and G-H, were compared and evaluated by plotting the  $B_{ij}$ 's of three one-size-fraction quartz feeds ground with both 1-inch and Bond ball charges. Time and breakage rate function restricted zero-order production of fines method fails at coarse sizes where abnormal breakage occurs. Moreover, it is difficult to determine the  $F_i$  values of zero-order method since the time that should be used in calculations is not exact for all the particle sizes. BII and G-H methods showed very close results to each other at coarsest and finest feed sizes although BII method is considered to be time restricted special case of G-H method (Kapur, 1982). G-H method provided more reliable results for a wide range of operating conditions as it is not time-restricted. The  $B_{ij}$  estimation methods showed dissimilarities in behavior at different feed sizes. This finding may be one of the reasons for the disagreements in the literature on the grinding kinetics of materials. On the other hand, all the  $B_{ij}$  estimation methods pointed out that  $B_{ij}$  of feed material depends on particle size and grinding media charge.

For both materials studied, the rate of grinding of coarsest fraction, 6x8 mesh, increased as the test sieve aperture becomes smaller, and, accordingly, the proportion of fine fraction in the mill increased. This means that the presence of fines enhances the grinding of coarse particles. The fines have little resistance to the falling balls at the grinding zone. Then, the energy associated with the falling ball is mostly consumed in the breakage of coarse particle. The specific energy consumed by the coarse particles increases as the initial fraction of coarse material in the feed decreases. This is the main reason for the increment in breakage rates with the decrease in the amount of coarse material in the feed.

The breakage rate functions are higher for 0.35  $\Phi_B$  compared to lower fractional charges since the number of collisions ending with breakage increases with increasing  $\Phi_B$  up to a certain point. There is no significant effect of  $\Phi_B$  on  $B_{ij}$ . The effect of specific grinding energy could not be observed since the variation of specific energy without changing the mill speed was insufficient in the tested range of operating conditions in the mill.

The Bond ball size distribution is more effective in grinding than 1 inch ball charge. The effect of ball charge was observed on both of the breakage parameters for 6x8 mesh quartz feed. However, even though there was no significant difference in breakage rate functions for 14x20 and 48x65 mesh quartz feeds, the  $B_{ij}$  values presented slightly finer size distributions when they were ground with Bond ball size distribution.

The variation of percent circulating load between 100% and 350% did not change the breakage rate functions significantly as variation of the material composition in the mill for this range is marginal.

Although  $B_{ij}$  is non-normalizable by size, it can be considered to be normalizable for quartz mineral in which the breakage rate functions of lower fractions are negligibly small.

According to the G-H method, the breakage parameters are not independent of each other.  $B_{ij}$  and  $K_1$  are utilized to determine  $K_i$  values for lower fractions. By utilizing this method a reasonable accuracy was achieved for the prediction of product size distribution of 6x8 mesh quartz mineral for 1.5 minutes of grinding time. It was thought that the environment independent  $B_{ij}$  may be utilized for the same size of feed ground in a milling environment having a size distribution. However, utilizing the same  $B_{ij}$  for the prediction of product size distribution of 6x8 mesh quartz ground in steady state milling environment failed at lower size fractions. This failure can not be attributed to  $K_i$  only as it is determined via  $B_{ij}$ . This means that  $B_{ij}$  of one-size-fraction feed cannot be satisfactorily used for the same material ground in a different milling environment.

It is more convenient to limit the grinding time by a few minutes in the researches done for investigating the grinding kinetics of material rather than using long time of grinding data since more than 50% of materials was reduced down to around 100 microns in a few minutes even the material was quartz.

The grinding kinetics of materials can be evaluated by the use of a single parameter using linear form of size discretized batch grinding equation as compensation condition is valid especially below 1 mm. Instead of describing grinding kinetics of materials by two breakage parameters, the use of single cumulative breakage rate parameter seemed to be both more practical and reliable. Furthermore, even for the materials which show abnormal breakage for the very first times of grinding, linear batch grinding equation provided reasonable estimations for 2.5 minutes of grinding time.

## REFERENCES

- Austin, L. G.; Bagga, P., 1981. An analysis of fine dry grinding in ball mills, *Powder Technology*, 28, 83-90.
- Austin, L. G.; Bagga, P.; Çelik, M., 1981. Breakage properties of some materials in a laboratory ball mill, *Powder Technology*, 28, 235-243.
- Austin, L. G.; Klimpel, R. R.; Luckie, P. T., 1984, *Process engineering of size reduction: Ball milling*, Society of mining engineering, AIME. 561 p.
- Austin, L. G.; Luckie, P. T., 1972. Methods for determination of breakage distribution parameters, *Powder Technology*, 5, 4, 215-222.
- Austin, L. G., Shoji, K., Bell, D., 1982. Rate equations for non-linear breakage in mills due to material effects. *Powder Technology*, Vol. 31, 127-133.
- Avşar, Ç., 2003. Breakage characteristics of cement components, Ph.D. Thesis, Mining Engineering Department, Middle East Technical University, Ankara, Turkey.
- Bond, F. C., 1952. The third theory of comminution, *Transactions AIME*, 193, 484-494.
- Bond, F. C., 1961. Crushing and grinding calculations, Part I-II, *British Chemical Engineering*, 6, 378-385, 543-548.
- Charles, R. J., 1957. Energy-size reduction relationships in comminution, *Transactions AIME, Mining Engineering*, 9, 80-88.
- Comminution-Theory and Practice. Society for Mining Metallurgy and Exploration, ed. Kawatra, S. K., Cussing-Malloy, Inc., Ann Arbor, MI, US.
- Daniel, M. J., 2006, Measurements of electrical energy consumption in a Bond ball mill, *Proceedings of the XXIII. International Mineral Processing Congress*, 3-8 September, Istanbul, G. Önal et al. (eds.), 1, 92-97.
- Encyclopædia Britannica, Hooke's Law., *Encyclopædia Britannica Online Academic Edition*. Encyclopædia Britannica Inc., 2012. Web. 10 July. 2012.
- Epstein, B., 1948. The logarithmico-normal distributions in breakage of solids. *Ind. Eng. Chem.*, 40, 2289-2291.
- Erdem, A. S.; Ergün, Ş. L., 2009. The effect of ball size on breakage rate parameter in a pilot scale ball mill, *Minerals Engineering* 22, 660-664.
- Fuerstenau, D. W., Abouzeid, A.-Z. M., 1991. Effect of fine particles on the kinetics and energetics of grinding coarse particles. *Int. Journal of Mineral Processing*, Vol. 31, 151-162.
- Fuerstenau, D. W., Abouzeid, A.-Z. M., 2002. The energy efficiency of ball milling in comminution. *Int. Journal of Mineral Processing*, Vol. 67, 161-185.

- Fuerstenau, D. W., Abouzeid, A.-Z. M., Phatak, P. B., 2010. Effect of particulate environment on the kinetics and energetics of dry ball milling. *Int. Journal of Mineral Processing*, Vol. 97, 52-58.
- Fuerstenau, D. W., Phatak, P. B., Kapur, P. C., Abouzeid, A.-Z. M., 2011. Simulation of the grinding of coarse/fine (heterogeneous) systems in a ball mill. *Int. Journal of Mineral Processing*, Vol. 99, 32-38.
- Fuerstenau, D. W., De, A., Kapur, P. C., 2004. Linear and nonlinear particle breakage processes in comminution systems. *International Journal of Mineral Processing*, 74S, 317-327.
- Griffith, A. A., 1921. The phenomena of rupture and flow in solids, *Philosophical Transactions. Royal Society*, 221, 163-198.
- Gumtz, G. D., and Fuerstenau D. W., 1970. Simulation of locked-cycle grinding. *Trans. Society of Mining Engineers, AIME*, 247, 330-335.
- Herbst, J. A., and Fuerstenau, W. D., 1973. Mathematical simulation of dry ball milling using specific power information. *Trans. Society of Mining Engineers, AIME*, 254, 343-348.
- Herbst, J. A.; Fuerstenau, D. W., 1968. The zero order production of fine sizes in comminution and its implications in simulation, *Trans. SME/AIME*, 241, 538-549.
- Herbst, J.A.; Fuerstenau, D.W., 1980, Scale-up procedure for continuous grinding mill design using population balance models, *Int. J. Miner. Process.*, 1-31.
- Hoşten, Ç., and Avşar, Ç., 2004. Variation of back-calculated breakage rate parameters in Bond-mill grinding. *Scandinavian Journal of Metallurgy*, 00: 1-8.
- Jankovic, A.; Dundar, H.; Mehta, R., 2010. Relationships between comminution energy and product size for a magnetite ore, *The Journal of the Southern African Institute of Mining and Metallurgy*, 110, 141-146.
- Kapur, P. C., 1982. An improved method for estimating the feed-size breakage distribution functions. *Powder Technology*, Vol. 33, 269-275.
- Katubilwa, F. M.; Moys, M. H.; Glasser, D.; Hildebrandt, D., 2011. An attainable region analysis of the effect of ball size on milling, *Powder Technology*, 210, 36-46.
- Katubilwa, F. M.; Moys, 2009. Effect of ball size distribution on milling rate, *Minerals Engineering* 22, 1283-1288.
- Kavetsky, A.; Whiten, W. J., 1982. Scale up relations for industrial ball mills, *Proceedings AusIMM*, 282, 47-55.
- Klimpel, R. R., and Austin, L. G., 1977. The back-calculation of specific rates of breakage and non-normalized breakage distribution parameters from batch grinding data. *International Journal of Mineral Processing*, Vol. 4. 7-32.
- Laplante, A. R.; Finch, J. A.; Villar, R. del., 1987. Simplification of grinding equation for plant simulation. *Trans. Instn Min. Metall. (Sect. C: Mineral Process. Extr. Metall.)*, 96, C108-C112).
- Loveday, B. K., 1979. Prediction of autogenous milling from pilot plant tests. *Proceedings 11<sup>th</sup> Commonwealth Mining and Metallurgical Congress. Hong Kong, May.*
- Lynch, A. J., 1977. *Mineral Crushing and Grinding Circuits; Their Simulation, Optimization, Design and Control.* Elsevier, Amsterdam, The Netherlands.

- Meloy, T. P.; Williams, M. C., 1992. A new comminution model to replace PBM comminution methodology, *Comminution-Theory and Practice*, ed. S. K. Kawatra. Soc. For Mining, Metallurgy, and Exploration, Inc., Littleton, CO.
- Mishra, B.K.; Rajamani, R.K., 1992. The discrete element method for the simulation of ball mills. *Appl. Math. Model*, 16, 598–604.
- Mosher, J. B.; Tague, C. B., 2001. Conduct and precision of bond grindability testing, *Minerals Engineering*, 14, 1187-1197.
- Morrell, S., 1996, Power draw of wet tumbling mills and its relationship to charge dynamics-Parts 1 and 2, *Transactions of Institution of Mining and Metallurgy, Sec. C: Mineral Process. Extr. Metall.*, 105, C43-C62.
- Morrell, S.; Man, Y.T., 1997, Using modeling and simulation for the design of full scale ball mill circuits, *Minerals Engineering*, 10/12, 1311-1327.
- Munjiza, A., 2004. *The combined finite-discrete element method*. Hoboken, NJ : Wiley, USA.
- Narayanan, S. S., 1987. Modelling the performance of industrial ball mills using single particle breakage data, *International Journal of Mineral Processing*, 20, 211-228.
- Narayanan, S. S.; Whiten, W. J., 1988. Determination of comminution characteristics from single particle breakage tests and its application to ball mill scale-up, *Trans. Instn. Min. Metall.* C97, 115-124.
- Purker, P.; Agrawal, R.; Kapur, P. C., 1986. A G-H Scheme for back-calculation of breakage rate functions from batch grinding data. *Powder Technology*, 45, 281-286.
- Rajamani, R.K.; Agrawala, S.; Mishra, B.K., 1993. Mill scale-up: ball collision frequency and collision energy density in laboratory and plant scale mills. XVIII International Mineral Processing Congress, vol. 1. Sydney, Australia, 103.
- Rajamani, R. K., Guo, D., 1992. Acceleration and deceleration of breakage rates in wet ball mills. *International Journal of Mineral Processing*, Vol. 34, 103-118.
- Ramasamy, M.; Narayanan, S. S.; Rao, Ch. D. P., 2005. Control of ball mill grinding circuit using model predictive control scheme, *Journal of Process Control*, 15, 273-283.
- Ramirez-Castro, J; Finch, J. A., 1980. Simulation of a grinding circuit change to reduce lead sliming. *CIM Bulletin*, 73, No: 816, 132-139.
- Rowland, C. A., 1998. Using the Bond work index to measure operating comminution efficiency. *Minerals and Metallurgical Processing*, 15, No. 4, 32-36.
- Sand, G. W., and Subasinghe, G. K. N., 2004. A novel approach to evaluating breakage parameters and modelling batch grinding. *Minerals Engineering*, Vol. 17, 1111-1116.
- Shoji, K., Austin, L. G., Smaila, F., Brame, K., Luckie, P. T., 1982. Further studies of ball and powder filling effects in ball milling. *Powder Technology*, 31, 121-126.
- Tavares, M. L.; Calvalho, R. M., 2009. Modeling breakage rates of coarse particles in ball mills, *Minerals Engineering*, 22, 650-659.
- Tromans, D., 2008. Mineral comminution: Energy efficiency considerations, *Minerals Engineering*, 21, 613-620.

Turner, R. R., 1982. Selection and sizing of primary autogenous and semi-autogenous grinding mills design and operation. Design and Installation of Comminution Circuits, eds. A. L. Mular and g. V. Jergensen II, Chapter 25. New York: SME-AIME.

Tuzcu, E. T. An approach for the modeling of batch grinding with single particle fracture studies and impact energy spectra. Dissertation of Doctor of Philosophy, Department of Metallurgical Engineering, The University of Utah, UT, USA, May 2010.

Tuzcu, E. T.; Rajamani, R. K., 2011. Modeling breakage rates in mills with impact energy spectra and ultra fast load cell data, Minerals Engineering, 24, 252-260.

Venkataraman, K. S.; Fuerstenau, D. W., 1984. Application of the population balance model to the grinding of mixtures of minerals, Powder Technology, 39, 133-142.

Verma, R., Rajamani, R. K., and 1992. Effect of milling environment on the breakage rates in dry and wet grinding. The Society of Mining and Metallurgical Engineers, chapt. 19, 261-271.

Walker, W. H.; Lewis, W. K.; McAdams, W. H.; Gilliland, E. R., 1937. Principles of Chemical Engineering, McGraw-Hill, NY, USA.

Whiten, W. J.; Roberts, A. N., 1974. Control of a multi-stage grinding circuit. Transactions Institution of Mining and Metallurgy, 83, C209-C212.

Yang, D. C., Mempel, G., Fuerstenau, D. W., 1968. A laboratory mill for batch grinding experimentation. Trans. Society of Mining Engineers, Vol. 241, 273-275.

Zambrano, A. R., 2002. General work input function for sizing grinding ball mills, Minerals & Metallurgical Processing, 19, 4, 178-186.

Zhang Y. M. and Kavetsky, A., 1993. Investigation of particle breakage mechanisms in a batch ball mill using back-calculation. International Journal of Mineral Processing, Vol. 39, 41-60.

## APPENDIX A: TORQUE AND POWER MEASUREMENTS

**Table A.1.** Mill torque versus mill speed for different ball sizes ( $\Phi_B=0.22$ )

Ball size, mm	19.05	25.4	31.75
Mill Speed, rpm	Torque, Nm		
30	12,27	11,93	11,38
40	12,5	11,95	11,63
50	12,57	12,08	11,67
60	12,79	12,16	11,77
70	12,83	12,17	11,88
75	12,86	12,13	11,82
80	12,87	12,18	11,93

**Table A.2.** % of Max. mill power versus ball charge for different ball sizes.

Ball Charge ( $\Phi_B$ )	Ball Size, mm		
	19.05	25.4	31.75
22	62,57	59,24	60,81
30	82,20	75,38	78,64
40	97,81	93,44	95,92
50	100,00	100,00	100,00

**Table A.3.** Torque measurements with aged and new balls (Ball size: 19.05 mm,  $n_c=0.75$ ).

Ball Charge ( $\Phi_B$ )	New Balls	Aged Balls
	Torque, Nm	
22	7.85	12.85
30	11.80	16.75
40	15.38	19.80
50	17.84	20.70

**Table A.4.** Material filling versus torque for different ball charges (Bond ball charge,  $n_c=0.75$ ).

Ball charge, %	Material filling, %				
	20	40	60	80	100
20	13	13,59	14,18	14,77	15,36
25	15,3	16,29	17	17,77	18,47
30	17,67	18,55	19,78	20,46	18,89
35	19,69	20,88	20,25	19,55	19
40	21,22	20,42	20	19,55	19,55
45	20,8	20,23	20,2	19,5	19,3

**Table A.5.** Material filling versus fineness of ground ( $\Phi_B=0.25$ ,  $n_c=0.75$ ).

Size, $\mu\text{m}$	Cum. Wt.% Passing					
	Material Filling%					
	Feed	20	40	60	80	100
3350	100	100	100	100	100	100
2360	80,84719	99,433	99,13153	99,73157	99,72658	99,83321
1700	60,93782	98,63194	98,27452	99,38857	99,5546	99,7373
1180	44,72226	96,74963	96,79881	98,87557	99,40025	99,65391
850	33,77028	91,64332	93,33868	97,6199	99,12683	99,57468
600	25,04754	82,00099	85,50642	93,76939	98,38596	99,46627
425	17,43739	65,95022	71,03346	82,39084	93,89663	99,12017
300	12,69572	53,54871	57,15628	69,38082	85,03263	97,71078
212	9,353886	42,87457	46,00825	55,72059	71,18539	91,86056
150	6,780758	33,99703	36,3428	44,89979	58,25983	80,36027
106	4,919691	26,41174	28,19432	35,08113	45,70471	66,49571
75	3,641219	19,99341	21,20761	24,63016	33,73611	51,81386
53	2,605494	15,31087	16,11824	18,71892	25,63944	38,45801
38	1,978395	11,85769	12,72456	14,7781	20,24167	30,26853
Pan	0	0	0	0	0	0

**Table A.6.** Energy Efficiency in the Bond Ball Mill.

No	Mat. Fill%	Wt., g	d <sub>50</sub>	Torque, Nm	Power, Watt	Sp. Energy (kWh/t)
1	20	896,48	46	15,3	96,023	5,356
2	40	1792,96	109	16,29	102,236	2,851
3	60	2689,43	180	17	106,692	1,984
4	80	3585,91	240	17,77	111,525	1,555
5	100	4482,39	291	18,47	115,918	1,293
6	20	1075,77	66	17,67	110,897	5,154
7	40	2151,55	124	18,55	116,420	2,705
8	60	3227,32	175	19,78	124,139	1,923
9	80	4303,1	230	20,46	128,407	1,492
10	100	5378,86	303	18,89	118,554	1,102
11	20	1255,07	64	19,69	123,574	4,923
12	40	2510,14	142	20,88	131,043	2,610
13	60	3765,21	220	20,25	127,089	1,688
14	80	5020,27	300	19,55	122,696	1,222
15	100	6275,34	380	19	119,244	0,950
16	20	1434,36	90	21,22	133,177	4,642
17	40	2868,73	193	20,42	128,156	2,234
18	60	4303,1	275	20	125,520	1,458
19	80	5737,46	342	19,55	122,696	1,069
20	100	7171,82	420	19,55	122,696	0,855
21	20	1613,66	118	20,8	130,541	4,045
22	40	3227,32	222	20,23	126,963	1,967
23	60	4840,98	294	20,2	126,775	1,309
24	80	6454,64	362	19,5	122,382	0,948
25	100	8068,3	430	19,3	121,127	0,751
26	20	717,18	44	13	81,588	5,688
27	40	1434,36	87	13,59	85,291	2,973
28	60	2151,55	148	14,18	88,994	2,068
29	80	2868,73	200	14,77	92,697	1,616
30	100	3585,91	257	15,36	96,399	1,344

**Table A.7.** Variation of fineness of material ( $d_{50}$ ) with charge conditions at 5 ( $n_c=0.75$ )

No	$d_{50}$	Mat. Fill., %	Ball load, %
1	73	20	25
2	65	40	25
3	62	60	25
4	68	80	25
5	76	100	25
6	60	20	30
7	56	40	30
8	62	60	30
9	68	80	30
10	72	100	30
11	70	20	35
12	62	40	35
13	67	60	35
14	73	80	35
15	80	100	35
16	74	20	40
17	71	40	40
18	75	60	40
19	80	80	40
20	84	100	40
21	73	20	45
22	70	40	45
23	68	60	45
24	73	80	45
25	78	100	45
26	78	20	20
27	67	40	20
28	64	60	20
29	68	80	20
30	75	100	20

**Table A.8.** Bond Grindability indices ( $W_i$ ) for quartz and calcite for different closing screens

Closing Screen, $\mu\text{m}$	Quartz	Calcite
	$W_i$ (kWh/ton)	$W_i$ (kWh/ton)
75	16,93	6,8
106	14,82	
150	12,03	5,75
212	9,54	
300	7,97	4,72

**APPENDIX B: PARTICLE SIZE DISTRIBUTIONS OF MINERALS AFTER SHORT-TIME GRINDING TESTS**

**Table B.1.** Short-time grinding tests for quartz steady-state mill feed generated by 75  $\mu\text{m}$  closing screen.

Size, $\mu\text{m}$	Cum Wt% Passing				
	Feed	30 sec	60 sec	90 sec	120 sec
3350	100.00	100.00	100.00	100.00	100.00
2360	92.44	96.30	97.88	98.89	99.41
1700	87.61	93.38	96.50	98.18	99.03
1180	84.23	91.23	95.32	97.55	98.69
850	81.92	89.35	94.09	96.90	98.34
600	80.26	87.50	92.63	95.96	97.82
425	78.50	84.85	90.06	93.88	96.40
300	76.55	81.90	86.71	90.54	93.44
212	72.18	77.03	80.80	84.70	87.90
150	59.25	64.27	68.02	70.60	74.43
106	30.39	37.18	38.59	42.48	47.33
75	1.77	7.32	9.97	12.62	16.35
53	1.09	3.40	5.45	7.22	9.24
38	0.74	2.12	3.64	4.55	5.79
Pan	0	0	0	0	0

**Table B.2.** Short-time grinding tests for quartz steady-state mill feed generated by 106  $\mu\text{m}$  closing screen.

Size, $\mu\text{m}$	Cum. Wt.% Passing						
	Feed	30 sec	45 sec	60 sec	90 sec	120 sec	150 sec
3350	100.00	100.00	100.00	100.00	100.00	100.00	100.00
2360	92.65	96.46	97.29	97.79	98.65	99.22	99.60
1700	87.59	93.48	94.91	95.97	97.55	98.53	99.22
1180	84.04	91.25	93.22	94.58	96.70	98.11	98.97
850	81.69	89.24	91.63	93.28	95.91	97.67	98.75
600	79.79	87.21	89.87	91.78	94.91	97.06	98.39
425	77.24	84.01	86.80	88.92	92.59	95.40	97.32
300	73.20	79.45	82.17	84.31	88.55	91.88	94.44
212	61.83	68.13	71.17	73.47	78.00	81.72	85.10
150	34.68	41.35	45.40	47.76	52.77	56.05	59.88
106	2.67	8.19	11.08	12.87	17.61	20.97	24.56
75	1.78	4.64	6.19	7.34	10.11	12.61	15.28
53	1.09	2.73	3.70	4.37	6.13	7.83	9.67
38	0.75	1.73	2.35	2.82	4.02	5.07	6.38
Pan	0	0	0	0	0	0	0

**Table B.3.** Short-time grinding tests for quartz steady-state mill feed generated by 150  $\mu\text{m}$  closing screen.

Size, $\mu\text{m}$	Cum Wt% Passing				
	Feed	30 sec	60 sec	90 sec	120 sec
3350	100.00	100.00	100.00	100.00	100.00
2360	91.64	95.86	97.21	98.35	98.82
1700	85.85	92.93	95.36	97.33	98.14
1180	81.78	90.18	93.90	96.50	97.64
850	78.86	87.80	92.49	95.72	97.22
600	76.09	85.10	90.64	94.52	96.53
425	70.39	78.94	85.65	90.66	93.88
300	57.13	66.32	74.45	80.87	85.65
212	32.62	41.45	49.74	57.07	63.09
150	3.85	12.54	19.19	25.63	31.21
106	2.67	7.73	12.12	16.18	20.21
75	1.78	5.06	7.96	10.69	13.40
53	1.09	3.15	5.07	6.83	8.60
38	0.75	2.11	3.44	4.48	5.73
Pan	0	0	0	0	0

**Table B.4.** Short-time grinding tests for quartz steady-state mill feed generated by 212  $\mu\text{m}$  closing screen.

Size, $\mu\text{m}$	Cum. Wt.% Passing						
	Feed	15 sec	30 sec	45 sec	60 sec	90 sec	120 sec
3350	100.00	100.00	100.00	100.00	100.00	100.00	100.00
2360	90.10	92.09	93.72	95.29	96.52	97.70	98.59
1700	82.90	87.00	89.03	92.02	94.07	96.18	97.59
1180	77.55	82.54	85.55	89.35	92.23	94.90	96.83
850	73.26	78.69	82.22	86.79	90.19	93.68	96.07
600	68.20	73.91	77.78	83.11	87.15	91.68	94.78
425	56.38	62.75	66.98	73.19	78.12	84.51	89.33
300	34.45	42.38	46.63	53.91	59.51	67.03	74.33
212	5.37	12.06	16.29	22.56	27.86	34.94	42.93
150	3.99	7.83	10.50	14.53	18.01	22.81	28.21
106	2.76	5.20	6.86	9.57	11.94	14.84	18.67
75	1.84	3.41	4.46	6.30	7.80	9.59	12.36
53	1.13	2.07	2.68	3.95	4.87	5.90	7.81
38	0.77	1.38	1.77	2.64	3.25	3.65	5.13
Pan	0	0	0	0	0	0	0

**Table B.5.** Short-time grinding tests for quartz steady-state mill feed generated by 300  $\mu\text{m}$  closing screen.

Size, $\mu\text{m}$	Cum Wt% Passing				
	Feed	30 sec	60 sec	90 sec	120 sec
3350	100.00	100.00	100.00	100.00	100.00
2360	86.35	91.23	95.24	96.85	97.82
1700	76.64	84.84	91.60	94.49	96.55
1180	68.86	79.32	88.31	92.55	95.55
850	61.92	74.23	84.85	90.43	94.45
600	52.43	66.66	78.73	86.47	92.24
425	33.04	48.81	61.93	72.52	81.98
300	6.58	22.70	36.73	48.00	59.57
212	5.20	15.15	24.46	32.97	41.53
150	3.87	10.43	16.74	22.55	28.47
106	2.68	7.06	11.27	15.19	19.19
75	1.78	4.68	7.50	10.07	12.71
53	1.10	2.86	4.66	6.39	8.13
38	0.75	1.92	3.10	4.21	5.35
Pan	0	0	0	0	0

**Table B.6.** Short-time grinding tests for calcite steady-state mill feed generated by 75  $\mu\text{m}$  closing screen.

Size, $\mu\text{m}$	Cum. Wt.% Passing						
	Feed	15 sec	30 sec	45 sec	60 sec	90 sec	120 sec
3350	100.00	100.00	100.00	100.00	100.00	100.00	100.00
2360	94.44	96.40	98.35	99.00	99.40	99.80	99.94
1700	88.67	94.19	97.02	98.32	99.02	99.57	99.87
1180	83.96	91.90	95.47	97.35	98.54	99.32	99.77
850	80.69	89.38	93.49	96.05	97.71	98.98	99.67
600	77.84	86.36	90.90	93.78	96.03	98.28	99.39
425	74.07	81.70	86.15	89.35	92.33	95.75	98.07
300	68.76	74.99	79.33	83.08	85.99	90.61	94.14
212	57.31	63.22	67.29	71.31	74.40	80.19	84.53
150	40.54	46.20	50.24	54.02	56.48	63.33	69.42
106	21.27	25.79	30.60	33.73	37.52	43.43	50.83
75	1.04	6.97	10.96	14.62	17.21	24.88	29.87
53	0.75	3.90	6.31	9.34	10.71	15.13	18.15
38	0.57	2.46	4.07	5.98	7.00	10.00	11.75
Pan	0	0	0	0	0	0	0
Torque. Nm		15.27	15.61	15.21	15.12	14.98	15.02

**Table B.7.** Short-time grinding tests for calcite steady-state mill feed generated by 150  $\mu\text{m}$  closing screen.

Size, $\mu\text{m}$	Cum. Wt.% Passing						
	Feed	15 sec	30 sec	45 sec	60 sec	90 sec	120 sec
3350	100.00	100.00	100.00	100.00	100.00	100.00	100.00
2360	93.70	96.60	97.49	98.01	99.16	99.60	99.75
1700	87.34	93.90	95.83	97.04	98.52	99.35	99.59
1180	81.92	90.88	93.93	95.64	97.83	99.02	99.47
850	77.58	87.50	91.46	93.81	96.55	98.43	99.25
600	72.51	82.90	87.45	90.60	94.14	97.17	98.59
425	63.08	73.43	78.48	82.51	87.17	92.51	95.66
300	48.80	58.91	64.59	69.56	75.14	82.37	88.01
212	27.64	37.18	43.46	48.57	54.52	63.47	71.09
150	1.94	11.90	17.96	24.02	28.90	39.08	46.77
106	1.41	7.66	11.96	16.08	19.76	27.59	34.50
75	1.04	5.51	8.55	11.74	14.51	20.01	24.60
53	0.75	3.90	6.01	8.40	10.45	15.00	18.20
38	0.57	2.82	4.20	5.90	7.60	10.60	12.60
Pan	0	0	0	0	0	0	0
Torque, Nm		15.18	15.08	15.05	15.12	15.12	15.08

**Table B.8.** Short-time grinding tests for calcite steady-state mill feed generated by 300  $\mu\text{m}$  closing screen.

Size, $\mu\text{m}$	Cum. Wt.% Passing						
	Feed	15 sec	30 sec	45 sec	60 sec	90 sec	120 sec
3350	100.00	100.00	100.00	100.00	100.00	100.00	100.00
2360	91.54	94.87	97.11	97.70	98.62	99.32	99.70
1700	83.13	90.45	94.24	95.81	97.46	98.83	99.41
1180	75.46	85.57	90.67	93.51	96.06	98.19	99.20
850	67.01	78.93	85.53	89.97	93.61	97.13	98.71
600	54.41	67.74	76.08	82.61	87.75	94.06	97.27
425	30.87	45.33	55.10	63.92	71.25	82.37	89.68
300	3.63	19.98	30.04	40.16	48.63	63.04	73.81
212	2.68	13.42	21.17	28.45	35.34	47.36	57.71
150	1.94	9.87	15.50	21.05	26.24	35.81	44.76
106	1.41	7.05	11.41	15.38	19.45	26.89	34.34
75	1.04	5.29	8.63	11.56	14.20	19.80	25.80
53	0.75	4.00	6.30	8.49	10.51	14.64	19.05
38	0.57	3.00	4.65	6.61	8.00	10.60	13.80
Pan	0	0	0	0	0	0	0
Torque, Nm		15.15	15.28	15.28	15.27	15.10	15.12

**Table B.9.** Short-time grinding tests for quartz steady-state mill feed generated by 150  $\mu\text{m}$  closing screen (100% CL.).

Size, $\mu\text{m}$	Cum. Wt.% Passing					
	Feed	30 sec	60 sec	90 sec	120 sec	150 sec
3350	100.00	100.00	100.00	100.00	100.00	100.00
2360	87.44	93.69	95.96	97.25	98.26	98.92
1700	78.78	89.01	92.71	95.18	96.97	98.18
1180	72.74	84.89	90.13	93.48	96.06	97.62
850	68.79	81.41	87.70	92.06	95.24	97.13
600	65.70	77.87	84.81	90.06	93.93	96.32
425	61.86	72.52	79.44	85.47	90.16	93.73
300	55.63	65.11	71.30	77.44	82.77	87.11
212	39.89	48.35	53.59	60.10	65.89	71.36
150	6.72	15.41	20.88	27.08	32.33	37.13
106	4.65	9.03	12.58	16.77	20.16	23.62
75	3.10	5.85	8.01	10.81	13.11	15.57
53	1.90	3.59	4.80	6.74	8.02	9.83
38	1.30	2.43	3.07	4.55	5.59	6.94
Pan	0	0	0	0	0	0

**Table B.10.** Short-time grinding tests for quartz steady-state mill feed generated by 150  $\mu\text{m}$  closing screen (350% CL.).

Size, $\mu\text{m}$	Cum. Wt.% Passing							
	Feed	15 sec	30 sec	45 sec	60 sec	90 sec	120 sec	150 sec
3350	100.00	100.00	100.00	100.00	100.00	100.00	100.00	100.00
2360	92.06	96.60	97.49	98.01	99.16	99.60	99.75	99.93
1700	86.99	93.90	95.83	97.04	98.52	99.35	99.59	99.86
1180	83.37	90.88	93.93	95.64	97.83	99.02	99.47	99.78
850	80.75	87.50	91.46	93.81	96.55	98.43	99.25	99.69
600	77.84	82.90	87.45	90.60	94.14	97.17	98.59	99.39
425	70.34	73.43	78.48	82.51	87.17	92.51	95.66	97.65
300	53.41	58.91	64.59	69.56	75.14	82.37	88.01	91.99
212	29.90	37.18	43.46	48.57	54.52	63.47	71.09	77.15
150	3.01	11.90	17.96	24.02	28.90	39.08	46.77	56.67
106	2.09	7.66	11.96	16.08	19.76	27.59	34.50	42.61
75	1.39	5.51	8.55	11.74	14.51	20.01	24.60	30.33
53	0.85	3.90	6.01	8.40	10.45	15.00	18.20	22.50
38	0.58	2.82	4.20	5.90	7.60	10.60	12.60	15.95
Pan	0	0	0	0	0	0	0	0

**Table B.11.** Short-time grinding tests for calcite steady-state mill feed generated by 150  $\mu\text{m}$  closing screen (100% CL.).

Size, $\mu\text{m}$	Cum. Wt.% Passing					
	Feed	30 sec	60 sec	90 sec	120 sec	150 sec
3350	100.00	100.00	100.00	100.00	100.00	100.00
2360	90.22	97.29	99.05	99.57	99.80	99.90
1700	80.14	94.78	98.03	99.21	99.65	99.85
1180	71.89	91.79	96.90	98.82	99.50	99.79
850	66.16	88.05	95.17	98.12	99.27	99.72
600	61.05	83.13	91.91	96.41	98.55	99.45
425	53.74	74.39	84.67	91.09	95.28	97.88
300	43.87	63.05	73.88	81.19	87.92	92.69
212	25.55	45.06	56.61	65.38	72.17	81.23
150	3.39	20.45	31.95	41.57	50.82	59.99
106	2.46	14.43	21.38	28.83	37.57	44.34
75	1.82	10.72	15.85	21.87	28.77	33.42
53	1.30	8.00	11.48	16.22	21.48	25.22
38	0.99	5.89	8.51	11.75	16.00	19.23
Pan	0	0	0	0	0	0

**Table B.12.** Short-time grinding tests for -6 mesh quartz (Bond charge.  $\Phi_B=0.22$ ).

Size, $\mu\text{m}$	Cum. Wt.% Passing					
	Feed	30 sec	60 sec	90 sec	120 sec	150 sec
3350	100.00	100.00	100.00	100.00	100.00	100.00
2360	59.45	76.69	85.23	90.49	93.22	95.46
1700	33.37	60.93	74.09	83.69	87.95	92.59
1180	20.77	48.26	64.93	76.66	83.64	90.20
850	15.58	39.52	56.76	69.98	78.99	87.33
600	12.17	32.22	48.26	61.80	72.26	82.64
425	9.12	24.67	38.07	49.75	60.80	72.20
300	7.05	19.01	29.56	38.96	48.66	58.98
212	5.16	13.90	21.65	28.52	36.01	44.10
150	3.59	9.61	14.97	19.67	25.11	30.85
106	2.39	6.33	9.91	13.15	16.82	20.95
75	1.54	4.15	6.52	8.73	11.00	13.92
53	0.91	2.51	4.07	5.53	7.25	9.12
38	0.59	1.80	2.75	3.72	4.85	6.30
Pan	0	0	0	0	0	0

**Table B.13.** Short-time grinding tests for -6 mesh calcite (Bond charge.  $\Phi_B=0.22$ ).

Size, $\mu\text{m}$	Cum. Wt.% Passing					
	Feed	30 sec	60 sec	90 sec	120 sec	150 sec
3350	100.00	100.00	100.00	100.00	100.00	100.00
2360	80.85	93.84	98.03	98.90	99.49	99.81
1700	60.94	88.66	96.29	98.24	99.24	99.66
1180	44.72	82.52	93.87	97.26	98.92	99.54
850	33.77	74.96	90.16	95.72	98.30	99.38
600	25.05	64.90	83.53	92.04	96.65	98.81
425	17.44	52.37	71.84	82.50	90.52	95.70
300	12.70	42.19	60.31	70.25	80.19	88.08
212	9.35	32.96	48.92	57.12	66.28	74.73
150	6.78	25.23	39.32	44.85	53.57	61.57
106	4.92	19.15	29.51	34.68	42.07	48.96
75	3.64	14.13	21.88	26.30	31.73	37.68
53	2.61	10.72	16.59	20.20	24.71	30.00
38	1.98	8.13	12.88	15.85	19.23	23.00
Pan	0	0	0	0	0	0

**Table B.14.** Short-time grinding tests for 6x8 mesh quartz (Bond charge.  $\Phi_B=0.22$ ).

Size, $\mu\text{m}$	Cum. Wt.% Passing					
	15 sec	30 sec	45 sec	60 sec	90 sec	120 sec
3350	100.00	100.00	100.00	100.00	100.00	100.00
2360	40.83	56.93	67.43	75.30	84.09	89.26
1700	23.96	40.06	51.76	61.62	74.33	82.67
1180	16.63	30.49	41.66	52.10	66.63	77.15
850	12.78	24.54	34.93	45.08	60.15	72.09
600	10.24	20.17	29.30	38.52	53.34	65.99
425	7.97	15.85	23.23	30.94	44.21	56.43
300	6.27	12.42	18.49	24.61	35.82	46.36
212	4.77	9.41	14.03	18.53	27.25	35.52
150	3.45	6.76	10.13	13.29	19.74	25.85
106	2.36	4.65	7.00	9.17	13.75	18.03
75	1.54	3.07	4.65	6.18	9.40	12.29
53	0.94	1.88	2.90	3.91	6.00	7.82
38	0.62	1.22	1.95	2.63	4.00	5.25
Pan	0.00	0.00	0.00	0.00	0.00	0.00
Torque. Nm	13.95	13.86	14.05	13.96	13.87	14.25

**Table B.15.** Short-time grinding tests for 6x8 mesh quartz (1 inch charge.  $\Phi_B=0.22$ ).

Size, $\mu\text{m}$	Cum. Wt.% Passing					
	15 sec	30 sec	45 sec	60 sec	90 sec	120 sec
3350	100.00	100.00	100.00	100.00	100.00	100.00
2360	40.67	56.09	65.84	71.13	78.17	82.70
1700	24.07	37.91	49.48	54.62	66.28	73.46
1180	16.69	28.90	40.84	46.51	59.57	68.14
850	12.89	23.30	34.61	40.22	54.31	63.99
600	10.23	19.17	29.34	34.92	49.00	59.32
425	7.83	15.00	23.55	28.47	41.50	51.57
300	6.22	11.91	18.77	22.81	33.99	43.12
212	4.69	8.95	14.27	17.33	26.06	33.46
150	3.34	6.45	10.24	12.45	18.86	24.33
106	2.28	4.42	7.05	8.55	13.06	16.93
75	1.47	2.94	4.66	5.66	8.70	11.43
53	0.90	1.86	2.92	3.53	5.50	7.34
38	0.59	1.25	1.99	2.37	3.68	4.99
Pan	0.00	0.00	0.00	0.00	0.00	0.00

**Table B.16.** Short-time grinding tests for 14x20 mesh quartz (Bond charge.  $\Phi_B=0.22$ ).

Size, $\mu\text{m}$	Cum. Wt.% Passing					
	15 sec	30 sec	45 sec	60 sec	90 sec	120 sec
1180	100.00	100.00	100.00	100.00	100.00	100.00
850	43.17	62.46	77.45	86.49	94.27	97.88
600	24.36	40.93	56.42	68.89	82.58	91.36
425	14.63	25.58	37.62	48.41	62.74	74.80
300	9.75	17.30	26.02	34.16	45.73	56.86
212	6.56	11.59	17.66	23.18	31.48	39.95
150	4.33	7.69	11.68	15.42	21.20	27.15
106	2.82	5.02	7.60	10.00	14.00	18.08
75	1.82	3.20	4.79	6.29	9.01	11.73
53	1.08	1.93	2.82	3.75	5.48	7.25
38	0.71	1.24	1.77	2.34	3.52	4.71
Pan	0.00	0.00	0.00	0.00	0.00	0.00
Torque. Nm	13.84	13.76	14.1	13.83	13.89	14.38

**Table B.17.** Short-time grinding tests for 14x20 mesh quartz (1 inch charge.  $\Phi_B=0.22$ ).

Size, $\mu\text{m}$	Cum. Wt.% Passing					
	15 sec	30 sec	45 sec	60 sec	90 sec	120 sec
1180	100.00	100.00	100.00	100.00	100.00	100.00
850	44.28	66.41	79.85	86.67	94.51	97.56
600	23.60	43.67	59.89	68.90	82.53	90.40
425	13.56	27.86	40.55	48.66	61.88	73.10
300	8.47	18.79	28.28	33.61	44.58	53.70
212	5.18	12.17	18.91	22.67	30.06	36.45
150	3.11	7.52	12.24	15.18	19.47	23.77
106	1.77	4.44	7.55	9.54	12.09	14.92
75	1.03	2.67	4.51	5.73	7.48	9.27
53	0.56	1.40	2.42	3.14	4.22	5.29
38	0.33	0.82	1.36	1.83	2.50	3.25
Pan	0.00	0.00	0.00	0.00	0.00	0.00

**Table B.18.** Short-time grinding tests for 48x65 mesh quartz (Bond charge.  $\Phi_B=0.22$ ).

Size, $\mu\text{m}$	Cum. Wt.% Passing						
	15 sec	30 sec	45 sec	60 sec	90 sec	120 sec	150 sec
300	100.00	100.00	100.00	100.00	100.00	100.00	100.00
212	9.75	18.73	24.67	30.33	39.90	49.43	56.65
150	4.83	9.08	12.23	15.74	21.66	27.73	32.74
106	2.63	4.95	6.79	8.89	12.56	16.36	19.46
75	1.52	2.83	3.94	5.20	7.47	9.71	11.89
53	0.84	1.57	2.23	2.92	4.36	5.86	7.21
38	0.54	0.87	1.37	1.81	2.72	3.76	4.70
Pan	0.00	0.00	0.00	0.00	0.00	0.00	0.00
Torque. Nm	14.3	14.87	14.63	14.4	14.72	14.3	14.3

**Table B.19.** Short-time grinding tests for 48x65 mesh quartz (1 inch charge.  $\Phi_B=0.22$ ).

Size, $\mu\text{m}$	Cum. Wt.% Passing						
	15 sec	30 sec	45 sec	60 sec	90 sec	120 sec	150 sec
300	100.00	100.00	100.00	100.00	100.00	100.00	100.00
212	13.36	22.03	28.73	35.39	44.13	56.04	62.59
150	4.74	9.14	12.21	17.43	22.24	30.26	35.84
106	2.63	5.08	6.91	10.06	12.89	18.15	21.99
75	1.55	3.10	4.36	6.12	8.00	11.37	14.04
53	0.87	1.83	2.71	3.78	4.88	6.97	8.89
38	0.55	1.15	1.90	2.51	3.34	4.64	6.01
Pan	0.00	0.00	0.00	0.00	0.00	0.00	0.00

**Table B.20.** Short-time grinding tests for 6x8 mesh quartz (Bond charge.  $\Phi_B=0.28$ ).

Size, $\mu\text{m}$	Cum. Wt.% Passing						
	15 sec	30 sec	45 sec	60 sec	90 sec	120 sec	150 sec
3350	100.00	100.00	100.00	100.00	100.00	100.00	100.00
2360	37.34	56.69	62.95	69.64	81.54	88.69	92.50
1700	18.92	37.44	45.33	53.40	69.55	81.25	87.97
1180	12.57	28.49	35.60	43.52	61.58	75.96	84.27
850	9.41	23.34	29.37	36.78	55.12	71.01	80.74
600	7.38	19.26	24.27	30.91	48.47	64.78	75.96
425	5.59	15.07	18.95	24.03	39.62	54.82	66.51
300	4.34	11.72	14.79	18.86	31.62	44.18	55.40
212	3.18	8.66	10.87	13.87	23.49	33.28	42.32
150	2.20	6.10	7.57	9.64	16.58	23.71	30.44
106	1.50	4.09	5.08	6.46	11.24	15.95	20.99
75	0.99	2.60	3.37	4.21	7.42	10.79	14.19
53	0.60	1.58	2.05	2.51	4.60	6.96	9.07
38	0.40	1.00	1.33	1.77	3.10	4.71	6.07
Pan	0.00	0.00	0.00	0.00	0.00	0.00	0.00
Torque. Nm	17.43	17.32	17.3	17.5	17.37	17.38	17.49

**Table B.21.** Short-time grinding tests for 14x20 mesh quartz (Bond charge.  $\Phi_B=0.28$ ).

Size, $\mu\text{m}$	Cum. Wt.% Passing						
	15 sec	30 sec	45 sec	60 sec	90 sec	120 sec	150 sec
1180	100.00	100.00	100.00	100.00	100.00	100.00	100.00
850	47.09	66.57	81.65	87.24	95.91	98.51	99.39
600	27.47	42.31	60.43	69.06	86.18	93.18	96.88
425	17.19	26.15	40.17	48.26	67.39	77.71	86.44
300	11.94	17.83	27.67	34.03	49.10	59.17	69.13
212	8.03	11.85	18.34	23.04	33.98	41.77	49.62
150	5.24	7.65	11.78	15.17	22.34	28.02	34.15
106	3.29	4.88	7.44	9.67	14.91	18.34	22.94
75	2.00	3.06	4.73	6.04	9.70	11.88	14.89
53	1.10	1.77	2.84	3.48	5.75	7.31	9.43
38	0.71	1.12	1.92	2.23	4.00	4.75	6.23
Pan	0.00	0.00	0.00	0.00	0.00	0.00	0.00
Torque. Nm	17.82	17.6	17.44	17.53	17.55	17.63	17.56

**Table B.22.** Short-time grinding tests for 48x65 mesh quartz (Bond charge.  $\Phi_B=0.28$ ).

Size, $\mu\text{m}$	Cum. Wt.% Passing						
	15 sec	30 sec	45 sec	60 sec	90 sec	120 sec	150 sec
300	100.00	100.00	100.00	100.00	100.00	100.00	100.00
212	15.54	22.42	30.73	36.14	47.71	57.25	65.16
150	6.04	9.92	14.04	17.44	25.96	31.81	39.06
106	3.43	5.56	8.04	10.13	15.74	19.22	24.22
75	2.07	3.34	4.84	6.18	9.78	12.08	15.67
53	1.21	1.98	2.92	3.71	6.04	7.31	9.83
38	0.83	1.42	2.01	2.55	4.17	4.78	6.84
Pan	0.00	0.00	0.00	0.00	0.00	0.00	0.00
Torque. Nm	17.62	17.6	17.43	17.53	17.58	17.56	17.54

**Table B.23.** Short-time grinding tests for 6x8 mesh quartz (Bond charge.  $\Phi_B=0.35$ ).

Size, $\mu\text{m}$	Cum. Wt.% Passing						
	15 sec	30 sec	45 sec	60 sec	90 sec	120 sec	150 sec
3350	100.00	100.00	100.00	100.00	100.00	100.00	100.00
2360	44.80	63.69	70.44	79.12	87.61	93.76	96.40
1700	24.90	44.99	53.95	66.57	79.68	89.16	93.76
1180	17.65	35.02	43.61	57.37	72.77	84.96	91.67
850	13.58	28.27	36.54	50.42	66.46	80.97	89.36
600	10.97	23.13	30.48	43.43	59.48	75.25	85.62
425	8.50	17.86	24.03	35.05	49.18	64.86	76.67
300	6.64	13.87	18.94	27.81	39.39	52.93	64.00
212	4.97	10.32	14.12	20.93	29.47	40.15	49.12
150	3.60	7.28	9.77	14.86	20.83	28.92	35.70
106	2.44	4.94	6.72	10.22	14.18	19.88	24.63
75	1.64	3.36	4.52	6.74	9.26	13.22	16.64
53	1.01	2.11	2.83	4.28	5.89	8.46	11.07
38	0.72	1.40	1.89	2.75	4.04	5.59	7.57
Pan	0.00	0.00	0.00	0.00	0.00	0.00	0.00
Torque. Nm	20.22	20.29	20.4	20.73	20.8	20.74	20.7

**Table B.24.** Short-time grinding tests for 14x20 mesh quartz (Bond charge.  $\Phi_B=0.35$ ).

Size, $\mu\text{m}$	Cum. Wt.% Passing						
	15 sec	30 sec	45 sec	60 sec	90 sec	120 sec	150 sec
1180	100.00	100.00	100.00	100.00	100.00	100.00	100.00
850	47.62	74.01	83.52	90.24	97.00	99.00	99.63
600	26.85	51.61	63.15	74.09	88.89	95.25	97.99
425	15.99	33.42	43.31	52.48	70.83	82.20	89.17
300	10.75	23.05	30.18	36.82	52.58	64.61	73.11
212	7.10	15.23	20.32	24.60	36.57	46.66	53.51
150	4.65	9.77	13.38	16.11	24.46	31.77	37.27
106	2.95	6.23	8.49	10.39	16.02	21.23	25.05
75	1.86	3.88	5.38	6.69	10.37	14.02	16.91
53	1.10	2.26	3.10	4.01	6.31	8.75	10.90
38	0.66	1.42	1.97	2.70	4.26	5.95	7.41
Pan	0.00	0.00	0.00	0.00	0.00	0.00	0.00
Torque. Nm	20.8	20.53	20.47	20.53	20.46	20.86	20.65

**Table B.25.** Short-time grinding tests for 48x65 mesh quartz (Bondcharge.  $\Phi_B=0.35$ ).

Size, $\mu\text{m}$	Cum. Wt.% Passing						
	15 sec	30 sec	45 sec	60 sec	90 sec	120 sec	150 sec
300	100.00	100.00	100.00	100.00	100.00	100.00	100.00
212	14.19	24.50	30.51	35.46	49.73	58.90	65.81
150	5.43	11.18	14.76	17.49	26.91	33.57	39.90
106	3.07	6.41	8.68	10.14	16.63	21.40	25.26
75	1.87	3.92	5.39	6.29	10.82	13.97	16.45
53	1.06	2.33	3.26	3.85	6.65	8.85	10.59
38	0.65	1.59	2.37	2.73	4.42	6.08	7.33
Pan	0.00	0.00	0.00	0.00	0.00	0.00	0.00
Torque. Nm	20.67	20.7	20.6	20.68	20.58	20.87	20.76

**Table B.26.** Short-time grinding tests for 6x8 mesh calcite (Bond charge.  $\Phi_B=0.22$ ).

Size, $\mu\text{m}$	Cum. Wt.% Passing						
	15 sec	30 sec	45 sec	60 sec	90 sec	120 sec	150 sec
3350	100.00	100.00	100.00	100.00	100.00	100.00	100.00
2360	66.06	80.35	88.84	93.37	97.08	98.97	99.74
1700	48.71	68.03	80.86	87.65	94.89	97.82	99.27
1180	36.24	55.96	71.85	80.62	92.04	96.82	98.88
850	27.12	44.97	60.59	71.44	87.18	94.83	98.24
600	19.69	34.34	48.56	59.81	78.50	90.32	95.98
425	13.22	24.27	35.47	45.52	64.21	79.66	88.89
300	9.57	17.97	26.71	35.05	51.52	66.56	77.62
212	6.95	13.26	19.83	26.41	40.08	53.18	63.33
150	5.10	9.83	14.84	19.96	30.78	41.68	50.23
106	3.76	7.39	10.81	15.04	23.33	31.95	39.70
75	2.76	5.46	8.15	11.21	17.48	24.22	30.91
53	1.92	3.96	5.93	8.12	12.86	17.71	23.18
38	1.30	2.78	4.71	5.95	8.91	12.00	15.90
Pan	0.00	0.00	0.00	0.00	0.00	0.00	0.00
Torque. Nm	14.58	14.59	14.64	14.7	14.76	15	14.95

**Table B.27.** Short-time grinding tests for 14x20 mesh calcite (Bond charge.  $\Phi_B=0.22$ ).

Size, $\mu\text{m}$	Cum. Wt.% Passing						
	15 sec	30 sec	45 sec	60 sec	90 sec	120 sec	150 sec
1180	100.00	100.00	100.00	100.00	100.00	100.00	100.00
850	52.51	74.36	85.03	91.52	97.26	99.06	99.73
600	28.77	49.00	64.46	76.33	89.77	95.97	98.64
425	17.08	31.60	44.52	57.04	74.27	86.05	93.00
300	11.69	22.34	32.34	43.03	59.09	72.10	82.06
212	8.38	16.01	23.53	32.12	45.69	57.48	67.20
150	6.15	11.75	17.40	24.02	34.94	44.67	53.53
106	4.52	8.68	12.77	18.13	26.59	34.08	41.86
75	3.36	6.52	9.60	13.73	19.89	26.05	32.77
53	2.40	4.63	6.78	10.47	14.62	19.33	25.13
38	1.71	3.09	5.28	7.50	10.99	15.13	19.95
Pan	0.00	0.00	0.00	0.00	0.00	0.00	0.00
Torque. Nm	15.02	15	15.23	14.98	15	15.15	14.9

**Table B.28.** Short-time grinding tests for 48x65 mesh calcite (Bond charge.  $\Phi_B=0.22$ ).

Size, $\mu\text{m}$	Cum. Wt.% Passing						
	15 sec	30 sec	45 sec	60 sec	90 sec	120 sec	150 sec
300	100.00	100.00	100.00	100.00	100.00	100.00	100.00
212	35.24	45.28	57.42	62.84	73.59	82.00	88.33
150	17.46	27.10	35.68	41.87	53.05	62.67	71.11
106	11.46	18.16	24.52	29.53	38.67	47.90	55.51
75	7.86	12.61	17.18	21.16	27.79	35.68	42.59
53	4.94	8.60	11.75	14.99	20.01	24.98	30.82
38	3.44	5.83	7.49	10.02	13.99	17.78	21.81
Pan	0.00	0.00	0.00	0.00	0.00	0.00	0.00
Torque. Nm	14.98	15.2	14.93	14.93	14.82	15.16	15

**Table B.29.** Short-time grinding tests for 6x8 mesh calcite (Bond charge.  $\Phi_B=0.28$ ).

Size, $\mu\text{m}$	Cum. Wt.% Passing						
	15 sec	30 sec	45 sec	60 sec	90 sec	120 sec	150 sec
3350	100.00	100.00	100.00	100.00	100.00	100.00	100.00
2360	66.41	85.04	91.78	95.35	98.34	99.42	99.72
1700	51.28	74.50	85.26	91.48	96.94	98.97	99.43
1180	39.22	63.51	77.17	86.01	95.11	98.39	99.24
850	29.91	52.25	66.72	77.63	91.72	97.21	98.96
600	22.04	40.82	55.08	66.30	84.52	93.77	97.78
425	15.17	29.45	41.28	51.51	70.89	84.45	92.69
300	11.15	22.17	31.60	40.17	57.83	71.71	82.82
212	8.14	16.61	23.89	30.65	45.51	58.08	69.36
150	5.99	12.46	17.99	23.26	35.26	45.58	55.59
106	4.39	9.29	13.51	17.35	26.92	35.00	44.24
75	3.34	6.89	10.14	13.08	20.25	26.59	34.30
53	2.44	4.81	7.40	9.50	14.79	19.52	25.03
38	1.69	3.31	5.30	6.70	10.31	13.51	17.51
Pan	0.00	0.00	0.00	0.00	0.00	0.00	0.00
Torque. Nm	18.45	18.2	18.27	18.54	18.2	18.5	18.45

**Table B.30.** Short-time grinding tests for 14x20 mesh calcite (Bond charge.  $\Phi_B=0.28$ ).

Size, $\mu\text{m}$	Cum. Wt.% Passing						
	15 sec	30 sec	45 sec	60 sec	90 sec	120 sec	150 sec
1180	100.00	100.00	100.00	100.00	100.00	100.00	100.00
850	55.65	76.44	86.94	93.69	98.40	99.52	99.87
600	32.38	52.65	67.59	80.18	92.13	97.36	99.18
425	19.51	34.18	47.99	61.04	77.79	88.63	94.95
300	13.30	24.24	35.20	46.52	62.33	75.76	85.48
212	9.48	17.29	25.81	34.93	48.42	61.10	71.67
150	6.88	12.51	19.06	26.03	36.94	47.87	57.68
106	5.03	8.94	14.03	19.61	27.82	37.05	45.89
75	3.65	6.62	10.42	14.83	20.98	28.40	35.84
53	2.75	4.57	7.30	11.00	15.48	20.51	26.66
38	2.00	3.40	5.51	7.99	11.11	14.50	18.84
Pan	0.00	0.00	0.00	0.00	0.00	0.00	0.00
Torque. Nm	18.38	18.5	18.26	18.38	18.43	18.15	17.96

**Table B.31.** Short-time grinding tests for 48x65 mesh calcite (Bond charge.  $\Phi_B=0.28$ ).

Size, $\mu\text{m}$	Cum. Wt.% Passing						
	15 sec	30 sec	45 sec	60 sec	90 sec	120 sec	150 sec
300	100.00	100.00	100.00	100.00	100.00	100.00	100.00
212	31.62	46.61	58.26	67.40	74.56	83.04	88.11
150	17.10	27.31	37.90	45.42	55.15	64.72	72.22
106	11.44	18.30	26.96	32.33	40.78	49.59	55.83
75	7.80	12.79	19.80	23.36	29.90	37.28	41.49
53	5.03	8.85	14.14	16.03	20.50	26.47	30.00
38	3.40	5.75	9.69	11.30	14.49	18.69	21.88
Pan	0.00	0.00	0.00	0.00	0.00	0.00	0.00
Torque. Nm	18.15	18.15	17.98	18.29	18.14	18.26	18.08

**Table B.32.** Short-time grinding tests for 6x8 mesh calcite (Bond charge.  $\Phi_B=0.35$ ).

Size, $\mu\text{m}$	Cum. Wt.% Passing						
	15 sec	30 sec	45 sec	60 sec	90 sec	120 sec	150 sec
3350	100.00	100.00	100.00	100.00	100.00	100.00	100.00
2360	65.86	86.90	93.05	97.10	99.01	99.65	99.87
1700	49.99	76.83	86.71	94.36	98.30	99.34	99.76
1180	37.97	65.25	77.90	89.25	96.95	99.03	99.65
850	28.48	53.72	71.40	81.29	93.29	98.10	99.37
600	20.85	41.98	61.36	70.11	86.22	95.01	98.25
425	14.26	30.38	46.05	54.58	72.22	85.41	92.68
300	10.45	22.85	35.33	42.90	58.77	73.19	82.53
212	7.57	17.05	26.70	32.83	46.38	59.45	69.52
150	5.58	12.73	20.20	25.08	36.01	46.99	56.36
106	4.07	9.45	15.19	18.93	27.45	35.84	44.60
75	2.96	7.17	11.47	14.40	20.64	27.47	35.31
53	2.08	5.23	8.32	10.48	15.25	20.31	26.02
38	1.48	3.89	6.16	7.70	10.48	14.20	19.48
Pan	0.00	0.00	0.00	0.00	0.00	0.00	0.00
Torque. Nm	20.9	20.96	20.85	20.92	20.96	21.25	21.06

**Table B.33.** Short-time grinding tests for 14x20 mesh calcite (Bond charge.  $\Phi_B=0.35$ ).

Size, $\mu\text{m}$	Cum. Wt.% Passing						
	15 sec	30 sec	45 sec	60 sec	90 sec	120 sec	150 sec
1180	100.00	100.00	100.00	100.00	100.00	100.00	100.00
850	56.05	75.71	87.23	93.84	98.36	99.52	99.86
600	32.22	51.79	67.67	79.69	92.40	97.21	99.11
425	18.95	33.81	47.74	59.97	77.83	88.34	94.69
300	12.97	23.98	34.97	45.71	63.05	75.26	84.97
212	9.15	17.30	25.65	34.31	49.29	60.90	71.65
150	6.62	12.66	19.09	25.84	38.16	48.12	59.10
106	4.81	9.19	14.48	19.29	29.09	37.47	47.32
75	3.48	6.93	11.01	14.54	22.09	28.83	35.73
53	2.50	5.20	8.18	10.77	16.51	21.87	27.50
38	1.82	3.68	6.11	7.90	12.50	16.22	20.90
Pan	0.00	0.00	0.00	0.00	0.00	0.00	0.00
Torque. Nm	20.6	21.29	20.9	21.19	21.44	20.88	20.98

**Table B.34.** Short-time grinding tests for 48x65 mesh calcite (Bond charge.  $\Phi_B=0.35$ ).

Size, $\mu\text{m}$	Cum. Wt.% Passing						
	15 sec	30 sec	45 sec	60 sec	90 sec	120 sec	150 sec
300	100.00	100.00	100.00	100.00	100.00	100.00	100.00
212	30.86	43.91	56.95	65.34	75.96	83.63	87.87
150	16.56	27.04	37.09	45.25	56.28	64.80	70.05
106	10.79	18.27	25.84	33.20	42.33	49.94	55.01
75	7.38	12.75	18.07	24.62	30.81	37.00	41.51
53	5.01	8.77	11.84	17.40	21.99	26.50	30.20
38	3.50	6.02	8.49	12.41	15.70	19.00	21.01
Pan	0.00	0.00	0.00	0.00	0.00	0.00	0.00
Torque. Nm	21.1	21.13	20.9	20.8	21.1	20.78	20.86

## CURRICULUM VITAE

### PERSONAL INFORMATION

Surname, Name : Acar, Cemil  
Nationality : Turkish (T.C.)  
Date and Place of Birth : 15 November 1980, Ankara, Turkey  
Marital Status : Single  
Phone : +90 312 210 26 73  
Fax : +90 312 210 58 22  
Email : cacar@metu.edu.tr

### EDUCATION

Degree	Institution	Year of Graduation
BS	9 Eylül University, Faculty of Engineering Mining Engineering Department İzmir, Turkey	2003
High School	Aktepe High School, Ankara, Turkey	1998

### WORK EXPERIENCE

Year	Place	Enrollment
2004-present	Middle East Technical University, Mining Engineering Department, Ankara, Turkey	Research Assistant
2011-2012	University of Utah Metallurgical Engineering Department Salt Lake City, UT, USA	Visiting Scholar
July, 2003	Özdođu İnş. Tic. Ltd. Şti., Bergama Ovacık Gold Mine Open Pit İzmir, Turkey	Construction Supervisor
July, 2002	Özdođu İnş. Tic. Ltd. Şti., Bergama Ovacık Gold Mine Open Pit Mining İzmir, Turkey	Summer Practice
June, 2002	ETİ BOR Kırka Boron Mine Ore Preparation Eskisehir, Turkey	Summer Practice
July, 2001	TKİ, ELİ Soma Lignite Corporation, Eyz Underground Mining Manisa, Turkey	Summer Practice

**PUBLICATIONS**

**BOOKS**

Gülsün M., Özün S., Sivrikaya O., Lüle M., Aydın G., Kaya R., **Acar C.**, Acar İ., Pekpak E., Sözeri H., Camalan M., Çırak, M., “*Mineral Processing Laboratory Manual*”, METU Printing House, Ankara, Turkey, 2010.

**PAPERS** (presented and published in the proceedings of refereed international congress and symposiums regularly held by international organizers)

1. **Acar, C.**, Hoşten, Ç., 2008. Power measurements in Bond Ball mill, Proceedings of the 11th International Mineral Processing Symposium, G. Özbayoğlu, A. İ. Arol, Ç. Hoşten, Ü. Atalay, ed., Oct. 21-23, 2008, Belek-Antalya, Turkey.

2. **Acar, C.**, Hoşten, Ç., 2009. A comparison of the experimental methods of determining the breakage distribution functions, Proceedings of the 13<sup>th</sup> Balkan Mineral Processing Congress, S. Krausz, L. Ciobanu, N. Cristea, V. Ciocan, ed., June 14-17, 2009, Bucharest, Romania.

3. **Acar, C.**, Hoşten, Ç., 2010. Graphical Evaluation of Energy-Size Distribution Relationship, Proceedings of the 12th International Mineral Processing Symposium, Ö. Y. Gülsoy, Ş. L. Ergün, N. M. Can, İ. B. Çelik, ed., Oct. 6-8, 2010, Cappadocia-Nevşehir, Turkey.

**PROJECTS**

1. The Effect of Size of Coal on the Performance of Heavy Medium Cyclones,
2. Purification of Turgutlu Clay for the Use of Ceramic Raw Material,
3. The effect of Clay on the Stability and Viscosity of Magnetite Heavy Medium,